

Oxidative Dehydrierung von Ethylbenzol zu Styrol im Mikrowellenfeld

DISSERTATION

zur Erlangung des akademischen Grades
Doktor der Naturwissenschaften
Dr. rer. nat.

vorgelegt von
Diplom-Ingenieur
Boriss Nigrovski
aus Tallinn, Estland

dem Rat der Chemisch-Geowissenschaftlichen Fakultät der
Friedrich-Schiller-Universität Jena

Jena, Oktober 2008

Gutachter:

1.
2.
3. Tag der öffentlichen Verteidigung:

to my mother

to my family

Danksagung

Allen, ohne die die vorliegende Dissertation nicht zustande gekommen wäre, möchte ich für die Unterstützung und Hilfe sehr herzlich danken.

Mein besonderer Dank gilt zuerst Herrn Prof. Dr. Bernd Ondruschka, ohne dessen Einsatz die Durchführung dieser Arbeit nicht möglich gewesen wäre, für sein Interesse am Fortgang dieser Arbeit sowie für seinen Beistand durch immerwährende Diskussionsbereitschaft, Anregungen und, soweit notwendig, Diplomatie.

Für die Übernahme des Zweitgutachtens bin ich Herrn Prof. Dr. R. Beckert sehr dankbar.

Meinen herzlichen Dank richte ich an Herrn Dr. Peter Scholz für die intensive und produktive Betreuung dieser Arbeit, die vielen kritischen und lehrreichen Fragen sowie die Durchsicht und Korrektur.

Herzlich danke ich Herrn Dr. Thomas Taubert, Frau und Herrn Fährndrich die mir beim Aufbau der Technik und bei Messungen an der Anlage geholfen haben.

Weiterhin danke ich Frau Dr. Zavyalova. Ohne die stundenlangen kreativen Diskussionen mit ihr und ohne ihre kritischen Anmerkungen wäre es mir unmöglich gewesen, die Dissertation in dieser Form durchzuführen.

Bei Herrn Dr. Kilian Pollok (Institut für Geowissenschaften, FSU Jena), Dr. Mathias Müller (Otto-Schott-Institut, FSU Jena) und Dr. T. Keller (Institut für Materialwissenschaft, FSU Jena) bedanke ich mich ganz besonders für die sehr gute Zusammenarbeit bei der Charakterisierung meiner Katalysatoren.

Darüber hinaus gilt mein Dank allen Mitarbeiterinnen und Mitarbeitern des Lehrstuhls für das freundliche Arbeitsklima.

Mein letzter Dank gilt jenen, denen ich am meisten zu verdanken habe und denen ich meine Arbeit widme, nämlich meiner Familie.

Table of Contents

	page
DEDICATION.....	iii
DANKSAGUNG.....	iv
TABLE OF CONTENTS.....	v
CHAPTER 1. Introduction.....	1
CHAPTER 2. Theoretical foundations.....	4
2.1 Styrene manufacture.....	4
2.1.1 Industrial styrene production	4
2.1.2 Alternative processes for the synthesis of styrene.....	7
2.1.3 Deactivation phenomena in oxidative dehydrogenation of ethylbenzene.....	10
2.1.4 Styrene production with sp^2 - nanocarbon materials.....	13
2.2 Microwave chemistry.....	16
2.2.1 Historical facts.....	16
2.2.2 Theoretical fundamentals.....	17
2.2.3 Application of microwave dielectric heating.....	24
CHAPTER 3. Experimental methods	41
3.1 Materials.....	41
3.2 Catalyst preparation.....	42
3.3 Experimental procedures.....	43
3.4 Characterization of catalysts.....	46
CHAPTER 4. Results and discussion.....	48
4.1 ODEB with industrial used catalysts and mild oxidant CO_2	48
4.1.1 ODEB over Fe_2O_3 - K_2CO_3 -based and V_2O_5 -based powder catalysts	48
4.1.2 Upshot.....	51

4.2 ODEB over iron oxide loaded carbon nanotubes.....	52
4.2.1 Characterization of the nanocomposites before the reaction.....	52
4.2.2 Catalytic tests.....	56
4.2.3 Discussion.....	61
4.2.4 Upshot.....	66
4.3 ODEB over Magnetite/Hematit nanopowders.....	67
4.3.1 Characterization of fresh Magnetite/Hematite nanopowders.....	67
4.3.2 Catalytic tests.....	70
4.3.3 Discussion.....	75
4.3.4 Upshot.....	77
4.4 ODEB over functionalized carbon nanotubes.....	79
4.4.1 Characterization of functionalized MWCNTs before ODEB.....	79
4.4.2 Catalytic tests.....	81
4.4.3 Discussion.....	84
4.4.4 Upshot.....	87
CHAPTER 5. Microwave-assisted synthesis of magnetite nanoparticles used as a catalyst for the irradiated pyrolysis of carbon nanotubes in fluidized-bed reactor.....	90
5.1 Selection of the MWCNTs preparation method	90
5.2 Synthesis of magnetite nanoparticles.....	91
5.3 Microwave-assisted fluidized-bed reactor.....	96
5.4 Fluidization characteristics of the magnetite nanopowder in fluidized-bed reactor.....	97
5.5 Upshot.....	100
CHAPTER 6. Conclusions.....	102
APPENDIX A. Energy consumption during 80-hour test for both heating methods.....	viii
APPENDIX B. Deconvolution of C1s and O1s XPS spectra around 288 and 533 eV respectively. ix	
APPENDIX C. Schematic drawing of the catalytic ODEB over carbon nanofilaments.....	x

APPENDIX D. Abbreviations.....	xii
APPENDIX E. List of figures.....	xiii
APPENDIX F. List of tables.....	xv
KURZZUSAMMENFASSUNG.....	xvi
Lebenslauf.....	xix
LIST OF THE PUBLICATIONS.....	xx

Chapter 1. Introduction

The first comment on styrene, presumably discovered by the research chemist Neumann in 18th century, was published in the “Dictionary of Practical and Theoretical Chemistry” of Nicholson in the year 1786 [1]. At a later time Bonastre isolated styrene from the probe of Styrax and the results of his work were represented in the scientific publication of 1831. Only eight years later Simon, pharmacist in Berlin, obtained an ethereal oil by steam distillation from Storax and named it styrene [2]. Certain amount of styrene was found in the xylene fraction of hard coal tar by Berthelot, whose advices for the technology of styrene production are in use even nowadays [3].

The development of dehydrogenation process by IG Farbenindustrie AG in Germany and Dow Chemical in the United States during the 1930s was the first step toward the modern technology. Several plants were built in Germany before 1940, primarily for making synthetic rubber. It also became a material of strategic importance in the United States when the supply of nature rubber from South Asia was cut off, and large-scale plants were built. In 1950s the demand for styrene monomer continued to grow, but its main use has shifted from synthetic rubber to polystyrene. The total worldwide production of styrene was approximately 16.5 millions tons in 1995 and was projected to grow at a rate of more than 4 % annually. Many factors contribute to its growth heretofore: it is a liquid that can be handled easily and safely, it can be polymerized and copolymerized under a variety of conditions by common methods of plastic technology to a large number of polymers of different properties and applications, polystyrene is easy to extrude and mold and is one of the least expensive thermoplastic volumetrically, the raw materials benzene and ethylene are produced in large quantities in refineries and can be supplied to styrene plants through pipelines [4]. Thus, styrene is related to the one of the most important products of organic chemistry.

Nowadays, the catalytic dehydrogenation of ethylbenzene to produce styrene accounts for >90% of the world capacity, with 25 million tons of monomer produced annually [5]. The industrial process is performed at high temperatures (600–700 °C) over a hematite catalyst promoted by potassium (10%) and other compounds (Al_2O_3 , Cr_2O_3 , V, Ce, W, Mo) to enhance both the catalyst selectivity and lifetime [6]. The average capacity of ethylbenzene dehydrogenation plants is over 100,000 metric tons per year and plants which have a capacity of 400,000 metric ton per year are not uncommon. However, a strong incentive for the development of alternative technologies arises from this dehydrogenation process and its thermodynamic limitations, the use of large amounts of overheated steam and irreversible

catalyst deactivation [7]. Therefore, the search for the cheaper and easier approaches of styrene production is still topical in the industry.

The objective of this research is to investigate the influence of microwave field as alternative heating source on the selectivity and activity of various catalytic systems in oxidative dehydrogenation of ethylbenzene (ODEB). However, the main target is to show the advantage of microwave dielectric heating over conventional heating in gas-phase heterogeneous catalysis. In the chapters of the present work the sequential solution of the problems and tasks formulated to achieve the aim is given. Chapter 2 covers the literature review. The general features of ethylbenzene dehydrogenation are briefly discussed. The theoretical and literature backgrounds are presented. Chapter 3 explains the experimental methods of ODEB. The experimental set-up and quantitative product analysis using GC are discussed. Chapter 4 describes and discusses the results of catalytic performance of iron (III) oxide loaded multi-walled carbon nanotubes (MWCNTs), magnetite/hematite nanomixtures and functionalized MWCNTs for ODEB in an integral fixed-bed reactor under conventionally-heated and microwave-assisted reaction conditions. The characterization of catalysts before and after reaction by X-Ray diffraction, transmission electron microscopy and X-Ray induced photoelectron spectroscopy allowed us to investigate the influence of reaction conditions on the structure and morphology of tested samples. Chapter 5 deals with theoretical interpretation of microwave-assisted fluidized-bed reactor for the preparation of carbon nanotubes by catalytic pyrolysis, as well as with the synthesis of magnetite nanoparticles by microwave assisted hydrothermal process. In Chapter 6 the most important conclusions of the presented research are summarized.

References

- [1] R.H. Boundy, F.R. Boyer. Styrene: its polymers, copolymers and derivatives. Reinhold, New York (1952) 535.
- [2] E. Simon. Justus Liebigs Ann. Chem. 31 (1839) 265.
- [3] M. Lieb, B. Hilderbrand. Ullmann's Encycl. Verlag Chemie, Weinheim 4th ed., vol. 22 (1995) 293-309.
- [4] J. Kroschwitz, M. Howe-Grant. Kirk-Othmer. Encycl. Chem. Tech. 4, vol. 22, John Willey&Sons: New York (1995) 956-995.
- [5] I. Serafina, A. Kotarbaa, M. Grzywaa, et al. J. Catal. 239 (2006) 137–144.
- [6] K. Weissermel, H.-J. Arpe. Industrielle Organische Chemie. Wiley-VCH: Weinheim 5th ed. (1998) 339-344.
- [7] F.Cavani, F. Trifido. Appl. Catal. A 133 (1995) 215-219.

Chapter 2. Literature review

2.1 Styrene manufacture

Styrene, also known as vinyl benzene or cinnamene, is an organic compound with the chemical formula C_8H_8 . Under normal condition, this aromatic hydrocarbon is an oily clear colorless liquid, evaporates easily and has a sweet smell. Styrene helps to create plastic materials used in thousands of remarkably strong, flexible, and lightweight products that represent a vital part of our health and well being. It is used in everything from food containers and packaging materials to cars, boats, and computers.

Are there any alternatives for styrene-based products?

When designers select one specific material for one specific application, they do it after considering the general cost-benefits balance. In many applications, no other material can provide the same combination of performance characteristics, quality, and cost-effectiveness of styrene-based products. For example, by using styrene, packaging is more sanitary and less costly, automobiles have lighter components making them more fuel-efficient, boats are more structurally sound, and building insulation quality has greatly improved, helping to cut energy costs.

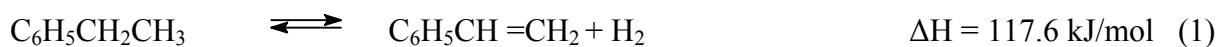
2.1.1 Industrial styrene production

Styrene is produced in industry mainly by two processes:

- I. dehydrogenation of ethylbenzene (DEB) in presence of steam over iron oxide based catalysts [1-3]
- II. as a by-product in the epoxidation of propene with ethylbenzene hydroperoxide and Mo complex-based catalysts [4].

Process I accounts for more than 90% of the worldwide capacity [5]. The DEB is an endothermic and reversible reaction with an increase in the number of mole due to reaction. High temperature favours dehydrogenation both kinetically and thermodynamically but also increases side-products and decreases the styrene selectivity.

Altogether, the dehydrogenation of ethylbenzene to styrene could be accompanied by several parallel-consecutive reactions, as follows [6]:



The main by-products in the dehydrogenation reaction are toluene and benzene. The formation of toluene (3) accounts for the highest yield loss, i.e., approximately 2% of styrene produced when a high selectivity catalyst is used. The formation of benzene (2) accounts for a yield of up to 1% of the styrene produced, mostly the result of thermal decomposition of ethylbenzene and styrene. The coke formed in reaction (4) is reformed with steam in reaction (5) [7-8]. Although other by-products, like carbon dioxide, methane, ethylene, phenylacetylene, allylbenzene, vinyltoluenes, xylenes, cumene, ethyltoluenes, butylbenzenes and heavy aromatics are rather insignificant in terms of the related yield losses, these compounds can affect the cost of purification and the quality of the styrene product.

Dehydrogenation catalysts usually contain 40-90% Fe_2O_3 and 10-30% K_2O ; the main promoter increases the activity and stability of the catalyst by an order of magnitude, as well as selectivity to styrene [9-10]. As found by Addiego et al. [11], the increase of potassium loading initially decreases the apparent activation energy to 88.2 kJ/mol and the further addition of potassium leads to an increase of the apparent activation energy to 142.8 kJ/mol, thereupon the unpromoted iron oxide yielded the apparent activation energy of 155.4 kJ/mol. The promotional role of potassium consists of the formation of a surface ternary compound, KFeO_2 , which constitutes the active phase [12-14]. Another further role played by potassium is the formation of well dispersed K_2CO_3 , which acts as catalyst for the gasification of carbonaceous deposit with the steam [8, 12-13]. The schematic life cycle of a potassium-promoted catalyst is shown in the figure in Fig.2.1 [8].

The role of other promoters in the Fe-K-O system is to uphold and support the KFeO_2 phase formation and to stabilize it under reaction conditions at a H_2O (steam)/ethylbenzene ratio as low as possible. The adding of Cr_2O_3 to the iron oxide catalysts enhances their activity, discourages sintering and quenching the volatilization of potassium from β -ferrite [14-18]. Ce, Mo and Al oxides considered to be structural promoters, as they can enter in the

Fe^{3+} compounds [8, 19]. Mn additive can increase the number of DEB active sites, as well as stabilize $\text{K}_2\text{Fe}_{22}\text{O}_{34}$ ferrite, one of the active phases of the catalyst [1-2, 20].

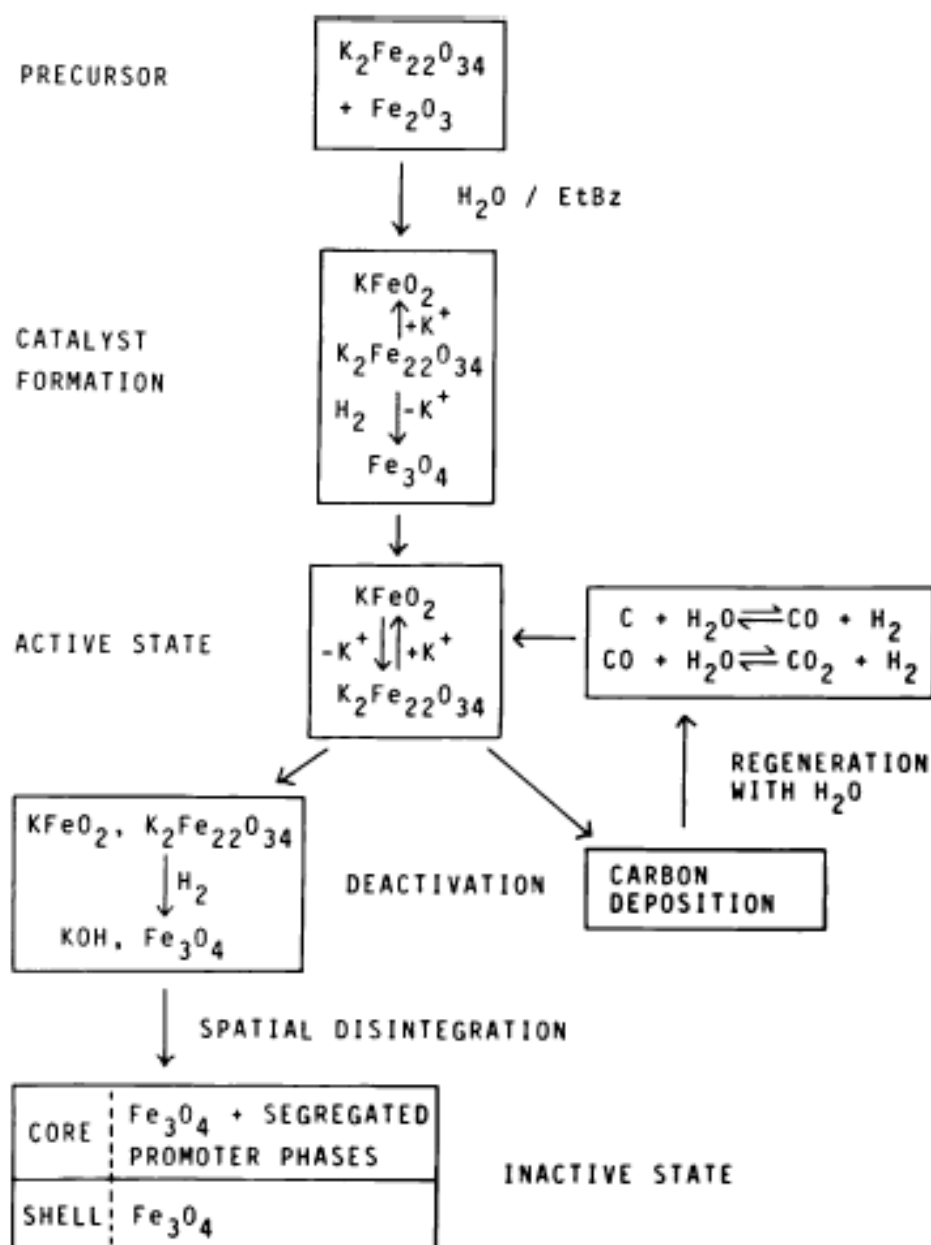


Figure 2.1. Schematic life cycle of a prototype styrene catalyst without any promoter additives as proposed by Muhler et al. [8].

The DEB can be run either adiabatically or isothermally over fixed bed in which the reactants are passed over the catalyst bed employing radial and axial flow. However,

isothermal dehydrogenation has the advantage of avoiding a very high temperature at the reactor inlet and maintaining a sufficiently high temperature at the reactor outlet. Two major types of isothermal reactor for DEB have been used by Lurgi and BASF [21]. The Lurgi reactor employs 20,000 to 30,000 tubes, 1 to 2-1/2 inch diameter and 8-10 ft length packed with catalyst using a molten salt mixture of sodium, lithium and potassium carbonates as the heating medium. In BASF plant the heat of reaction is supplied by hot flue gas from a fired heater at 760°C. The packed tubes are fewer in number and larger; 4-8 in diameter and 8-13 ft length. High conversion and selectivity are claimed but due to formidable heat-transfer problems and high costs of multitubular construction isothermal reactors are not applied in industry.

In an adiabatic reactor, the endothermic heat of reaction is supplied by the preheated steam that is mixed with ethylbenzene upstream of the reactor. As the reaction progresses, the temperature decreases. To obtain the higher conversion of ethylbenzene to styrene, usually two, and occasionally three, reactors are used in series with a re-heater between the reactors to raise the temperature of the reaction mixture. The superheated steam is co-fed with ethylbenzene and serves several purposes. Firstly, it provides the heat to maintain the reaction temperature and acts as a diluent resulting in a shift to higher equilibrium conversion through a decrease of the partial pressures of ethylbenzene and hydrogen. Furthermore, it limits the carbonaceous deposition by gasification. Finally, as an oxidant agent, it renders the iron oxide in an appropriate oxidation state. Typical steam/ethylbenzene ratio entering the reactor is 6-12. The modern adiabatic dehydrogenation plant, operating at a pressure of 41 kPa (6 psia) at the second reactor outlet, can give styrene selectivity as high as 97% at ethylbenzene conversion of 60-70%. A choice of a desired conversion is a matter of economic organisation. A low conversion gives a high selectivity but increases energy consumption; a high conversion decreases the energy cost but increases the raw material cost [22].

2.1.2 Alternative processes for the synthesis of styrene

As important as DEB is in the production of styrene, it suffers from two theoretical disadvantages: it is endothermic and is limited by thermodynamic equilibrium. The endothermicity requires heat input at high temperatures, which is difficult. The thermodynamic limitation necessitates the separation of the unreacted ethylbenzene from styrene, which are closed-boiling compounds. Therefore, the economically cheaper and

technically easier routes for styrene synthesis are of topical interest of the commercial establishment and many research institutes.

As alternatives to the industrial DEB the following technologies could be taken into account:

- The DEB followed by oxidation of hydrogen
- Oxidative dehydrogenation of ethylbenzene (ODEB)
- Dehydrogenation in membrane reactors

By dehydrogenation/oxidation process, DEB and oxidation of hydrogen are carrying out alternately in separate reactors charged with different catalysts. A gas mixture containing the oxygen injects either in the effluent or in the feed of a dehydrogenation reactor, in order to catalytically oxidize, either in part or totally, the co-produced or co-fed hydrogen. The oxidation of hydrogen not only reheats the reaction mixture from dehydrogenation reactor but also shifts the reaction equilibrium, thus allowing a higher conversion of ethylbenzene in the following dehydrogenation reactor. Such an oxidative reheat technology was patented [23-25] and developed by Universal Oil Products (UOP), and implemented in a demonstration-scale unit at Mitsubishi Chemical in Japan. However, this approach has not attained commercial acceptance, probably because of the high cost of palladium catalyst and the necessity of diluting the oxygen with steam prior to its injection into the reaction mixture. There are also concerns about the safety of the oxygen, and the possibility of contaminating the styrene product with oxygenates.

The SMART (styrene monomer advanced reactor technology) process for the synthesis of styrene in combination with the UOP concept for oxidative reheating by selective catalytic oxidation of hydrogen was licensed by ABB Lummus Crest. The SMART process can be used to revamp conventional dehydrogenation plants, in order to increase the capacity with low investment costs. Romantier et al. [26] discovered that the revamping of an existing plant producing 272,000 t/year of styrene has been increased in capacity to 400,000 t/year by adding two new reactors in a three-stage dehydrogenation process; the existing reactors are not modified, and the new reactors are added in series.

One of the possibilities to overcome the thermodynamic limit on conversion of ethylbenzene in industrial styrene synthesis is seen in the application of hydrogen permselective membranes which are able to remove the produced hydrogen from the catalyst bed, thus minimizing undesired oxygen insertion reactions and avoiding problems related to flammability of mixtures and to runaway [27]. Ten to fifteen percent higher ethylbenzene conversion than the fixed-bed reactor could be achieved in a Pd membrane reactor due to the

instantaneously removal of hydrogen by the permeation wall of Pd membrane [28-29]. However, Pd membranes belonging to non-porous (dense) membranes are prohibitive for industrial application due to their exorbitant price. The porous membranes, which are made of cheaper materials such as Vycor glass, alumina, ceramics etc., have been investigated more for dehydrogenation reactions than dense metallic membranes, but still did not find any application in the industry. Fig.2.2 shows the configuration of catalytic membrane reactor for dehydrogenation of hydrocarbons developed by Shell [30]. The first reactor is necessary to obtain hydrogen and the task of the membrane reactor is to decrease the amount of hydrogen. Hydrogen, with small amounts of hydrocarbons, permeates through the membrane walls. The post-dehydrogenation reactor treats the hydrogen-rich permeate stream, in order to transform the reagents which have permeated together with hydrogen through the membrane walls.

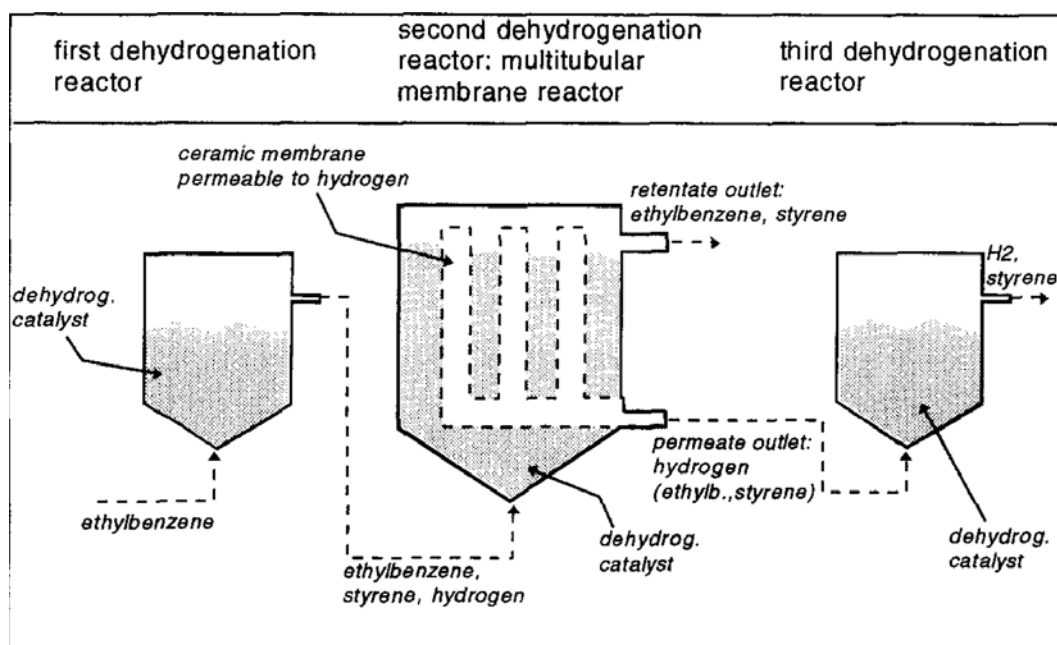


Figure 2.2. Reactor configuration in the process for hydrocarbons dehydrogenation (Shell) [30].

In ODEB the strong exothermic and irreversible for all practical purposes reaction is used:



This approach could greatly reduce the cost of styrene production due to the several reasons. First of all, the formation of water thermodynamically enables complete conversion of ethylbenzene and thus decreasing the separation costs. Secondly, this reaction flows

without excess of steam and the elimination or minimization of superheated steam could deeply decrease the process costs. Unfortunately, this technique has not resulted in commercial processes mainly because the selectivity to styrene is too low, in comparison with the dehydrogenation technology, to be economical. However, the theoretical elegance and potential benefit of the concept are so promising that it is still a topic of extensive research of many universities worldwide.

Particularly, in order to minimize the oxygen insertion reactions and to eliminate the problems which arise in the presence of molecular oxygen (mixture flammability, run away) interesting solutions have been proposed. For example, the use of CO₂, as soft oxidant, can give several advantages in ODEB, such as enhancement of product selectivity, suppression of the total oxidation and prevention of hot-spots on catalyst surface [31-32]. Nitrous oxide appeared to be also much more selective oxidant compared to oxygen and can be used in ODEB [33]. Moreover, utilization of N₂O and CO₂, which contribute the greenhouse effect and ozone layer depletion, has been of global interest from both fundamental and practical viewpoints in green and catalytic chemistry. Additionally, the catalytic oxidation in the presence of molecular oxygen with oxides possessing medium strength acidity (Co, Mo and CoMo catalysts supported on a montmorillonite clay and Al-pillared forms [34]) or with redox-type oxides in the absence of molecular oxygen (Mg₃(VO₄)₂, Mg₂VO₄ [35-36]) can undergo interconversion via reduction–oxidation and play a catalytically active role in the process.

Other technologies for producing of styrene from alternative raw materials such as side-chain alkylation of toluene with methanol or formaldehyde and cyclodimerization of 1,3-butadiene followed by oxidative dehydrogenation of the vinylcyclohexene to styrene have also been seriously investigated, but are deemed uneconomical [37].

2.1.3 Deactivation phenomena in oxidative dehydrogenation of ethylbenzene

The useful life of potassium promoted Fe-catalyst varies from 18 to 24 months, depending on the nature of the catalyst, the design and operation of the reactor system and the quality of the feedstock, and then the catalyst needs to be replaced. In view of this scale this is a very costly operation owing to the large quantity (approximately 120 m³ or 120-160 t depending on the density of the catalyst, for a plant of 300,000 t/year capacity) required [37-38]. Several main reasons of the deactivation are generally brought forward, i.e. loss

and/or redistribution of promoters (mainly potassium), build up of carbonaceous deposits, (change in) oxidation state of the Fe-oxide and physical degradation.

Loss or redistribution of promoters

The active state of the catalyst is believed to be equilibrium between potassium ferrite, KFeO_2 , and $\text{K}_2\text{Fe}_{22}\text{O}_{34}$ (Fig. 2.1). Potassium promoter loss, changes in composition or migration will alter the catalytic properties of the Fe-oxide. At the reaction conditions the potassium compounds, especially KOH, are slightly volatile, leading to a gas-phase transport to the outlet of the reactor. Also, potassium migrates from exterior to the core of the catalyst pellet due to a temperature gradient resulting from the endothermicity of the reaction. As well, hydrogen, formed as product of the reaction, can play havoc with catalyst here: it reduces the active catalyst to KOH and magnetite, Fe_3O_4 . The addition of different metal stabilizers such as chromium could significantly increase K and K^+ desorption energy and reduce the flux of potassium volatilization by an order of magnitude [14].

Oxidation state shifting

As already observed above (Fig. 2.1), the iron compound in fresh catalyst consisted of mainly Fe_2O_3 (hematite) which is reduced to Fe_3O_4 (magnetite) [39]. However, ions Fe^{3+} form a ternary compound $\text{K}_2\text{Fe}_{22}\text{O}_{34}$, which is unstable at typical styrene synthesis conditions resulting in the formation of KFeO_2 , which is considered to be the active phase. At the same time Fe_2O_3 slowly reduced to Fe_3O_4 , which is regarded to be an inactive phase. During the run KFeO_2 is also slowly reduced to Fe_3O_4 . However the $\text{K}_2\text{Fe}_{22}\text{O}_{34}$ serves as a potassium storage medium supplying the surface with near-monolayer coverage of potassium ions and preventing the reduction of the Fe^{3+} ions. Irreversible deactivation occurs when the $\text{K}_2\text{Fe}_{22}\text{O}_{34}$ become exhausted [7-8]. Thus, the reduction of Fe^{3+} -containing phase should be prevented. Probably the formation of KFeO_2 serves this function and it is also considered, that the addition of Cr as structural promoter stabilizes the Fe^{3+} oxidation state [40-41].

Physical degradation

The cause of the physical degradation of a Fe-oxide catalyst during styrene synthesis is closely related to the change in oxidation state of the Fe-oxide [13] as described in the

previous section. Under reaction conditions Fe_2O_3 (hematite) undergoes a reduction to Fe_3O_4 (magnetite). Hematite has a hexagonal lattice structure whereas magnetite has a cubic lattice structure. The structure change, along with the high mechanical forces in the catalyst bed, results in degradation or a pulverization of the catalyst particles. Also, the local density is changing due to the migration of the potassium promoter contribute in a weakening of the catalyst crush strength. Moreover, due to the local depletion of the promoter higher coking levels are attained and the pores of the catalyst can become plugged. The overall result of the above processes is the pressure drop over the catalyst bed becomes larger, which adversely affects the selectivity and the catalyst needs to be changed.

Coke deposition

Two reactions that have been suggested really not welcome in ODEB are the formation of carbonaceous deposits on the catalyst surface and their subsequent gasification by the diluent steam, leading to the production of small amounts of CO_2 (eq.5). The effect of these reactions on the overall conversion and selectivity is twofold. First, ethylbenzene and styrene are irreversibly converted into coke and/or CO_2 , which represents a loss in selectivity. Second, the presence of CO_2 in the reactant mixture strongly affects the catalyst activity [42]. The rate of coke deposition during DEB depends on many factors, among which steam/ethylbenzene ratio and reaction temperature play the most important role. Indeed, an excessively high operation temperature enhances the cracking side reactions, occurring on the acidic surface sites of the catalyst. On the other hand, the simultaneous gasification of coke by steam, during normal activity, usually leads to a 3–6 wt% steady-state concentration of carbonaceous deposits [43].



With no steam present reduction of the Fe-oxide takes place and excessive carbon formation is observed. An intermediate metastable carbide phase is formed which rapidly decomposes. The model scheme is presented below.



The presence of steam helps in preventing Fe^{3+} reduction, leading to the subsequent formation of Fe_3C , which is considered a key intermediate in coke formation.

2.1.4 Styrene production with sp^2 - nanocarbon materials

As it was discussed in the previous chapter, one of the peculiar features observed with most DEB catalytic systems was the formation of a coke layer, which was found to be the real catalytic surface [44-46]. This carbonaceous over-layer is initially deposited on the surface of the original catalyst, which fulfils the role of a catalyst for the formation of the carbonaceous deposit and a support for that deposit. That is why the catalysts exhibited induction periods in their activities. Additionally, it was proposed that quinone-type groups on the surface of this coke are the active sites for oxidative dehydrogenation [49]. Moreover, carbon itself assumes a large variety of forms because of its unique position in the periodic table. The various bonding states of carbon are related to certain structural arrangements. sp^1 -hybridization gives rise to carbon chain structures, sp^2 -hybridization to planar carbon structures, and sp^3 -hybridization to tetrahedral carbon structures. These results suggested that carbon materials such as activated carbon and synthetic graphite, carbon nanotubes (CNTs) and nanofibers, onion-like carbons and ultra-dispersed diamonds could be used as catalysts for the reaction.

Activated carbon

Activated carbon is mainly used as a catalyst support, but its use as a catalyst on its own is growing quickly. The ODEB is one of the reactions where activated carbon has been tested as a catalyst, due to its industrial relevance. Alkhazov et al. [50] were the first who tested activated carbon. They observed that ODEB could be performed at lower temperatures (350–400 °C) than those normally used with mixed oxide catalysts (450–550 °C). The group of scientists headed by Pereira also deeply investigated ODEB with activated carbon catalyst [51-54] and observed that initially (first ten minutes) the conversion is high, but the formation of gaseous reaction products does not take place. In principle, in this stage ethylbenzene and most probably the styrene formed lead to coke deposition in the pores of the carbon, which is confirmed, as it was found later, by an increase of the catalyst weight and by a reduction in the pore volume. The main precursor for the formation of coke is styrene, because it (being an unsaturated hydrocarbon) has higher tendency to form coke, in addition to its known great tendency to polymerize. The blockage of the pores occurs mainly in the first instants of the reaction and after 30 min, the carbon loses already 70% of its micro porosity. The kinetic results obtained in 5 h runs in ODEB showed that activated carbon in comparison with conventional catalysts (metal oxides) exhibited higher conversion and selectivity at lower

temperature (350 °C). However, due to the formation of an oxygenated coke, which also takes place by ODEB over commercial catalytic systems, the activated carbon catalysts displayed a low stability as a function of time on stream in an oxidative atmosphere, hindering the potential use of activated carbons as catalyst.

Carbon nanofibers and nanotubes

Recently, new carbon forms like graphite nanofibers or nanofilaments and CNTs have gained enormous attention in the scientific community. However, the production of graphite nanofibers is even older and the first reports date of more than a century [55-56]. Carbon nanofibers did not actually attract much attention of the academic community until the 1980s when their excellent electric conductivity, adsorbability and mechanochemical properties were found, made them applicable to composite, electrode materials, catalyst support materials, etc. [57]. There are mainly three types of carbon nanofibers: the fishbone or herringbone, their graphene layers stacking obliquely with respect to the fiber axis; the platelet carbon nanofibers, their graphene layers being perpendicular to the axis; and the ribbon carbon nanofibers, their graphene layers paralleling to the growth axis [58]. An increasing number of their applications in catalysis, either as supports or as catalysts have been investigated [59-61]; including application in synthesis of styrene [62-63].

Ideal CNTs may be described as nanoscaled graphene cylinders that are closed at each end by half a fullerene. Structures comprising only one cylinder are termed single walled carbon nanotubes, whereas multi-walled nanotubes (MWCNTs) contain two or more concentric graphene cylinders. CNTs have been the focus of considerable study because of their unusual strength along with excellent mechanical, electrical, thermal and magnetic properties. These properties make CNTs attractive for applications in nanoelectronics and quantum computing, as gas sensors, or fillers in polymer, ceramic or metal composites [64]. The applications of CNTs as catalysts have also attracted much interests in catalysis community due to their unique porous microstructure and chemical properties. One of the promising results is the use of CNTs in ODEB to styrene [65-66]. A few works were reported on the use of CNTs to catalyze the oxidative dehydrogenation of light hydrocarbons [67]. However, the high price and low density are the main disadvantages for their possible use in the industry.

Onion-like carbon and ultra-dispersed diamonds

In 1992 Ugarte, during the examining of carbon non-nanoparticles filled with gold and lanthanum oxide found fascinating particles consisting of concentric graphite-like shells [68] and these particles were called carbon onions. The onion-like carbons belong to the non-planar carbon materials, as well as ultra-dispersed diamonds with sp^2 - and sp^3 -atomstructure respectively. Last two decades many research groups and institutes have intensively investigated the methods of synthesis and properties of sp^2 - and sp^3 -hybridized carbons [69-70], mechanism of carbon onion core transformation into diamond-like structure [71] and reversely [72], but only a few articles report the catalytic application of these materials. Maksimova et al. have studied the effect of the unique structural variety of carbon, *i.e.* the carbon allotropies with sp^2 - and sp^3 -local electronic configurations, on the catalytic behaviour in ODEB to styrene [73-74]. The participation of newly-formed sp^2 -carbons over ultra-dispersed diamonds indicated that the same active sites formed during the reaction as these on onion like carbons. However, both materials exhibited high and stable ethylbenzene conversion and selectivity to styrene but the economic drawbacks of their synthesis make their application in industry impractically nowadays.

2.2 Microwave chemistry

2.2.1 Historical facts

The existence of electromagnetic waves, of which microwaves are part of the frequency spectrum, was assumed by Maxwell in 1864 from his theoretical calculations. In 1888, Hertz was the first to demonstrate the existence of electromagnetic waves by constructing an apparatus that produced and detected microwaves in the ultra-high vacuum region and only six years later Bose publicly demonstrated radio control of a bell using millimeter wavelengths, and conducted research into the propagation of microwaves. In the Second World War, the core of all microwave devices, the magnetron, was designed by Randall and Booth and used for RADAR (**R**adio **D**etection **A**nd **R**anging). It was soon concluded that microwaves could heat water in a very effective manner, and microwave-heating appliances became available in the US from the 1950's. These devices were widespread by the 1980's, and it was around this time that the application of microwave heating upon chemical reactions began to develop [75].

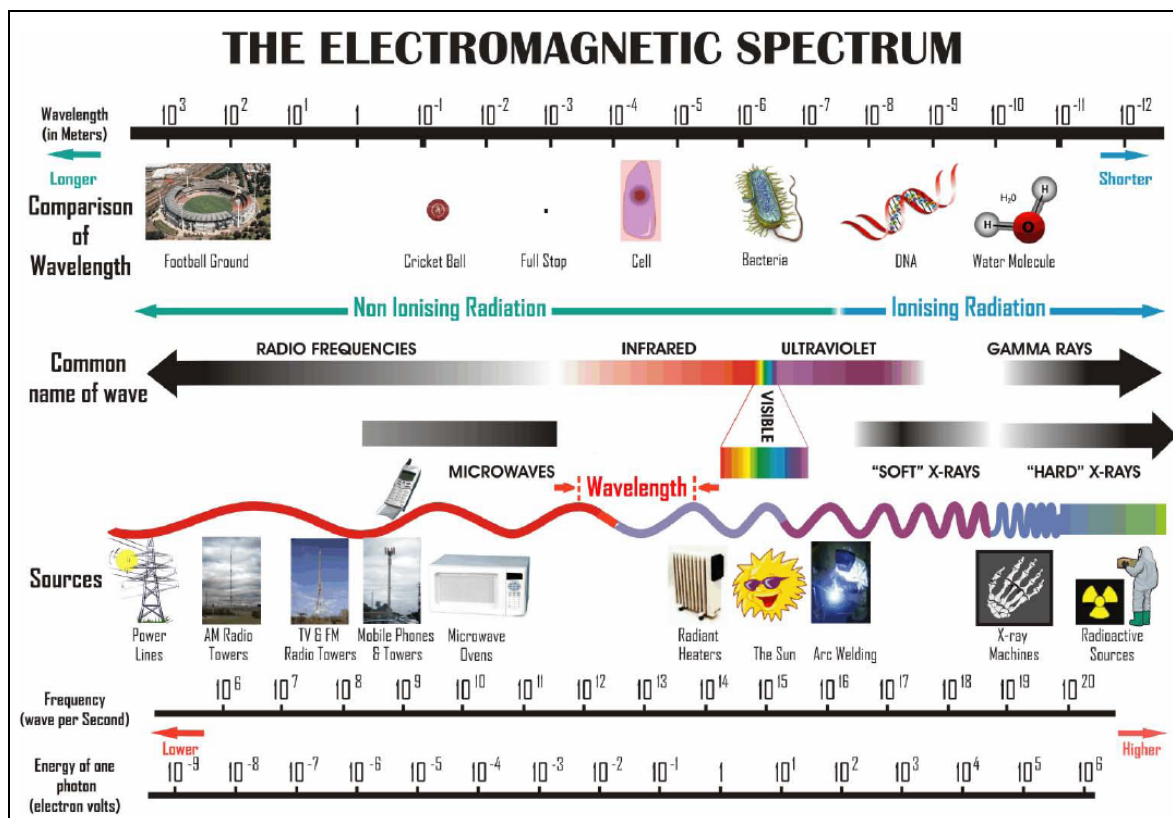


Figure 2.3. The electromagnetic spectrum [76].

2.2.2 Theoretical fundamentals

Microwaves are part of the electromagnetic spectrum, with wavelengths from 1 mm to 1 m, corresponding to frequencies from 300 GHz to 300 MHz (Fig.2.3) [76]. As such they have oscillating electrical and magnetic components orthogonal to each other and the direction of reproduction. Most of the microwaves spectrum is used for telecommunications or RADAR, but a few frequencies are applied for heating devices, the most common being 2.45 GHz [77]. Over the last decade the development of microwave-assisted chemistry has witnessed an explosive growth. For example, there were about 50 papers published in this area in 1993, but this figure increased more than 100-fold in 2004, and to date, the total number of related papers is around 2000. It is estimated that, at present, about 25 000 – 30 000 chemists use microwave technology to conduct chemical reactions worldwide [78].

Microwave volumetric heating

A distinguishing feature of microwave heating is its volumetric nature whereby the microwave power is dissipated in a dielectric and the electromagnetic energy converted directly to heat inside the material. Generally, there are three qualitative ways in which a material may be categorized with respect to its interaction with the microwave field: transparent (low dielectric loss materials) – microwaves pass through with little, if any, attenuation; opaque (conductors) – microwave field are reflected and do not penetrate; and, absorbing (high dielectric loss materials) – absorb microwave energy to a certain degree based on the value of the dielectric loss factor [79]. The absorbed energy will vary depending on the properties of both the microwave and the material itself. Because the microwave is losing energy as it journeys through the material, it will at some point have lost all its energy and become extinct. After this point, any heating does not continue by means of the direct interaction of microwave with the material, but through the conduction from the regions which have interacted with the microwave radiation. A fourth type of interaction is that of a mixed absorber. This type of interaction is observed in composite or multi-phase materials where one of the phases is a high-loss material while the other is a low-loss material, for example the mixture of magnetite and maghemite used further in tests. Mixed absorbers take advantage of one of the significant characteristics of microwave processing, that of selective heating. The microwave are absorbed by the component that has high dielectric loss while passing through the low loss material with little drop in energy. In some processes and

products heating of a specific component while leaving the surrounding material relatively unaffected would be of a great advantage. This selective heating process is not possible in conventional heating environments.

Even though the total charge on a molecule is zero, the nature of chemical bonds is such that the positive and negative charges do not completely overlap in most molecules. Such molecules are said to be polar because they possess a permanent dipole moment. A good example is the dipole moment of the water molecule. Molecules with mirror symmetry like oxygen, nitrogen, carbon dioxide, and carbon tetrachloride have no permanent dipole moments. However, when a dipole is placed in a static electric field, it will align itself with the field to minimize free energy and a finite time, known as the response time, is required for this to occur. If the field is oscillating there are three possibilities. At low frequency the dipole is able to remain aligned with the field as the response time is much smaller than the period of the perturbation. At high frequency the response time is much greater than the period; the dipole is unable to react to the changing field, and remains static. However, at intermediate frequencies where the response time is of the same magnitude as the period of the electric field, the dipole experiences a force that causes a rotation, but the polarization of the molecules lags behind that of the field. As the dipoles are not in phase with the field, they are not in the lowest energy state, and energy transfer must be occurring. The dipoles are absorbing energy from the electromagnetic field and it is being converted into heat.

The complex dielectric constant (ϵ^*) completely describes the dielectric properties of a homogeneous material. It can be expressed as the sum of two parts, the real (ϵ') and imaginary (ϵ'') dielectric constants:

$$\epsilon^* = \epsilon' - i \epsilon'' \quad (10)$$

The real part of the dielectric constant is approximately equal to ϵ^* at very high or low frequencies and exactly equal in static fields. Where an energy transfer (heating) is occurring ϵ'' is non-zero. This value is related to the efficiency of conversion between electromagnetic and thermal energy. The loss angle, δ , is also commonly quoted, although usually expressed in the form of its tangent. It is defined thus:

$$\tan \delta = \frac{\epsilon''}{\epsilon'} \quad (11)$$

The angle is the phase difference between the electric field and the polarization of the material. Magnetic polarization can also lead to a heating effect in a similar manner, for example in ferrites, although this is much less common [80].

Two important parameters for microwave processing are the depth of microwave penetration (D_p) and absorbed power (P_{abs}). Unlike conventional heating, these parameters are highly dependent on the dielectric properties of the material and, in practice, can provide another degree of process flexibility. The penetration depth (D_p) is defined as the depth at which the power has fallen to $1/e$ (~36.8%) of its incident value, and depends not only on the properties of the material but also on the wavelength. The power absorbed per unit volume during the microwave heating of the object could be given by the following equation [81]:

$$P_{abs} = 2\pi f \varepsilon_0 \varepsilon'' E^2 \quad (12)$$

where E is the magnitude of the internal electric field, f is the microwave frequency and the ε_0 is the permittivity of free space. However, the penetration depths as well as the knowledge of how the electric field decreases from the surface are very important in processing thick materials. Materials with a small penetration depth have a similar temperature profile to that of a conventionally-heated object, because all of the power is lost near the surface of the material. If the material has a large penetration depth, heating will occur deeper within the material and can lead to an inverted temperature profile. For small samples this means that the radiation may pass through the sample without losing much power and therefore only cause a very slight temperature rise. Thus, it could be concluded that microwaves transfer most effectively to materials which have dielectric loss factor in the middle of the conductivity range (Fig.2.4) [80]. In contrast, the conventional heating transfers heat more efficiently to materials with higher conductivity, because this form of heating is cause of the conduction of charged particles such as electrons or ions; and the time scale for these particles is much shorter than that for microwave radiation.

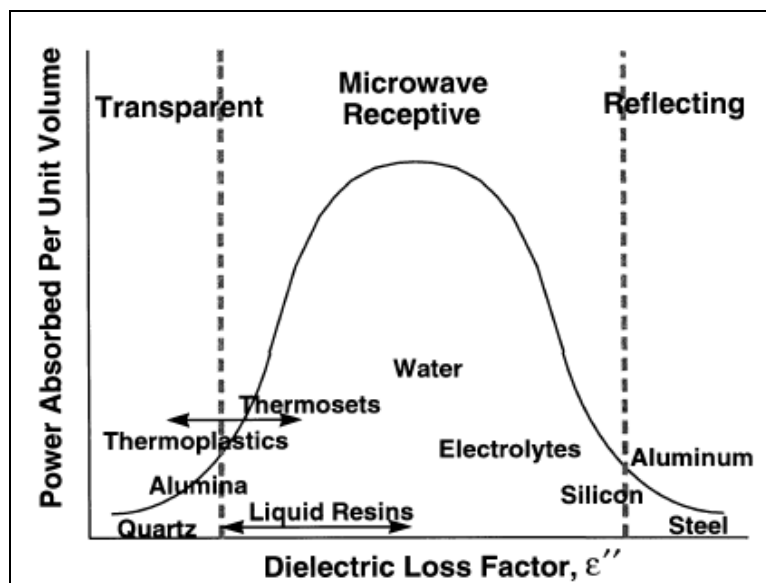


Figure 2.4. Relationship between the dielectric loss factor and ability to absorb microwave power for some common materials [80].

In addition, the conductivity of materials plays significant role in the heterogeneous catalysis at low temperatures, as the main source of heat loss through the walls of the quartz tubing in which the catalyst is held. The rate of heat loss is directly proportional to the difference between temperature of the sample T_s and the ambient temperature T_0 and can be presented by following equation:

$$\text{rate of heat loss} = \alpha(T_s - T_0) \quad (13)$$

where α is the heat transfer coefficient. Consequently, the rate of rise of bulk temperature during the microwave heating is depended on the power absorbed and the lost heat to the surrounding environment. Its simplified model can be given by the equation:

$$C_p \left(\frac{dT_s}{dt} \right) = 2\pi \cdot f \cdot \varepsilon_0 \cdot \varepsilon_{eff}'' \cdot E^2 - \alpha(T_s - T_0) \quad (14)$$

where C_p is the heat capacity of the sample. If the relative dielectric loss factor does not vary greatly with the temperature, the material will heat rapidly at first and then reach a steady state, at which the power absorbed per unit volume will be equal to the rate of heat loss from the sample.

$$2\pi \cdot f \cdot \varepsilon_0 \cdot \varepsilon_{eff}'' \cdot E^2 = \alpha(T_s - T_0) \quad (15)$$

The achievement of steady temperature then depends upon whether there are solutions to this equilibrium. However, for the materials, such as alumina, MoS₂ etc.[81-82], the analytical solutions of the equation are not possible because the relative dielectric loss

factor of these materials shows a strong variation with temperature, leading to a thermal “runaway” in which the temperature continues to rise uncontrollably. In this case the solution can be found by plotting the two terms separately and observing the crossover points as described by Zhang et al. [81].

However, before the use of microwave radiation in most popular catalytic reactions will be reviewed it is necessary to discuss the microwave effects occurred during the microwave-irradiated reactions.

The first attempts to explain the microwave thermal effect were undertaken by Sun [82] in his article on the hydrolysis of adenosine-tri-phosphate, in which he used the concept of spectroscopic heating to explain the microwave-induced acceleration of the rate of hydrolysis of the phosphor-anhydride bond of nucleotide tri-phosphate. Indeed, his co-worker Jahngen explained later that the increase in reaction rate was most likely due to the thermal gradients [83]. It was proposed, that in conventional heating thermal energy is transferred from the environment through the surface of the capillary to the solvent, whereas in the spectroscopic heating the increase in the kinetic energy of the solvent is due to the direct absorption of radiated energy by molecules, which accrue excessive amounts of energy in the form of vibrational and rotational modes and dissipate it to the environment [84]. It seems to be that microwave irradiation raises the temperature of the whole volume simultaneously, whereas in the oil-heated tube the reaction mixture in contact with the vessel wall is heated first.

The Fig.2.5 shows typically the heating modes and the temperature distributions in solid objects (for example catalyst bulk). Indeed, the typical thermal effects observed under microwave irradiation are overheating, hot spots and selective heating, which can be applied efficiently to improve processes, modify selectivity or even to perform reactions that do not occur under classical reaction conditions [77, 85].

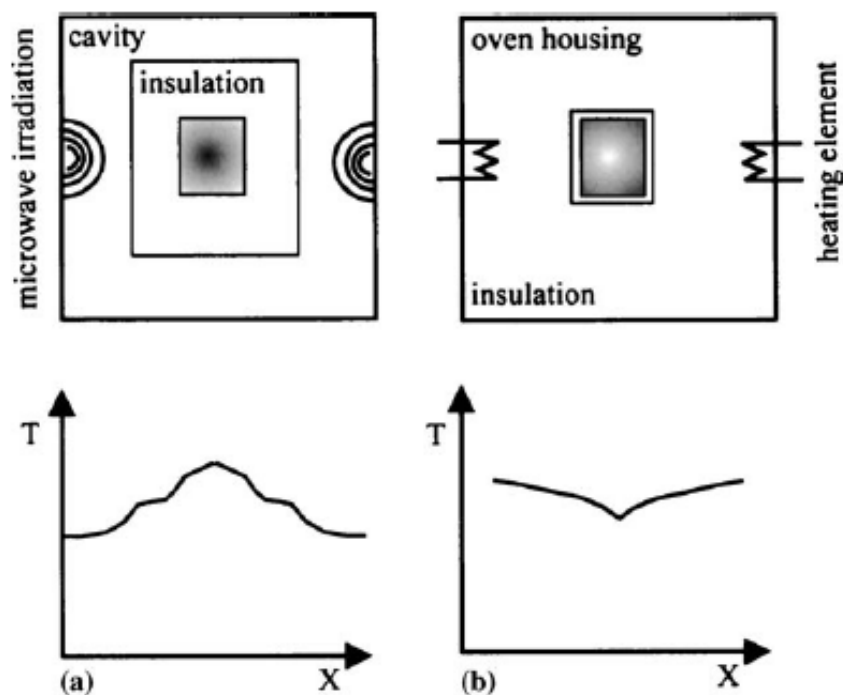


Figure 2.5. Inverse temperature profile by microwave heating (a) and conventional heating (b). [77].

Overheating of polar liquids can be explained by the “inverted heat transfer” effect (from the irradiated medium towards the exterior) since boiling nuclei are formed at the surface of the liquid. This thermal effect, which is not easily reproduced by conventional heating, can be used to improve the yields and the efficiency of certain processes in organic and organometallic chemistry.

The formation of so-called “Hot Spot” is a thermal effect that arises as a consequence of the inhomogeneity of the applied field, resulting in some regions that have higher temperatures than their surroundings. Mingos and Zhang [86] investigated the endothermic catalytic decomposition of H_2S over $\gamma\text{-Al}_2\text{O}_3$ as well as $\text{MoS}_2\text{-}\gamma\text{-Al}_2\text{O}_3$ and found that experiments yielded higher conversions than those expected from thermodynamic equilibrium and tests under thermal conditions. The higher conversion under microwave irradiation was attributed to the presence of hot spots, which temperature was proposed to be about 100–200 °C higher than the bulk temperature.

Temperature measurement in microwave field

There is a great interest in developing a thermoanalytical technique able to perform dielectric measurements during the microwave heating. However, the measurement of temperature under microwave heating is a difficult matter. As microwaves heat materials

differentially depending on their dielectric constant, the introduction of a temperature-measuring device that has a dielectric loss is unsatisfactory. A number of several methods currently used to measure the temperature in microwave field have been proposed.

A typical conventional thermometer works through conduction of heat. However, the expansive liquid is commonly either mercury or alcohol, both of which couple with microwaves. If these are placed in a sample within a microwave field, they will not only give a measure of the temperature, but also that of the heating effect upon the expansive liquid within the thermometer [87]. It is possible to use a thermometer where the expansive liquid used has a very low dielectric loss tangent such as xylene [88]. A good indication of the sample temperature can readily be achieved by the use of miniature gas thermometer, connected by capillary to a pressure transducer mounted external to the microwave cavity. Instancing, a thermometer constructed of Pyrox does not itself interact significantly with microwaves and can be used to the softening point of Pyrox, which is around 500°C.

In 1821, the German–Estonian physicist Seebeck discovered that any conductor (such as a metal) is proposed to generate a voltage, when a thermal gradient exists between two ends of a metal bar [89]. A thermocouple exploits this effect and consists of two dissimilar metal wires, joined together by welding. A potential difference exists between these two wires which vary with temperature. Because of the thermocouples small size, fast response, flexibility, ruggedness and low cost they are probably the most favored method of temperature measurement up to 1800 °C for both conventional and microwave heating. However, it is not possible to insert wires into a microwave cavity without interference to the microwave field and inducing currents in the wires.

The infrared thermography plays an essential role in experimental tests since (due to the electromagnetic field and the metal probes interactions) traditional techniques for temperature measurements cannot be applied inside microwave ovens [90]. Principal work of the infrared thermography is based on the property of the hot body to lose its energy by emitting radiation. The energy of the radiation that is emitted is a function of the temperature. For a perfect emitter, known as a black body, the relationship is given by the Stefan-Boltzmann law:

$$J^* = \sigma T^4 \quad (16)$$

where J^* is the energy flux density, σ is the Stefan-Boltzmann constant and T is the thermodynamic temperature [91]. The schematic diagram of the infrared camera used for thermographic measurements of plasma torches is displayed in Fig. 2.6 [92].

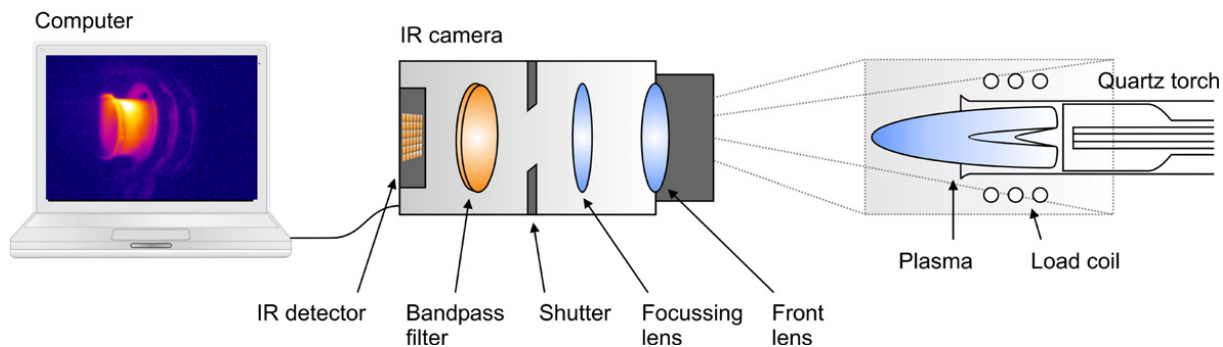


Figure 2.6. Schematic diagram of the inductively coupled plasma infrared imaging system [92].

Optical measurements such as these have the advantage that the instrument does not have to be in contact with the sample. Nearly everything gets hot before it fails, making infrared cameras extremely cost-effective, valuable diagnostic tools in many diverse applications. However, as it is only possible to observe radiation from the outside of samples, only the temperature of the surface can be measured.

While for surface temperatures IR thermography can be used, the inner temperatures may be measured by fibre optic probes that use the fluorescence of phosphors and/or phosphors co-doped with various auxiliary activators at their tips to measure temperature based on optical signals [93-95]. Since the fluoroptic thermometers are non-electrical and non-metallic, they are immune to electromagnetic interference and can measure temperatures in a broad variety of applications where conventional thermocouple sensors are ineffective. This method seems to be the ‘gold standard’ of temperature measurement in a microwave; however it is also not without drawbacks. The probes are not very durable and have a restricted maximum working temperature and it has also been shown that where an intense illumination source is present, temperature measurements may not be accurate [96]. Moreover, the price of fluoroptic thermometer is extremely high and amounts thousand euros.

2.2.3 Application of microwave dielectric heating

In 1945 the engineer Spencer, a self-taught engineer with the Raytheon Corporation, was testing a new vacuum tube called a magnetron when he discovered that the candy bar in his pocket was melted. This intrigued him, so he tried another experiment with popcorn kernels, sputtered, cracked and popped all over his lab and egg, exploded and splattered hot yolk all over amazed face of his curious colleague [97-98]. Quickly coming to the conclusion that other types of food could be heated by that way, the Raytheon Company filed the first patents for a microwave oven later that year and in 1947 demonstrated the world's first

microwave oven, called a "Radarange" and showed in Fig.2.7A [97]. Housed in refrigerator-sized cabinets, the first microwave ovens were sold at the considerable price of about US\$4000 [99]. Prices came down to US\$1200, and then remained in the US\$1000-1200 range until the early 1960s. In 1967 the first countertop, domestic oven was introduced. It was a 100-volt microwave oven, which cost just under \$500 and was smaller, safer and more reliable than previous models (Fig.2.7B). Presently, the cheapest portable model cost well below US\$100 (Fig.2.7C). Yearly sales in the USA have stabilized since the mid-1980s above the 10 million units. As a matter of fact, the number of households in the USA, Japan and Europe that have microwaves nowadays is more than 90%.

All microwave ovens used for heating food operate at 2450 MHz, the frequency at which microwaves interact strongly with water molecules in the food, while passing through other things (like plastic and dishes) without heating them. There is enough water in most foods to allow the microwaves to do their work. However, the main reason why microwaves became so popular is that microwave heating in comparison to conventional heating offers substantial savings in terms of energy. In general, microwave heating consumes 10-100 less energy and requires 10-200 times less time [100].

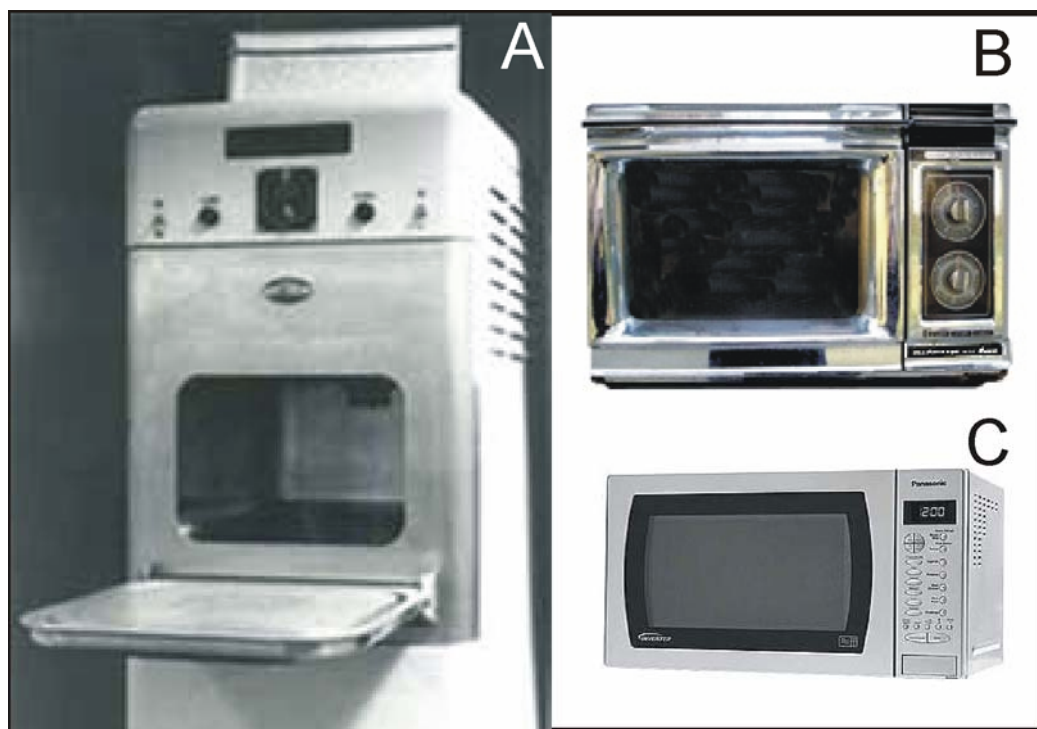


Figure 2.7. The evolution of microwave oven from gigantic "Radarange" (A) to the retro oven from 60s (B) and modern Panasonic microwave (C) [97].

Microwave equipment

A microwave system typically consists of a generator to produce the microwaves, waveguide to transport the microwaves, an applicator or a cavity to manipulate the microwave field for specific purpose, and a control system.

A magnetron is usually used to generate microwaves. The magnetron is a vacuum tube containing a cylindrical cathode and a coaxial anode as shown in Fig. 2.8 [101]. The anode, which has a set of vanes projecting inward forming slots between them, and are approximately $\frac{1}{4} \lambda$ (wavelength) deep and therefore are resonant at the operating microwave frequencies. The slots are mutually coupled via the fringing field at their open ends and the whole structure forms a resonant circuit. When the filament is heated, a cloud of electrons is formed around the cathode. When the anode is supplied with high voltage DC (direct current), these electrons will travel from the cathode to the anode. The magnetic field provided by the permanent or electromagnet installed outside the anode will provide a strong magnetic field that changes the path of these electrons. Since the field lines are parallel to the axis of the anode and perpendicular to the electron path, the electrons are forced to travel in a quasi-circular path around the cathode. By increasing the DC anode voltage or decreasing the magnetic field, some of the electrons will travel on a path closer to the anode, reaching the anode cavities where they will generate a resonant microwave field [80].

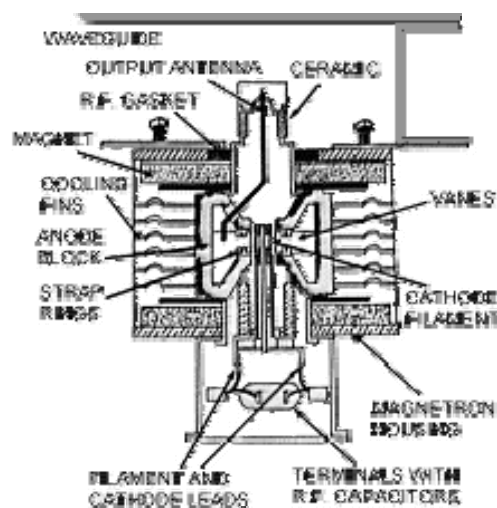


Figure 2.8. Sectional view of a typical magnetron [101].

Afterwards the energy emitted into the microwave field antenna connected to the anode will transmit it into the waveguide. Waveguides are metallic tubes of circular or rectangular cross-section, which are dimensioned for the current frequency.

The microwave applicator is the component of a processing system in which energy is applied to the product to be heated [102]. Common microwave applicators include traveling wave applicators, single mode cavities, and multimode cavities. However, the most used form of the applicator, comprising well over 50% of industrial systems and almost all household microwaves, is the multimode type. In a multimode system created by one or two magnetrons microwave irradiation is directed into the cavity through the waveguide and distributed by a mode stirrer [103]. The mode stirrer is a moving device introduced in the oven to perturb the field distribution continuously. Usually, it consists of a metal multi-blade fan rotated inside the oven. Even though it is a crude device, it contributes significantly to the achievement of uniform heating. However, the multimode modes result in regions of high and low electric fields i.e. non-uniformity within the cavity. To provide a more even energy distribution, the samples should be continuously rotated. While the generated microwave power is high (1000-1400 W), the power density of the field is generally rather low, what makes the heating of small individual samples practically difficult, a major drawback especially for research and development purposes. Therefore, the use of multimode instruments for small-scale synthetic organic research applications has become much less extensivity as compared to the use of the much popular in this area single-mode cavities.

In single mode resonant cavities the superposition of the incident and reflected waves gives a standing wave pattern which is very well defined in space. This enables the dielectric material to be placed in the position of maximum electric field for optimum transfer of the electromagnetic energy. A typical single mode resonant applicator consists of a rectangular waveguide, into which a co-sinusoidal electric field distribution of n half-wavelengths is established, connected to a flange with a coupling iris on one side and a non-contacting short-circuit plunger on the other side. Unfortunately, the single mode applicators couple efficiently only with small samples and the maximum output power is typically limited to 300 W. However, despite a limited processing volume the single mode systems become very popular in many synthetic laboratories and have been particularly effective in plasma processing as well as joining [103-104].

Generally, the microwaves with cavities of different types and sizes have found the application in a number of fields where the advantages of microwave energy may lead to a significant savings in energy consumption, process time and environmental remediation. In the following sections the employment of microwave ovens for various industrial technologies of material processing such as joining, sintering, wastes remediation, synthesis and heterogeneous catalysis is reviewed.

Joining and Sintering

The pioneering work in the area of application of the various microwave techniques for welding metals using microwave induced plasma jet, and joining polymers and ceramics utilizing electromagnetic field focusing facilities was performed by Siores and Rego [100]. Investigation of dielectric properties of engineering thermoplastic materials, such as ultrahigh molecular weight polyethylene, polycarbonate and acrylonitrile-butadiene-styrene polymers, and various ceramic materials was continued by Yarlagadda in Australia [105-106]. The ceramics that are commonly sintered using microwaves are Al_2O_3 , ZrO_2 , MgO , and SiC [107-108]. However, various fundamental problems are usually encountered during the microwave sintering of ceramic materials [109]. Firstly, the low-frequency (2.45 GHz) microwave applicators do not couple microwave power efficiently to many ceramics at room temperature and poor microwave absorption characteristics make initial heating difficult. Secondly, for a wide variety of ceramic materials, including Al_2O_3 , SiO_2 , Fe_3O_4 , β -alumina, ZrO_2 , etc., thermal instabilities may occur and it can lead to the phenomenon of temperature runaway; i.e., the specimen overheats catastrophically. Thus, although some advantageous application of microwave processing in sintering has been demonstrated, the perceived potential of the technology has gone largely unrealized on a production scale due to the same problems as described for microwave assisted synthesis of materials.

Waste treatment

Microwave heating has a significant potential for the current heating technologies in the treatment of waste streams and environmental remediation. Every year thousands of tons of printed circuit boards (in TVs, Stereos, computers, phones, etc) end up in landfill [110]. It is desirable to reduce the volume of this waste, immobilize the hazardous components into leach resistant forms and also reclaim and re-use potentially valuable products. With use of microwave energy, organic constituents can be removed during an initial lower-temperature processing step ($T < 700\text{ }^\circ\text{C}$), greatly reducing volume and weight of the waste material. During high-temperature processing ($T > 1200\text{ }^\circ\text{C}$), the remaining ash and glass fiber reinforcement mats can combine to form a vitreous mass. The metals are generally agglomerate to one or more spheroids, drop to the bottom of the melt, and are easily recovered [111-112].

Synthesis

One of the earliest applications of microwave radiation to the synthesis of inorganic compounds was performed by Frazer and Holzmann and followed quickly by Shriver and Jolly, where Frazer and Holzmann performed the reductive dimerization of BCl_3 to B_2Cl_4 , while Shriver and Jolly observed the transformation of GeCl_4 to Ge_2Cl_6 under microwave radiation [113-114]. Continuing this early application of microwaves, Mingos and his co-workers found that some metal oxides were sensitive to dielectric heating. Copper (I) oxide reached $550\text{ }^\circ\text{C}$ after irradiation for 1 minute at 500 W. In addition, the oxides of tungsten and vanadium heated to $750\text{ }^\circ\text{C}$ under the same conditions, and melted upon further heating [115]. From these early applications microwave radiation has been applied to the synthesis of modern, advanced materials such as nano-materials, thin films, and porous ceramics [116-118]. There has been intense interest in the development of nano-materials because of their size dependent properties stemming from varying degrees of quantum confinement of the electrons in the material. El-Shall et al. have developed a microwave-assisted synthesis for highly uniform, ultra narrow semiconductor (ZnS , ZnSe , CdS , CdSe) nanorods and nanowires [119]. The fast and volumetric dielectric heating from microwaves made their synthesis very fast, and produced uniform materials. The development of thin films is also an important area of materials chemistry, which has a large impact on the microelectronics industry. There are many methods for depositing thin films, and, of course, the morphology of the film is highly dependent on the method of deposition [120]. The microwave energy has been also used for the fabrication of carbon nanomaterials [121]. As an instance of microwave energy superiority over conventional heating the direct comparison of the 4-acyl-1,2,3,4-tetrahydroquinoxalin-2-one synthesis for both heating methods was investigated by Kappe et al. [122].

Heterogeneous catalytic reactions in the liquid phase where the formation of the temperature gradients in a stirred suspension of fine powdered catalyst is rather limited were well examined by Hajek and Radoiu in the transformation of *t*-butylphenols on montmorillonite KSF [123]. The authors proposed that the reaction rate enhancement observed under microwave conditions could be related to the interaction of microwave energy with species adsorbed on the surface of catalyst, particularly on the polarized molecule in the transition state. This effect was named in further as “microwave-induced polarization”. Lipshutz et al. [124] described the remarkable effect of microwaves on various types of cross-coupling of organozirconium species using Ni/C as catalyst. In the liquid phase synthesis of 3,4-dihydropyrimidine-2(1H)-ones catalyzed by aluminated mesoporous silica maximum

yield was obtained also under microwave conditions [125]. Inexpensive and relatively nontoxic reagents with graphite were used for reliable and environmentally benign method of 4-arylidene-2-phenyl-5(4*H*)-imidazolones synthesis under microwave irradiation [126]. It was found that the microwaves make the method advantageous in comparison to other existing methods. Chemat-Djenni et al. [127] investigated the microwave selective phenomena and its impact on heterogeneous chemical reactions. Several reactions of industrial interest have been studied: isomerization of *m*-xylene to *p*-xylene, Wacker oxidation of cyclohexene in the presence of heptanes as solvent, hydrolysis of hexanenitrile to hexanoic acid and esterification of stearic acid. The 20-fold reduction in energy demand on switching from electrical heater power supply to microwave reactor was determined during the experiments. The microwave heating was also applied to the degradation of 4-chlorophenol and phenol over mix-valenced nickel oxide [128-129]. Thus, it could be concluded that the application of microwave heating in liquid-phase heterogeneous systems is to be perspective.

Catalysis

The microwave phenomena was rapidly applied to catalysis, and the first report of altered selectivity came in 1988 from Thiebault et al. in the transformation of 2-methylpentane [130]. Further reports of different selectivity for the conversion of small organic molecules followed later [131]. Since this time, microwave heating of catalysts has been applied to a number of systems. In the automotive area, microwave heating has been investigated to decrease the cold start problems of three-way catalysts [132], and the catalytic combustion of diesel soot on particulate traps [133].

It is evident that microwave irradiation is a selective mode of heating, because microwaves generate rapid intense heating only of polar substances while apolar substances do not absorb the radiation and are not heated. Particularly, selective heating can be successfully exploited in heterogeneous reactions to heat selectively a polar catalyst, whereas the temperature of the fluid remains much lower than the catalyst temperature, and thus, the process might be performed more energy efficient than under thermal heating conditions. All those advantages of microwave heating in combination with the advantages of catalysis could be applied by chemists in order to perform the reactions cheaper, faster, with less waste and with a higher purity product. Further down, the use of microwave heating in heterogeneous gas-phase catalysis is briefly reviewed for several reactions including the oxidative coupling of methane, the oxidation of carbon monoxide, the reduction of NO_x and SO₂, automotive

exhaust gas purification and environmental catalysis. Particularly, several examples of heterogeneous liquid phase reactions activated by microwave irradiation will be also reported.

The oxidative coupling of methane is of a great commercial interest as it may provide a route to long chain hydrocarbons from natural gas deposits. As oil reserves dwindle, a synthesis of higher hydrocarbons by this method becomes both more desirable and financially viable. As a result, this is the area of many researches in microwave assisted heterogeneous gas phase catalysis. For the reaction to occur, methane is heated with oxygen and a catalyst. The desired reactions are shown in Fig. 2.9 [77-79].

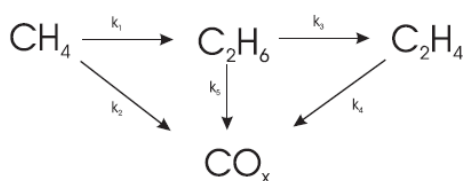


Figure 2.9. Reaction network for the oxidative coupling of methane [77].

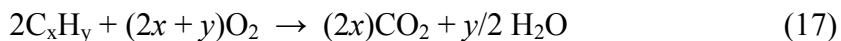
However, this reaction is problematic, as the products are unstable under conventional reaction conditions and may undergo further oxidation to CO or CO₂. Conventional heating of this reaction typically results in 10–15% methane conversion with 80–85% selectivity for C₂ hydrocarbons [77]. The first report of the application of microwave heating to this reaction was in a review by Bond et al. [134] using a sodium aluminates catalyst. It was confirmed that when microwave heating is used instead of conventional heating, the C₂ formation occurs at almost 125°C lower temperatures with higher selectivity. Roussy et al. [135] have also revealed an enhancement in higher hydrocarbons selectivity in oxidative coupling of methane over several microwave-irradiated catalysts like La₂O₃, La₂ZrO₇, SmLiO₂, (SmLiO₂)_{0.8}(CaOMgO)_{0.2}, Li/MgO and BaBiO_{3-x}. They found that microwave irradiation resulted in an increased ratio of ethylene to ethane, which is desirable, and also an increased selectivity of CO, which appears to be more useful than CO₂. Furthermore, it was observed that the selectivity to C₂ products was maximal at low conversions, decreasing at higher methane conversion. In contrast, the conventional heating of reaction resulted in minimal selectivity at low conversion, which increased with greater conversion. Although many catalytic systems [136-143] have been developed for the conversion of methane to higher hydrocarbons, this reaction is still under deep-rooted attention of many scientific and industrial laboratories due to daily increase of hydrocarbons prices as well as their consumption world-wide.

The study of the oxidation of carbon monoxide as a separate oxidation has received little attention, with the work of Perry et al. [144] being the sole exception. The reaction has been performed on Pt/Al₂O₃ and Pd/Al₂O₃ in a packed bed reactor heated by microwave energy and via conventional heating. It was concluded that the reaction kinetics (order of reaction) and the rate of reaction for the microwave heated CO oxidation were comparable to those for the conventionally heated reactor. A detailed analysis of the problems associated with temperature measurement in a microwave field is given, and it is postulated that any perceived temperature difference between microwave and conventional heating can be assigned to a poor measurement regime. As such they conclude that the Pt and Pd crystallites in a supported catalyst are not significantly hotter than the alumina support in a microwave heated reactor. However, whilst the oxidation of CO is particularly promising for the various applications including CO detection devices, the reduction of CO in industrial and automotive emissions, the purification of air in homes and offices, as well as lasers used for weather monitoring, the research of such catalyst being able to oxidize CO at room temperature will be always of the huge technical interest [145-148].

The oxides of nitrogen or NO_x, as they are collectively known, are formed as the ubiquitous byproducts of high-temperature combustion and are a sizeable pollution problem. They are also produced naturally from volcanic activity, biological decay and lightning. NO_x contributes to acid rain smog, eutrophication of water and the formation of toxic compounds in the atmosphere. Reduction of NO_x has been investigated by Wan [149] using copper and nickel catalysts, and Ringler et al. [150] have worked with a Pt/Al₂O₃ catalyst that showed differences in activity under microwave heating. The direct decomposition has also been carried out over metal-doped zeolites by Zhang and Tang [151-152], showing interesting results. Additionally, the removal of NO_x to nitrogen with the purifying efficiency of 95% in the microwave reactor filled with zeolite and ammonium bicarbonate was greatly demonstrated by Wei et al. [153-154].

Sulfur dioxide is another important pollutant of the environment and it is generally to be the main precursor to acid rain. This gas causes systemic disorders such as nasopharyngitis, chronic bronchitis, fatigue and alterations of the sense of smell [155]. Being water soluble, its local effects on the human body are manifested mainly as respiratory disorders. For these reasons the removal of sulfur oxide has attracted a lot of attention [155-158]. Comparative studies carried out in different reactors, however, only few works studied the catalytic reduction of sulfur under microwave heating condition [78, 82, 86,154,159].

The automotive three-way catalyst in vehicle exhaust systems is designed to remove the most harmful components emitted from internal combustion engines and involves the following reactions:



Automotive catalysts are involved in a complex interplay between these and other reactions under a wide array of conditions and thus contain a veritable cocktail of catalytic metals. A current state of the art catalyst reported by Turner et al. [160] contains ten catalytic compounds. Present automotive catalysts are very effective, but still have two greatest weaknesses: low temperature at the moment of engine start and the susceptibility to poisoning. Unfortunately, they are not active at ambient temperatures, and only become effective after being heated by the hot exhaust gas from the engine. However, the microwave heating of the catalyst to reduce emissions immediately after starting the engine has recently been shown to be highly effective, and conversions at abnormally low measured temperatures has been observed [132,161]. Furthermore, the microwave energy can induce carbon monoxide light-off (the temperature where 50% of final conversion is achieved) more efficiently than conventional heating and can reverse the poisoning by SO₂ for a commercial three-way catalyst.

Environmental catalysis is an ill-defined term that is generally used to refer to catalysis when applied to reduction or elimination of noxious emissions. The destruction of volatile and harmful solvents has been demonstrated in a pilot system by Cha et al. [162]. They used the microwave-based fume hood exhaust purification process to capture hazardous air pollutants in the fume hood exhaust using granular activated carbon and natural zeolite. Subsequently, the desorbed pollutants were recovered or destroyed by microwave energy during the regeneration of the saturated adsorbents. The microwave heated catalytic reactor contained Pd and Pt to form CO₂, H₂O and HCl. In further, the HCl was removed by a separate system, and the CO₂ and H₂O were vented to the atmosphere. Particularly, the organohalogenated compounds used widely in industry (solvents, extractants, dry-cleaning agents, degreasing agents, etc.), are also considered to be very dangerous environmental pollutants, and their release into the environment is a subject to stringent regulations. The microwave assisted decomposition of trichloroethylene as one of the aliphatic organochlorine

compounds was greatly demonstrated by Takashima et al [163]. They used 10% Ni/ γ -Al₂O₃ and 10% Co/ γ -Al₂O₃ to compare thermal trichloroethylene decomposition results with microwave mode. It was demonstrated that the microwave heating could greatly reduce the reaction temperature, accelerate the TCE decomposition speed and improve the TCE decomposition ratio. Hartmann et al. [164-165] deeply investigated the total oxidation of volatile organic compounds such as n-heptane, ammonia and methane in the microwave field. Finally, comparative studies of the influence of conventional and microwave heating methods on the catalytic and heating behavior of nanoscaled perovskites is excellently presented by Möser and Krech [166-168]. The perovskite powders of the types La_{0.5}Ca_{0.5}Al_yM_{1-y}O_{3- δ} (y = 0-0.8), M = Fe, Cr, Mn, Co and La_xSr_{1-x}Mn_yCo_{1-y} (x = 0.5-1, y = 0-1) were used as catalysts in total oxidation of propane at atmospheric pressure under both heating methods.

Heterogeneously catalyzed selective oxidation of aliphatic and aromatic hydrocarbons is of great commercial importance for fuels, polymers and as a starting point for production of many industrial chemicals. The enhancement of these reactions with microwaves could save significant amounts of energy. However, the mechanism of catalyst activation under microwave heating for most reactions is still unclear and needs to be extensively studied. In the present work, the ODEB as a great example for gas-solid phase selective oxidation of aromatic hydrocarbons was performed in conventionally heated and microwave assisted reactors in order to determine the advantages and/or disadvantages of each method.

References

- [1] A. Miyakoshi, A. Ueno, M. Ichikawa. *Appl. Catal. A* 219 (2001) 249–258.
- [2] A. Miyakoshi, A. Ueno, M. Ichikawa. *Appl. Catal. A* 216 (2001) 137–146.
- [3] T. Mathew, S. Malwadkar, S. Pai, et al. *Catal. Lett.* 91 (2003) 217-224.
- [4] Wikipedia, the free encyclopaedia: <http://en.wikipedia.org/wiki/Styrene> (29.10.2007).
- [5] L. Shijie, Y. Cheng, M. Changxi, et al. *React.Kinet.Catal.Lett.* 84 (2005) 247-254.
- [6] N. Dulamita, A. Maicaneanu, D. C. Sayle, et al. *Appl. Catal. A* 287 (2005) 9-18.
- [7] M. Muhler, R. Schlögl, A. Reller, et al. *Catal. Lett.* 2 (1989) 201-210.
- [8] M. Muhler, J. Schütze, M. Wesemann, et al. *J. Catal.* 126 (1990) 339-360.
- [9] Shibata, K.; Kiyoura. *Bull. Chem. Soc. Japan* 42 (1969) 871.
- [10] K. Coulter, D.W. Goodman, R.G. Moore. *Catal. Lett.* 31 (1995) 1-8.
- [11] W.P. Addiego, C.A. Estrada, D.W. Goodman, et al. *J. Catal.* 146 (1994) 407-414.
- [12] O. Shekhah, W. Ranke, R. Schlogl. *J. Catal.* 56 (2004) 225-236.
- [13] D.E. Stobbe, F.R. van Buren, A.J. van Dillen. et al. *J. Catal.* 135 (1992) 533-548.
- [14] I. Serafin, A. Kotarba, M. Grzywa, et al. *J. Catal.* 239 (2006) 137-144.
- [15] K.K. Kearby. US Patent 2,426,829 (1947).
- [16] B.D. Herzog, H.F. Raso. *Ind. Eng. Chem. Prod. Res. Dev.* 23 (1984) 187.
- [17] T. Hirano. *Appl. Catal.* 28 (1986) 119-352.
- [18] S. Elsanashaie, B.K. Abdallah, S.S. Elshishini, et al. *Catal. Today* 64 (2001) 151-168.
- [19] A. Trovarelli, C. De Leitenburg, M. Loaro, et al. *Catal. Today* 50 (1999) 353-362.
- [20] A. Kotarba, I. Kruk, Z. Sojka. *J. Catal.* 221 (2004) 650-661.
- [21] K. Kochlöfl. Dehydrogenation of Ethylbenzene. In *Handbook of Heterogeneous Catalysis*. VCH: Weinheim 5 (1997) 2151-2152.
- [22] Google: <http://www.che.cemr.wvu.edu/publications/projects/styrene/styrene1.PDF> (12.03.2008).
- [23] T. Imai, D.Y. Jan. US 4 788 371 (1988).
- [24] T. Imai. US 4 418 237 (1983).
- [25] T. Imai. US 4 435 607 (1984).
- [26] J. Romatier, M. Bentham, T. Foley, et al. *Proc. Dewitt Petrochem. Rev.* (1992) K1.
- [27] R. Dittmeyer, V. Höllein, P. Quicker, et al. *Chem. Eng. Sci.* 54 (1999) 1431-1439.
- [28] Y. She, J. Han, Y.H. Ma. *Catal. Today* 67 (2001) 43–53.
- [29] Y.L. Becker, A.G. Dixon, Y.H. Ma, et al. *J. Memb. Sci.* 77 (1993) 233-240.
- [30] Y.M. Sun, S.J. Khang, *Ind. Eng. Chem. Res.* 29 (1990) 232-239.

- [31] X. Li, W. Li, K. Xie. *Catal. Lett.* 105 (2005) 223-227.
- [32] D.Hong, V. P. Vislovskij, S. Park et al. *Bull. Korean Chem. Soc.* 26 (2005) 1743-1748.
- [33] P. Kustrowski, L. Chmielarz, A. Rafalska-Lasocha. *Catal. Com.* 7 (2006) 1047-1052.
- [34] A. Moronta, M. E. Troconis, E. Gonzalez, et al. *Appl. Catal. A* 310 (2006) 199–204.
- [35] W.S. Chang, Y.Z. Chen, B.L. Yang, *Appl. Catal. A* 124 (1995) 221-228.
- [36] W. Oganowski, J. Hanuza, L. Kepinski, et al. *J. Mol. Catal. A* 136 (1998) 91-100.
- [37] Kirk-Othmer. *Encycl. Chem.* John Wiley&Sons: New York. 4th ed., vol. 22 (1995) 957-995.
- [38] D.H. James, W.M. Castor. *Ullmann's Enc. Ind. Chem.* Wiley-VCH: Weinheim 5th ed., vol. 25, (1994) 329.
- [39] E.H. Lee. *Catal. Rev.* 8 (1973) 285-298.
- [40] W.J. Pöpel, W. Büchele, A. Deimling, et al. DE 4324905 A1 (1995) to BASF AG.
- [41] G.E. Lewis, A.R. Smith, F.A. Sherrod. US Patent 4,804,799 (1989) to DOW Chemical.
- [42] I. Rossetti, E. Bencini, L. Trentini, et al. *Appl. Catal. A* 292 (2005) 118–123.
- [43] K.R. Devoldere, G.F. Froment. *Appl. Catal. A* 212 (2001) 239-245.
- [44] T.G. Alkhozov, A.E. Lisovskii, M.G. Safarov et al. *Kinet. Catal.* 13 (1972) 509-516.
- [45] A. Schraut, G. Emig, H.G. Sockel. *Appl. Catal.* 29 (1987) 311-319.
- [46] G. Emig and H. Hofmann. *J. Catal.* 84 (1983) 15-28.
- [47] G.E. Vrieland, P.G. Menon. *Appl. Catal.* 77 (1991) 1-12.
- [48] A.E. Lisovskii, C. Aharoni. *Catal. Rev.-Sci. Eng.* 36 (1994) 25-38.
- [49] L.E. Cadus, O.F. Gorriz, J.B. Rivarola. *Ind. Eng. Chem. Res.* 29 (1990) 1143-1156.
- [50] T.G. Alkhozov, A.E. Lisovskii, Yu.A. Ismailov. *Kinet. Catal.* 19 (1978) 611-621.
- [51] M.F.R. Pereira, J.L. Figueiredo. *Appl. Catal. A* 184 (1999) 153-160.
- [52] M.F.R. Pereira, J.J.M. Orfão, J.L. Figueiredo. *Appl. Catal. A* 196 (2000) 43-54.
- [53] M.F.R. Pereira, J.J.M. Orfão, J.L. Figueiredo. *Appl. Catal. A* 218 (2001) 307-318.
- [54] M.F.R. Pereira, J.J.M. Orfão, J.L. Figueiredo. *Coll. Sur. A* 241 (2004) 167-171.
- [55] P. Schützenberger, L. Schützenberger, C. R. Acad. Sci. Paris 111 (1890) 774-785.
- [56] C. Pelabon, H. Pelabon, C. R. Acad. Sci. Paris 137 (1903) 706-720.
- [57] F. Yuan, H.K. Yu, H. Ryu. *Elect. Acta* 50 (2004) 685–691.
- [58] Y.A. Zhu, Zh.J. Sui, T.J. Zhao, et al. *Carbon* 43 (2005) 1694–1699.
- [59] N.M. Rodriguez, M.S. Kim, R.T.K. Baker. *J. Phys. Chem.* 98 (1994) 13108-13119.
- [60] K.P. De Jong, J.W. Geus. *Catal. Rev. Sci. Eng.* 42 (2000) 481-500.
- [61] P. Serp, M. Corrias, P. Kalck. *Appl. Catal. A* 253 (2003) 337-352.
- [62] T. Zhao, W. Sun, X. Gu, et al. *Appl. Catal. A* 323 (2007) 135-146.

- [63] J.J. Delgado, D.S. Su, G. Rebmann, et al. *J. Catal.* 244 (2006)126-129.
- [64] M. Paradise, T. Goswami. *Mater. Design* 28 (2007) 1477-1489.
- [65] G. Mestl, N. Maksimova, N. Keller, et al. *Angew. Chem. Int. Ed.* 40 (2001) 2066-2068.
- [66] M.F.R. Pereira, J.L. Figueiredo, J.J.M. Órfão. *Carbon* 42 (2004) 2807-2813.
- [67] Z.J. Sui, J.H. Zhou, Y.C. Dai, et al. *Catal. Today* 106 (2005) 90-94.
- [68] D. Ugarte. *Nature* 359 (1992) 707-716.
- [69] T. Gorelik, S. Urban, F. Falk, et al. *Chem. Phys. Lett.* 373 (2003) 642-645.
- [70] Y.P. Kudryavtsev, S.E. Evsyukov. *Diamond Relat. Mater.* 6 (1997) 1743-1746.
- [71] I.V. Ponomareva, L.A. Chernozatonskii. *J. Microel. Eng.* 69 (2003) 625–628.
- [72] V.L. Kuznetsov, A.L. Chuvilin, Y.V. Butenko, et al. *Chem. Phys. Lett.* 222 (1994) 343-348.
- [73] D. Su, N. Maksimova, J.J. Delgado, et al. *Catal. Today* 102-103 (2005) 110-114.
- [74] D. Su, N. Maksimova, G. Mestl, et al. *Carbon* 45 (2007) 2145-2151.
- [75] R.Gedye, F.Smith, K.Westaway, et al. *Tetrahedron Lett.* 27 (1986) 279–282.
- [76] Google: <http://www.satcom.co.uk/article.asp?article=16> (20.03.2008)
- [77] H. Will, P. Scholz, O. Ondruschka. *Chem. Eng. Technol.* 27 (2004) 1-10.
- [78] X. Zhang, D.O. Hayward. *Inorg. Chim. Acta* 359 (2006) 3421-3433.
- [79] W.H. Sutton. *Am. Ceram. Soc. Bull.* 68 (1989) 376–386.
- [80] E.T. Thostenson, T.W. Chou. *Composites: Part A* 30 (1999) 1055–1071.
- [81] X. Zhang, D.O. Hayward, D.M.P. Mingos. *Ind. Eng. Chem. Res.* 40 (2001) 2810-2817.
- [82] W.C. Sun, P.M. Guy, J.H. Jah, et al. *J. Org. Chem.* 53 (1988) 4414-4416.
- [83] E.G.E. Jahngen, R.R. Lentz, J.P.S. Pesheck, et al. *J. Org. Chem.* 55 (1990) 3406-3409.
- [84] C.O. Kappe, A. Stadler. *Microwaves in Organic and Medicinal Chemistry*. WILEY-VCH, Weinheim 25 (2005) 15.
- [85] A. Hoz, A. Diaz-Ortiz, A. Moreno. *Chem. Soc. Rev.* 34 (2005) 164–178.
- [86] X. Zhang, D.O. Hayward, D.M.P. Mingos. *Chem. Commun.* (1999) 975-976.
- [87] G. Bond, R.B. Moyes, S.D. Pollington, et al. *Meas. Sci. Technol.* 2 (1991) 571-572.
- [88] A. Whittaker, D. Mingos. *Chemistry under Extreme or Non-Classical Conditions*. Wiley: New-York, 1st ed. (2002) 479–514.
- [89] Wikipedia, the free encyclopaedia: <http://en.wikipedia.org/wiki/Thermocouple> (20.04.2008).
- [90] G. Cuccurrullo, P.G. Berardi, R. Carfagna, et al. *Infr. Phys. Technol.* 43 (2002) 145-150.
- [91] N. Schuster, V.G. Kolobrodov. *Infrarotthermografie*, VCH: Weinheim 2 (2004) 25-30.

- [92] C. Engelhard, A. Scheffer, T. Maue, et al. *Spectrochim. Acta Part B* 62 (2007) 1161–1168.
- [93] V.C. Fericola, R. Galleano. *Meas.* 37 (2005) 1-8.
- [94] H. Aizawa, H. Uchiyama, T. Katsumata, et al. *Meas. Sci. Technol.* 15 (2004) 1484–1489.
- [95] M. Ollivon, S. Quinquenet, M. Seras, et al. *Thermochim. Acta* 125 (1988) 141-153.
- [96] A.D. Reid, M.R. Gertner, M.D. Sherar. *Phys. Med. Biol.* 46 (2001) 149-157.
- [97] Google: <http://www.ieee-virtual-museum.org/collection/tech.php?id=2345891&lid=1> (15.03.2008).
- [98] Google: <http://www.gallawa.com/microtech/history.html> (15.03.2008).
- [99] L.P. Kok, P.E. Visser, M.E. Boon. *J. Neurosci. Meth.* 55 (1994) 119-124.
- [100] E. Siores, D. Do Rego. *J. Mater. Process. Technol.* 48 (1995) 619-625.
- [101] Google: <http://www.gallawa.com/microtech/magnetron.html> (17.03.2008).
- [102] B. Ondruschka, W. Bonrath, D. Stuerger. *Microwaves in Organic Synthesis*. Wiley-VCH: Weinheim 2nd ed., vol.1 (2006) 62-103.
- [103] C.O. Kappe, A. Stadler. *Microwaves in Organic and Medicinal Chemistry*. Wiley-VCH: Weinheim 1st ed., vol. 25 (2005) 29-55.
- [104] D.E. Clark, W.H. Sutton. *Annu. Rev. Mater. Sci.* 26 (1996) 299-331.
- [105] P.K.D.V. Yarlagadda, T.C. Chai. *J. Mater. Process. Technol.* 74 (1998) 199–212.
- [106] P.K.D.V. Yarlagadda, R.C.T. Soon. *J. Mater. Process. Technol.* 84 (1998) 162–174.
- [107] A.K. Mukhopadhyay, M.R. Chaudhuri, A. Seal et al. *Bull. Mater. Sci.* 24 (2001) 125–128.
- [108] A. Chatterjee, T. Basak, K.G. Ayappa. *AIChE J.* 44 (1998) 2302-2311.
- [109] R.R. Menezes, P.M. Souto, R.H.G.A. Kiminami. *J. Mater. Process. Technol.* 190 (2007) 223–229.
- [110] T.J. Appleton, R.I. Colder, S.W. Kingman et al. *Appl. Energy* 81 (2005) 85–113.
- [111] D.A. Jones, T.P. Lelyveld, S.D. Mavrofidis, et al. *Resources Conserv. Recycl.* 34 (2002) 75-90.
- [112] R.L. Schulz, D.C. Folz, D.E. Clark, et al. *Microwaves: Theory and Application in Materials Processing III*, *Ceram. Trans.* Westerville, OH: Am. Ceram. Soc. (1995) 107-116.
- [113] J.W. Frazer, R.T. Holzmann. *J. Am. Chem. Soc.* 80 (1958) 2907-2908.
- [114] D. Shriver, W.L. Jolly. *J. Am. Chem. Soc.* 80 (1958) 6692-6693.
- [115] D.R. Baghurst, M.P. Mingos. *J. Chem. Soc., Chem. Commun.* 12 (1988) 829-830.
- [116] B.L. Cushing, V. L. Kolesnichenko, C.J. O'Connor. *Chem. Rev.* 104 (2004) 3893-3946.
- [117] G.D. Wilk, R.M. Wallace, J.M. Anthony. *J. Appl. Phys.* 89 (2001) 5243-5275.

- [118] H. Li, M. Eddaoudi, M. O'Keeffe et al. *Nature* 402 (1999) 276-279.
- [119] A.B. Panda, G. Glaspell, M.S. El-Shall. *J. Am. Chem. Soc.* 128 (2006) 2790-2791.
- [120] R. Zhai, S. Wang, H. Xu et al. *Mater. Lett.* 59 (2005) 1497-1501.
- [121] Y.C. Choi, D.J. Bae, Y.H. Lee et al. *Synthetic Metals* 108 (2000) 159–163.
- [122] C.O. Kappe, D. Dallinger. *Nature Rev. Drug Disc.* 5 (2006) 51-63.
- [123] M. Hajek, M. Radoiu. *J. Mol. Catal.* 160 (2000) 383-392.
- [124] B. Lipshutz, B. Frieman. *Tetrahedron* 60 (2004) 1309-1316.
- [125] A. Dubey, B. Mishra, D. Sachdev, et al. *React. Kinet. Catal. Lett.* 93 (2008) 149-155.
- [126] S. Fozooni, A. Tikdari. *Catal. Lett.* 120 (2008) 303-306.
- [127] Z. Chemat-Djenni, B. Hamada, F. Chemat. *Molecules* 12 (2007) 1399-1409.
- [128] T. Lai, C. Lee, K. Wu, et al. *Appl. Catal. B:* 78 (2008) 151–157.
- [129] T. Lai, C. Lee, G. Huang, et al. *Appl. Catal. B:* 78 (2008) 151–157.
- [130] J. Thiebaut, G. Roussy, M.S. Medjram, et al. *Catal. Lett.* 21 (1993) 133-138.
- [131] G. Roussy, S. Hilaire, J.M. Thiebaut, et al. *Appl. Catal. A: Gen.* 156 (1997) 167-180.
- [132] Y. Zhenming, Z. Jinsong, C. Xiaoming, et al. *Appl. Catal. B: Environ.* 34 (2001) 129–135.
- [133] J. Ma, M. Fang, P. Li, et al. *Appl. Catal. A: Gen.* 159 (1997) 211-228.
- [134] G. Bond, R. Moyes, D. Whan. *Catal. Today* 17 (1993) 427–437.
- [135] G. Roussy, E. Marchal, J. Thiebaut, et al. *Fuel Process. Technol.* 50 (1997) 261–274.
- [136] C. Chen, P. Hong, S. Dai, et al. *React. Kinet. Catal. Lett.* 61 (1997) 175-180.
- [137] R.H. Nibbelke, J. Scheerova, M. Decroon, et al. *J. Catal.* 156 (1995) 106-119.
- [138] L.M. Ioffe, T. Lopez, Y.G. Borodko, et al. *J. Mol. Catal. A: Chem.* 98 (1995) 25-34.
- [139] H. Will, P. Scholz, B. Ondruschka, et al. *Chem. Ing. Technol.* 74 (2002) 1057-1067.
- [140] H. Will, P. Scholz, B. Ondruschka, et al. *Chem. Ing. Technol.* 74 (2002) 1258-1262.
- [141] H. Will, P. Scholz, B. Ondruschka, et al. *Chem. Ing. Technol.* 26 (2003) 1146-1149.
- [142] F. Basile, P. Benito, G. Fornasari, et al. *Stud. Surf. Sci. Catal.* 162 (2006) 761-768.
- [143] A. Dominguez, Y. Fernandez, B. Fidalgo, et al. *Energy Fuels* 21 (2007) 2066-2071.
- [144] W. Perry, J. Katz, D. Rees, et al. *J. Catal.* 171 (1997) 431–438.
- [145] M.M. Schubert, M.J. Kahlich, H.A. Gasteiger, et al. *J. Power Sour.* 84 (1999) 175-182.
- [146] M.A. Bollinger, M.A. Vannice. *Appl. Catal. B: Environ.* 8 (1996) 417-443.
- [147] M.J. Kahlich, H.A. Gasteiger, R.J. Behm. *J. Catal.* 182 (1999) 430-440.
- [148] I. Silverwood, G. McDougall, A. Whittaker. *Phys. Chem. Chem. Phys.* 8 (2006) 5412-5416
- [149] J.K.S. Wan. *Res. Chem. Intermed.* 19 (1993) 147–158.
- [150] S. Ringler, P. Girard, G. Maire, et al. *Appl. Catal. B: Environ.* 20 (1999) 219–233.

- [151] J. Tang, T. Zhang, D. Liang, et al. *Appl. Catal. B: Environ.* 36 (2002) 1–7.
- [152] J. Tang, T. Zhang, L. Ma, et al. *Catal. Lett.* 73 (2001) 193-197.
- [153] Z. Wei, Z. Dub, Z. Lin, et al. *Energy* 32 (2007) 1455–1459.
- [154] Z. Wei, Z. Lin, H. Niu, et al. *J. Hazard. Mater.* (2008) in press.
- [155] R. Pisani, D.K. de Moraes. *J. Hazard Mater.* 109 (2004) 183-189.
- [156] K.T. Lee, S. Bhatia, A.R. Mohamed. *Chem. Eng. Sci.* 60 (2005) 3419-3423.
- [157] W.Z. Khan, B.M. Gibbs. *Environ. Int.* 23 (1997) 227-236.
- [158] S.J. Wu, N. Sumie, C.L. Su et al. *Ind. Eng. Chem. Res.* 41 (2002) 1352-1356.
- [159] X. Wang, A. Wang, N. Li, et al. *Catal. Lett.* 1-2 (2006) 109-113.
- [160] M. Turner, R. Laurence, K. Yngvesson, et al. *Catal. Lett.* 71(2001) 133–138.
- [161] J. Tang, T. Zhang, L. Ma, et al. *J. Catal.* 211 (2002) 560–564.
- [162] C. Cha, S. Wallace, A. George, et al. *J. Environ. Eng.* 130 (2004) 338–348.
- [163] H. Takashima, L. Ren, Y. Kanno. *Catal. Commun.* 5 (2004) 317–319.
- [164] I. Hartmann, H. Mäurer, S. Morkwa, et al. *Chem. Ing. Tech.* 77 (2005) 1609-1617.
- [165] I. Hartmann, W. Einicke. *Chem. Ing. Tech.* 79 (2007) 1205-1209.
- [166] T. Krech, C.Moser, R. Emmerich, et al. *Chem. Eng. Technol.* 31 (2008) 1000-1006.
- [167] C. Möser. Final thesis for MSc. degree, Jena, Germany, 2006.
- [168] T. Krech. Final thesis for MSc. degree, Jena, Germany, 2007.

Chapter 3. Experimental methods

"We have to learn again that science without contact with experiments is an enterprise which is likely to go completely astray into imaginary conjecture."

Hannes Alfvén

3.1 Materials

Multi-walled carbon nanotubes (MWCNTs) for the present investigations were received commercially from Bayer Technology Services Ltd. (Germany). As reported by manufacturer, MWCNTs with a high degree of purity (low concentration of free residual catalyst and absence of free amorphous carbon) were produced in a high-yield process based on catalytic chemical vapour deposition. The main properties of MWCNTs are presented in Tab. 3.1.

Table 3.1

The properties of MWCNTs

Property	Value
C-purity	>95%
Number of walls	3-15
Outer mean diameter	13-16 nm
Inner mean diameter	4 nm
Length	1-10 μm
Apparent density	150-350 kg/m^3

The following chemicals were purchased from Sigma-Aldrich Inc.: iron (III) nitrate nonahydrate $\text{Fe}_2(\text{NO}_3)_3 \cdot 9\text{H}_2\text{O}$, purity >99%; iron (II, III) oxide (magnetite nanopowder), purity >98%; iron (II, III) oxide <5 micron, purity >98%; vanadium (V) oxide, purity 98+%; zirconium (IV) oxide < 5micron, purity >99%; cerium (IV) oxide, purity >99%; potassium carbonate, purity 98+%; ferric acetylacetonate, purity >97%; nitric acid, purity min. 69%. The nitrogen (5.0; UN1066) was supplied in the gas cylinder by Linde AG. Ethylbenzene (purity >99%) and glycerin (purity >98%) was purchased from VEB Jenapharm, Labor Chemie Apolda and Fluka respectively. Titanium (IV) oxide with purity of >99% was purchased from Merck KGaA.

3.2 Catalyst preparation

The catalysts used in this study were prepared as follows by impregnation method, by simple mechanical mixing and by treatment with various oxidizing agents.

Fe₂O₃-K₂CO₃-based powder catalysts

The composition and abbreviation of Fe₂O₃-K₂CO₃-based powder catalysts is presented in the Tab. 3.2. The catalysts were prepared as follows: the mixture of solid components was mixed with distilled water for 1 h; the obtained wet paste was replaced in the crucible and dried for 4 h at 120 °C. Then the catalyst was calcinated in the furnace for 1 h at 750 °C on air and cooled at the room temperature. The same method was used for the preparation of V₂O₅-based powder catalysts, which composition is presented also in the Tab. 3.2.

Table 3.2

Compositions and abbreviations of powder catalysts prepared by the simple mixings

Catalyst	Composition (wt.%)							
	Fe ₂ O ₃	Cr ₂ O ₃	K ₂ CO ₃	TiO ₂	CeO ₂	V ₂ O ₅	MnO ₂	ZrO ₂
CAT1	75	3	10	6	6	-	-	-
CAT2	55	-	5	-	-	-	20	20
CAT3	75	-	5	-	-	-	20	-
CAT4	-	-	-	-	-	50	25	25
CAT5	-	-	-	-	-	75	12.5	12.5

Iron oxide loaded carbon nanotubes

The modification of MWCNTs with iron oxide nanoparticles is specified. Initially, MWCNTs were preheated in a stream of air in the muffle furnace at 400 °C for 2 h in order to remove undesirable impurities and the rest of free residual catalyst. An iron solution concentration of 20.9 mg/ml was obtained by dissolving 15.2 g of iron (III) nitrate nonahydrate in 100 ml of deionised water. Deposition of iron oxide nanoparticles onto the surface of MWCNTs was performed by the incipient wetness impregnation using iron nitrate solution of appropriate amount to obtain the desired loading of promoter. During the impregnation the black solution was heated up to 80 °C and stirred continuously in the glassware until the liquid was totally evaporated. After further drying at 110 °C for 12 h the

samples were calcined at 500 °C for 4 h in the presence of air to get the catalysts. The temperature of 500 °C was taken as optimal for thermal decomposition of iron nitrate nonahydrate to the iron (III) oxide [1-2]. The catalysts with theoretical Fe₂O₃ nanoparticles content 3, 6 and 9 wt.% were successfully obtained and are abbreviated in the text as CNT3, CNT6, and CNT9, respectively.

Magnetite/Hematite nanomixture

The magnetite/hematite catalyst was obtained by the simple mixing of corresponding nanopowders. The nanopowder of hematite was prepared by polyol method [3]. During the preparation procedure the iron acetylacetonate (19.05 g) was dissolved in 150 ml of ethylene glycol; and then stirred for 2 h at 130 °C. Added nitric acid (3 ml) changed the colour of solution immediately from red to black brown. The obtained solution was stirred at 200 °C overnight. Next day the residue of the solvent was evaporated at 230 °C. Finally, the sample was dried in the drying oven for 4 h at 180 °C.

Functionalized MWCNTs

The functionalization of MWCNTs using nitrogen stream containing 5% of oxygen was carried out in conventionally heated and microwave assisted reactors for 10 h at 400 °C.

In a typical HNO₃ oxidation [4], MWCNTs (5 g) were added to HNO₃ (6 M) and mixed for 24 h at 80 °C. MWCNTs were filtered and washed with distilled water until the filtrate was neutral. The resulting MWCNTs were dried under normal condition at 110 °C overnight.

3.3 Experimental procedures

The experimental set-up is shown schematically in Fig. 3.1. The catalytic activity measurements for the conventionally-heated ODEB were performed in a fixed-bed quartz-tube reactor with inner diameter of 20 mm and 330 mm length. The catalyst was fixed with a quartz wool plug, to escape any possibility removal by gas stream. The typical loading of catalyst sample was 1.0 g. A flow of nitrogen was used for evaporation of the liquid ethylbenzene at

25 °C (ethylbenzene partial pressure 1350 Pa). The flow rates of nitrogen and air were controlled by mass flow controllers so that the ethylbenzene concentration of 2.5 vol.% and an ethylbenzene/oxygen volume ratio of 1:1 in accordance to the reactor pressure were obtained. The actual reaction temperature was determined by inserting a thermocouple into the catalyst bed. The gas composition at inlet and outlet of reactor were analyzed by gas chromatography method. Gas chromatography is a type of chromatography (firstly dates to 1903 in the work of the Russian scientist, Mikhail Semenovich Tswett) in which the mobile phase is a carrier gas, usually an inert gas such as helium or a nonreactive gas such as nitrogen, and the stationary phase is a microscopic layer of liquid or polymer on an inert solid support, inside glass or metal tubing, called a column. Gas Chromatography is different from other forms of chromatography (High pressure liquid chromatography, thin layer chromatography, etc.) because the solutions travel through the column in a gas state. The interactions of these gaseous analytes with the walls of the column (coated by different stationary phases) causes different compounds to elute at different times called retention time. The comparison of these retention times is the analytical power of gas chromatography [6]. The instrument used to perform gas chromatographic separations in the present work is on-line gas chromatograph (Hewlett Packard G1800D) equipped with a Plot Fused Silica column (0.32 mm i.d., 25 m length) and electron-impact ionization detector.

The performance of catalysts was evaluated by means of the ethylbenzene conversion, the styrene selectivity and the styrene yield:

$$\text{ethylbenzene conversion: } X = \frac{F_{EB_i} - F_{EB_o}}{F_{EB_i}},$$

$$\text{styrene selectivity: } S_{ST} = \frac{F_{ST}}{F_{EB_i} - F_{EB_o}},$$

$$\text{styrene yield: } R_{ST} = F_{ST} / F_{EB_i},$$

$$\text{space velocity: } V_{sp} = \frac{\dot{V}}{V_{cat}}$$

where F = molar flow rate, ST = styrene, EB_i = inlet ethylbenzene, EB_o = outlet ethylbenzene, V_{sp} = space velocity (h^{-1}), \dot{V} = gas flow rate (l/h) und V_{cat} = catalyst volumen (l).

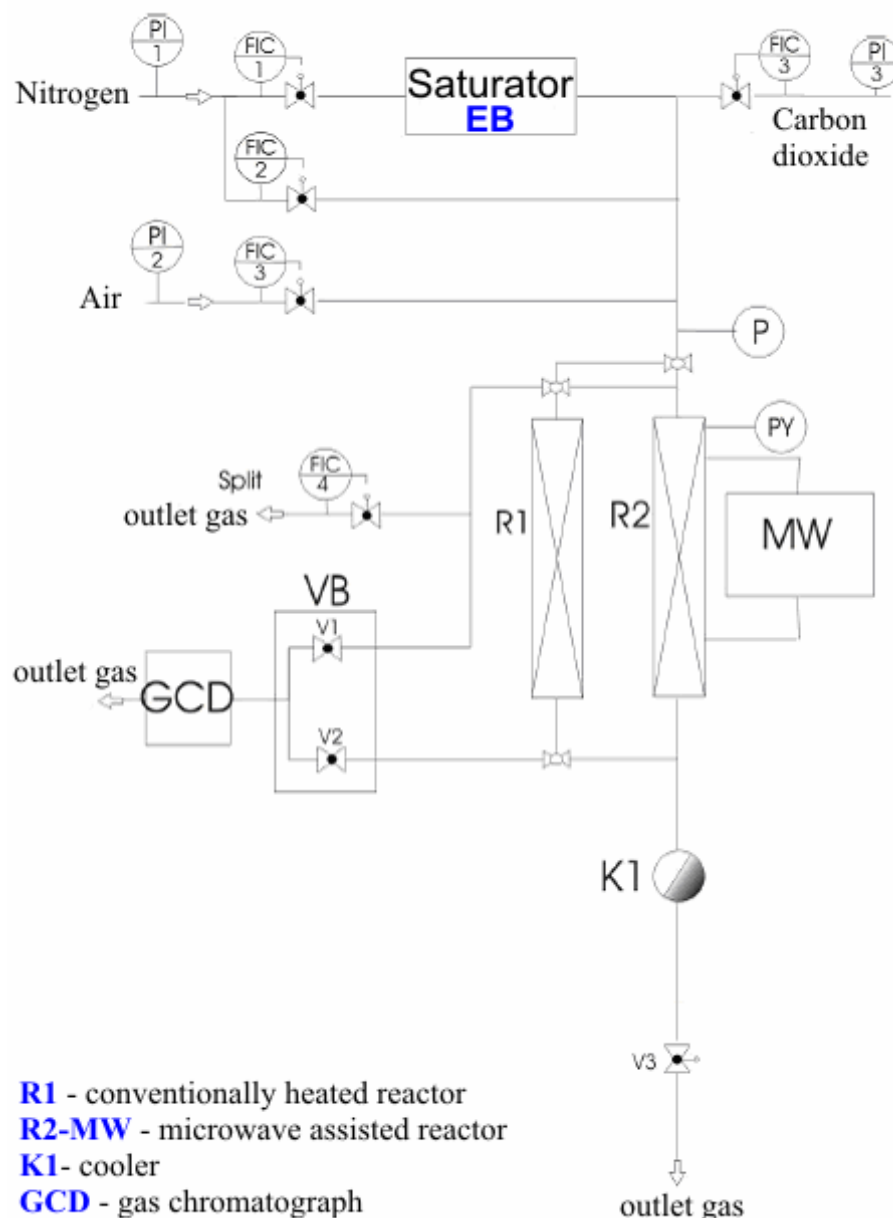


Figure 3.1. Scheme of the experimental set-up.

Investigation of the catalytic activity of the prepared composites under microwave irradiation was performed at the same reaction conditions as in the conventionally-heated reactor in order to obtain comparable results. Indeed, two different types of microwave oven were used. During the performance of ODEB with MWCNTs/Fe₂O₃ and Magnetite/Hematite catalytic systems the quartz-tube fixed-bed reactor (20 mm i.d., 610 mm length) with catalyst (1.0 g) was inserted into the multimode microwave oven (Panasonic NE – 1846). Microwave energy input was controlled by switched-mode power supply from 40 to 1800 W. On the back-side of the oven an integrated pyrometer was directed straight against the catalyst location in the reactor, and its readings were used by the software to control the microwave oven input power thereby maintaining a constant reaction temperature. Because a regular

thermocouple is sensitive to microwave irradiation its continuous presence in the reactor is prohibited. Therefore, the inner temperature was measured by a rapid insertion of thermocouple through the special quartz capillary onto a catalyst at the moment, when microwave irradiation was shortly interrupted, as described in detail by Will et al. [5]. The same method of the temperature measurements was used during the long term stability tests of functionalized MWCNTs in the microwave oven MLS-Ethos 1600 with switched-mode power supply from 10 to 1000 W. Finally, it should be noted, that all tests were repeated at least three times to improve the accuracy of the measured data.

3.4 Characterization of catalysts

The BET specific surface area S_{BET} and pore volume of the prepared composites were determined from the adsorption and desorption isotherms of nitrogen using a Quantachrome Autosorb-1 apparatus.

X-ray diffraction (XRD) experiments were performed on a Siemens DS000 diffractometer with $\text{Cu K}\alpha$ radiation using a Ni filter to identify the crystalline phases of the fresh and the catalysts spent in catalytic runs.

The particle size, morphology and distribution of iron (III) oxide on the MWCNTs were studied before and after ODEB by transmission electron microscopy (TEM) using a LEO922 operating at 200 keV. The instrument is equipped with an in-column Omega energy filter and an energy dispersive X-ray (EDX) detector. All TEM images were zero-loss filtered.

The amount of reactive groups on the surfaces of functionalized MWCNTs before and after ODEB was characterized by means of XPS using an ESCA Microprobe spectrometer with XPS Microscope at room temperature.

References

- [1] K. Wieczorek-Ciurowa, A.J. Kozak. *J. Therm. Anal. Calor.* 58 (1999) 647-651.
- [2] L. Hannevold, O. Nilsen, A. Kjekshus, et al. *Appl. Catal. A* 284 (2005) 177-184.
- [3] U. Zavyalova, B. Nigrovski, K. Pollok, et al. *Appl. Catal. B: Environ.* 83 (2008) 221–228.
- [4] A. Rasheed, J.Y. Howe, M.D. Dadmun, et al. *Carbon* 45 (2007) 1072-1080.
- [5] H. Will, P. Scholz, B. Ondruschka. *Top. Catal.* 29 (2004) 175-182.
- [6] Wikipedia: http://en.wikipedia.org/wiki/Gas-liquid_chromatography (12.09.2008).

Chapter 4. Results and discussion

4.1. ODEB with industrial used catalysts and mild oxidant CO₂

The goal of each catalytic reaction study is to enhance the rates of reaction through improvement of already existed catalytic systems, reaction parameters as well as to achieve detailed knowledge about the various processes taking place inside the reactor and on the catalyst surface during the reaction. As it was noted before, the reaction investigated in this work is dehydrogenation of ethylbenzene. Being one of the most important industrial processes, this reaction attracts an interest of thousand research groups all over the world. The main problems encountered in ethylbenzene dehydrogenation are the high endothermicity of the reaction, high steam-to-hydrocarbon ratios and irreversible deactivation of the catalyst. Therefore, the techniques such as oxidative dehydrogenation and the employment of alternative heating sources have been proposed to give a solution to above described problems. The scrupulous analysis of the literature made possible to choose for our investigations the catalytic systems which could exhibit the highest ethylbenzene conversion and styrene selectivity in ODEB [1-5]. Particularly, the reaction was performed over Fe₂O₃-K₂CO₃-based CAT1, CAT2 and CAT3 in the presence of oxygen and over V₂O₅-based CAT4 and CAT5 with carbon dioxide as soft oxidant.

4.1.1. ODEB over Fe₂O₃-K₂CO₃-based and V₂O₅-based powder catalysts

Potassium promoted iron oxide catalyst is known to be favourable in the synthesis of styrene. However, magnesium, zirconium and chromium oxides were added to the Fe₂O₃-K₂CO₃ system in order to improve the activity and stability of the catalyst [1-3]. Fig. 4.1 shows the effect of temperature on the ethylbenzene conversion and styrene selectivity over CAT1, CAT2 and CAT3. It seems to be that all prepared catalysts exhibited the similar catalytic activity, whereas the highest selectivity of 82% was obtained on CAT3, which is promoted with manganese oxide, and the lowest selectivity of 62% was achieved on MnO₂ and ZrO₂ promoted CAT2. The increase in temperature favours the reaction. However, in the present system, the styrene selectivity decreased with increasing of the reaction temperature because of the increased rate of side reactions like formation of toluene and benzene as well as total oxidation.

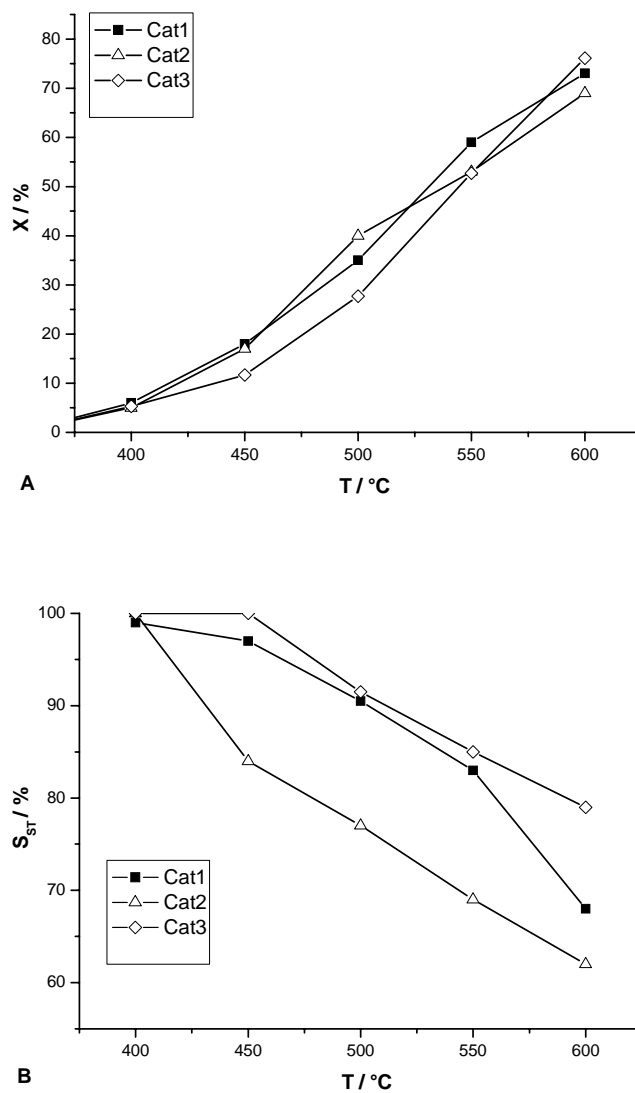


Figure 4.1. Effect of reaction temperature in ODEB over CAT1, CAT2 and CAT3 catalysts.

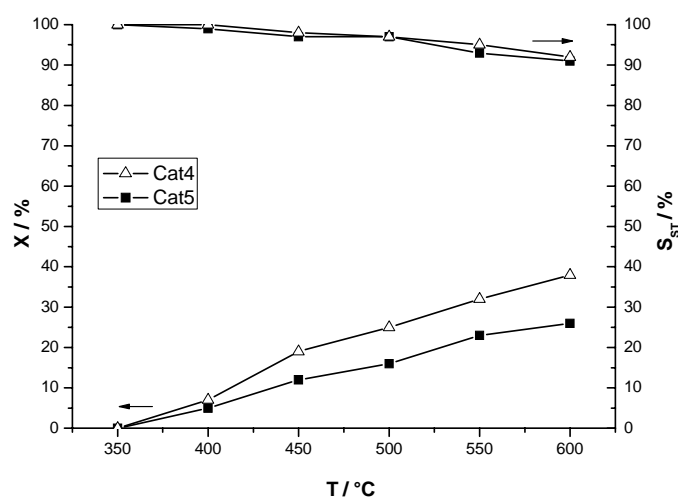


Figure 4.2. Effect of reaction temperature in ODEB in the presence of carbon dioxide over CAT4 and CAT5.

Carbon dioxide could also be used as an oxygen source or oxidant and can be considered as a non-traditional mild oxidant and oxygen transfer agent [4-5]. ODEB with CO₂ could be effective in respect of utilization of CO₂ resource, which is a main contributor to the greenhouse effect. However, the Fe₂O₃-K₂CO₃-based catalysts do not work effectively in the presence of CO₂, because even small amount of carbon dioxide inhibits the activity of commercial potassium-promoted iron oxide catalyst. V-containing catalysts are known to be rather active and selective in mild oxidation reactions, such as partial oxidation, oxidative dehydrogenation, and ammoxidation of hydrocarbons [5-9]. Thus, V₂O₅-based catalytic systems were chosen for the investigation of ODEB with carbon dioxide as a mild oxidant. Fig. 4.2 presents the effect of temperature on the performance of V₂O₅-based catalysts on ODEB with CO₂. With an increase of the reaction temperature from 350 to 600 °C, styrene selectivity decreased slightly from 100% at initial temperature to 90% at final temperature over both catalysts, whereas ethylbenzene conversion increased from 0% at 350 °C to 26 and 40% at 600 °C over CAT4 and CAT5 respectively. For all reactions, styrene is predominantly observed together with unconverted ethylbenzene. Only insignificant amounts of benzene and toluene are obtained as by-products.

Before the catalytic experiments in the microwave field were started the effect of microwave irradiation on the temperature of Fe₂O₃-K₂CO₃- and V₂O₅-based powder catalysts was investigated and the results are summarized in Tab. 3.1. All samples were radiated for minutes by microwave power input of 1800 W. However, the results obtained were not convincing, and the highest temperature of 260 °C was obtained over V₂O₅-based CAT4, which seems to be too low for the performance of ODEB. MWCNTs, which are expected to have remarkable microwave absorbing characteristics due to their dielectric structure [10], were also tested in the microwave field and the temperature of 440 °C was achieved after 5 minutes of irradiation by microwave power input of only 90 W. Particularly, MWCNTs, belonging to the one of the most promising class of the non-planar sp²-nanocarbon systems, are expected to be a good catalyst itself or catalyst support for ODEB due to its high mechanical strength, uniform nano-structure, electrical properties, ideal porous structure and thermal stability as well as stability against oxidation.

Table 4.1.

Effect of microwave irradiation on the temperature of powder catalysts.

Material	Power W	Time of radiation min	Temperature effect °C	
			Thermometer	Pyrometer
CAT1	1800	15	198	172
CAT2		15	201	170
CAT3		15	162	145
CAT4		15	262	235
CAT5		15	232	180
MWCNTs	90	5	440	235

4.1.2. Upshot

The catalytic activity of Fe₂O₃-K₂CO₃-based powder catalysts in ODEB was investigated. The highest ethylbenzene conversion and styrene selectivity were found for MnO₂ promoted CAT3 at the reaction temperature of 600 °C. During ODEB in the presence of carbon dioxide high styrene selectivity was obtained on V₂O₅-based powder catalysts; however, the ethylbenzene conversion seems to be too low even at the temperature of 600 °C. All powder catalysts exhibited low microwave absorbability, whereas the temperature of 440 °C was achieved during microwave treatment of MWCNTs for 5 minutes by microwave power input of only 90 W. Moreover, there was not found any literature report on the application of microwave dielectric heating in heterogeneous gas-phase catalysis with MWCNT. Hence, the investigation of MWCNTs as catalyst and catalyst support in microwave-assisted ODEB has to be the main item of present research.

4.2. ODEB over iron oxide loaded carbon nanotubes

Most developments in ethylbenzene and styrene technologies in recent years have centered on process optimization, catalyst upgrades and equipment improvements that have led the way for large- scale capacities and enhanced project economics. A decade ago, typical capacities for single-train grassroots ethylbenzene/styrene plants averaged 200,000 metric tons per year. Today, unit capacities greater than 700,000 metric tons per year are being considered and built. The thousand tons of catalyst are necessary to make this industrial process more productive, cheaper and less energy consumptive. However, due to deactivation problems of the catalyst used currently in industry, resource depletion as well as the appreciation of energy costs, the exploration of new catalytic materials and compositions in conjunction with application of alternative heating resources is the main item of many scientists all over the world as well as the topic of the present work.

4.2.1 Characterization of the nanocomposites before the reaction

The pore volume and surface area of the prepared composites are summarized in Tab. 4.2. According to the obtained results, the addition of iron oxide resulted in an increase of the catalyst S_{BET} . Modification of the MWCNTs by 3 wt.% of iron oxide leads to the S_{BET} being 13% higher than that for the unpromoted carbon. However, further increase of the promoter content from 3 to 9 wt.% resulted only in a small increase of S_{BET} . However, a slight decrease of total pore volume (V_{total}) was observed for the Fe_2O_3 supported on MWCNTs catalysts, concluding that all promoted MWCNTs were approximated to have the same size of deposited iron oxide nanoparticles.

Table 4.2

Effect of the iron oxide loading on the pore volume and surface area of the prepared composites.

Sample	Loading amount (wt.%)	V_{total} (cm ³ /g) ±0,04	S_{BET} (m ² /g) ±0,08
CNTs	-	2.599	284.5
CNT3	3	2.244	321.7
CNT6	6	2.153	337.9
CNT9	9	2.164	339.1

TEM and high resolution TEM (HRTEM) images of the unpromoted MWCNTs are shown in Fig. 4.3. The MWCNTs consist of a hollow inner cavity (light region) and graphene sheets as outer walls (dark region) with an outer mean diameter of 13-16 nm. The length of the nanotubes is up to several microns and they form interlocked clusters. It could be seen in the Fig. 4.3A, that the inner and outer parts of MWCNTs are distinguishable by different grey scales. However, the inner diameter of MWCNTs (approximately 4 nm) was measured with the nanotubes oriented parallel to the beam, which spherical shape with a hollow inner cavity could be clear observed in Fig. 4.3B. The walls of the nanotubes are formed by graphene sheets.

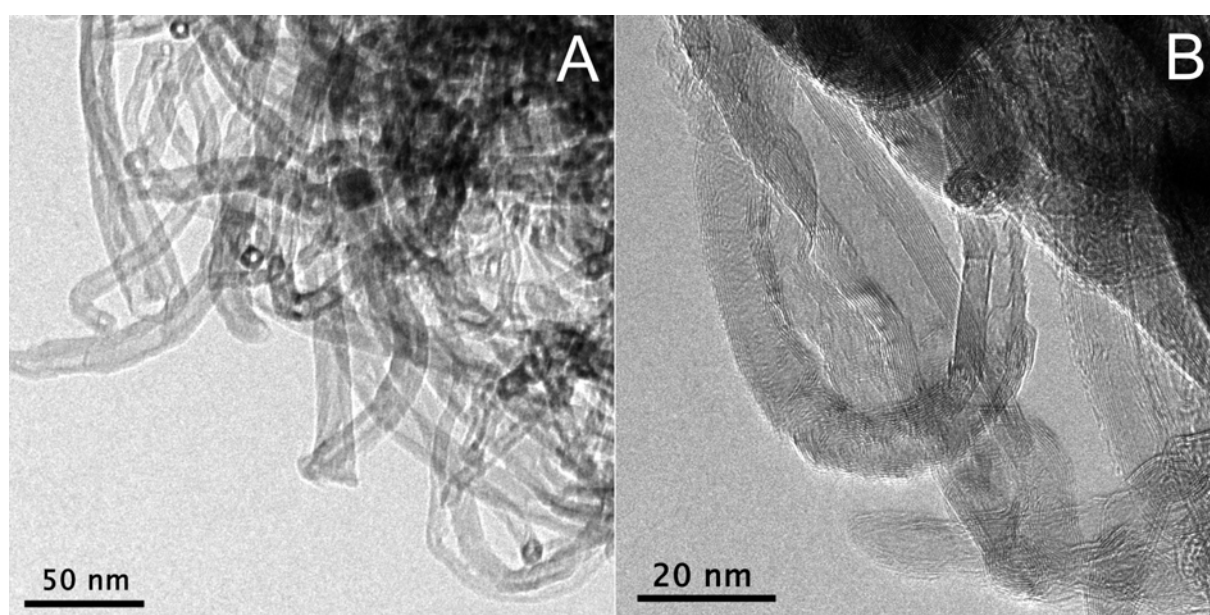


Figure 4.3. (A) TEM and (B) HRTEM images of unpromoted MWCNTs before the reaction.

TEM images of the fresh Fe_2O_3 modified MWCNTs (Fig. 4.4A) shows that iron oxide nanoparticles are randomly adhered on the outer surface of the MWCNTs. Under high resolution (Fig. 4.4B) the iron oxide nanoparticles are confirmed to be crystalline with a particle size of about 10 nm. Most Fe_2O_3 nanocrystals have an almost isometrical morphology; however, some seem to develop flat crystal faces. Selected area electron diffraction (SAED) shows that the iron oxide particles are hematite.

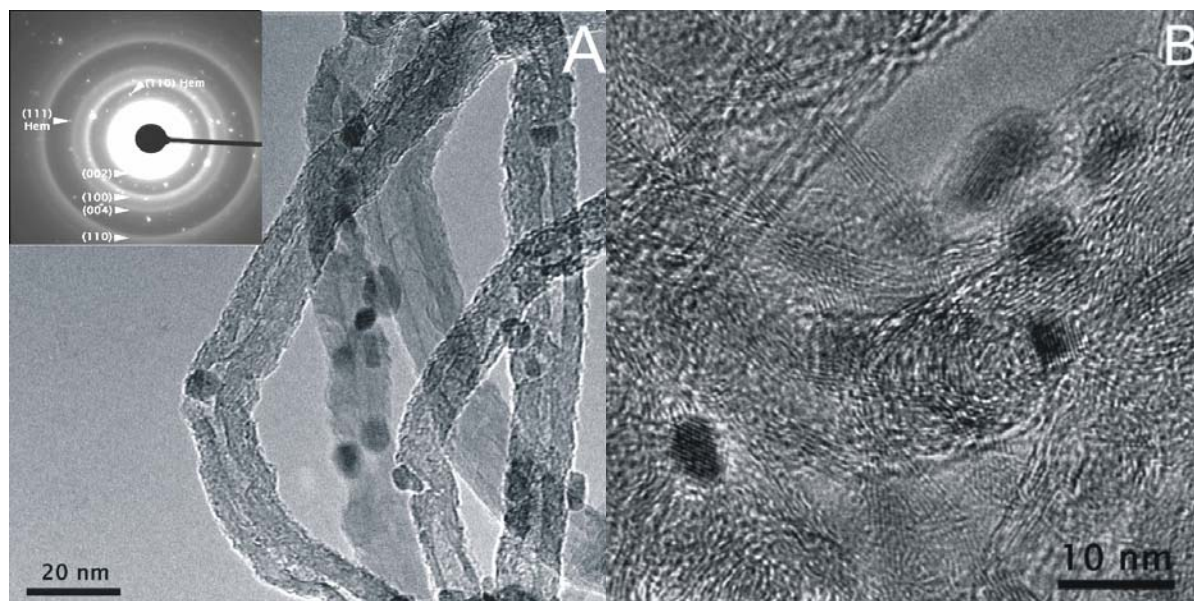


Figure 4.4. TEM micrographs of fresh Fe_2O_3 decorated MWCNTs. **a)** The nanoparticle adhere to the outer surface of the nanotubes and are randomly distributed. **b)** High-resolution images. The nanocrystals are crystalline and have a grain size of less than 10 nm.

Fig. 4.5 shows the XRD patterns of pure MWCNTs and iron oxide loaded MWCNTs before ODEB. Four Bragg peaks, which are typical of sp^2 -carbon materials, could be clearly observed in the XRD pattern of pure MWCNTs (Fig. 4.5a). The XRD pattern of iron oxide loaded MWCNTs confirms the existence of iron oxide polycrystals in the probe as well as the crystal structure of MWCNTs, indicating that the deposition of Fe_2O_3 did not damage the crystallinity of MWCNTs (Fig. 4.5b). However, it should be noted that peak intensities of MWCNTs slightly decreased after decorating.

The diffraction angles at $2\theta = 35.52^\circ$, 43.52° , 53.54° and 62.64° can be assigned to (3 1 1), (4 0 0), (4 2 2), (4 4 0) crystal planes of $\gamma\text{-Fe}_2\text{O}_3$, respectively. The mean particle size of iron oxide nanoparticles calculated by Scherrer equation is about 9.5 nm, being in accordance with particle size obtained during the TEM characterization.

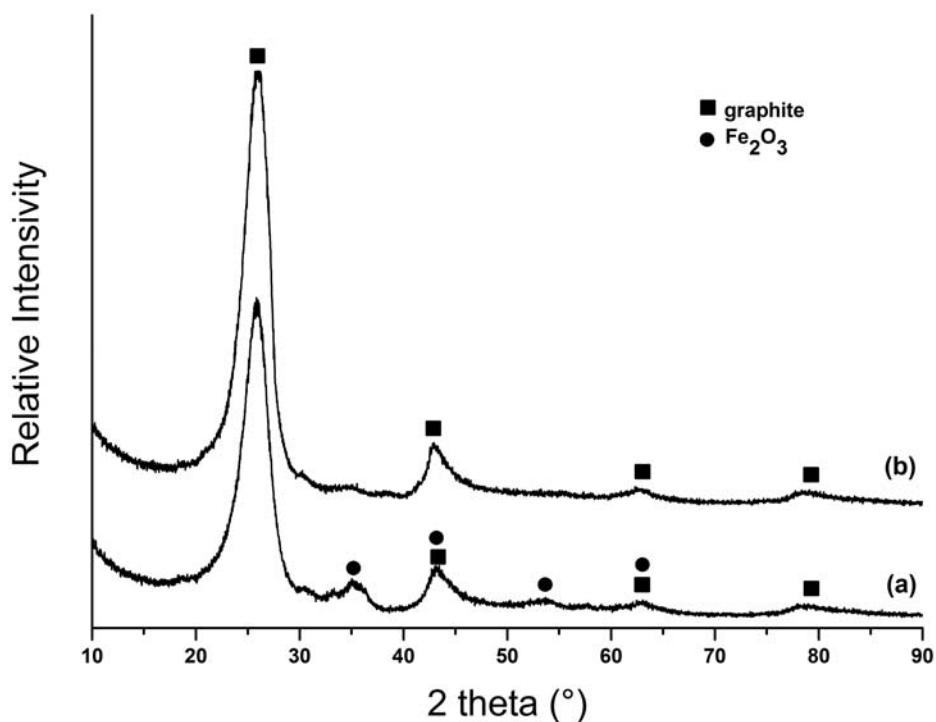


Figure 4.5. XRD pattern of (a) pure MWCNTs and (b) Fe₂O₃/MWCNTs nanocomposite before dehydrogenation.

Before the catalytic reactions were started the stability of by microwave irradiation heated MWCNTs against combustion were investigated. As reported by Su et al. [11], sp²-carbon materials displayed excellent stability in conventionally-heated ODEB in comparison to activated carbon, which high catalytic activity results showed in the beginning of dehydrogenation continuously decreased under reaction conditions due to its combustion in oxidative atmosphere and the catalyst was completely burned after 720 minutes on stream. Therefore, the series of tests including the heating of MWCNTs by various microwave input power were performed. The concentration of oxygen corresponds to that used in further catalytic reactions.

Fig. 4.6 presents the effect of microwave input power on the temperature of catalyst. It seems to be, that the necessary for dehydrogenation temperature could be achieved by the microwave input of 60W (Panasonic NE – 1846). No changes in catalyst weight were observed indicating that the microstructure of MWCNTs is stable against combustion under reaction conditions used in further tests.

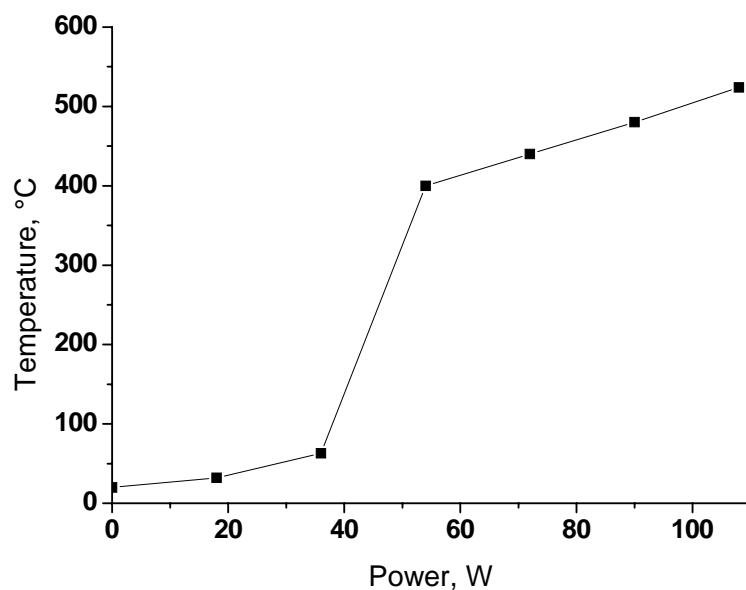


Figure 4.6. The effect of microwave power input on the temperature of catalyst bulk.

4.2.2 Catalytic tests

The catalytic performance of MWCNTs modified by iron oxide has been investigated for ODEB in an integral fixed-bed reactor conventionally-heated and under microwave-assisted conditions.

Influence of the iron oxide loading

Fig. 4.7 shows ethylbenzene conversion and styrene selectivity as a function of the iron oxide loading onto 1.0 g of the MWCNTs for both heating methods. Ethylbenzene conversion in conventionally-heated ODEB reaction was 30% for pristine MWCNTs. The ethylbenzene conversion increased with loading level of iron oxide and reached a maximum of 50% over CNT9 sample with 9 wt.% of Fe_2O_3 . The same influence of iron oxide loading on the activity of the prepared composites was observed in microwave-assisted reactions. Unpromoted MWCNTs exhibit the lowest ethylbenzene conversion of 28%, and the highest ethylbenzene conversion of 58% was obtained over CNT9. Fig. 4.7B shows that styrene selectivity decreased with increasing iron oxide loading under microwave irradiation as well as with the conventional heating method. However, the styrene selectivity over CNT6 sample was 5% lower using conventional heating and 35% lower using microwave heating than that

obtained on CNT3 sample. The lowest selectivity to styrene of 52 and 54% was observed over CNT9 sample in conventionally-heated and microwave-assisted ODEB respectively. Presumably, at the promoter loading higher than 3 wt.% the styrene selectivity decreases, because the catalyst surface becomes sufficiently acidic at this iron oxide concentration, followed by the formation of undesirable by-products [12].

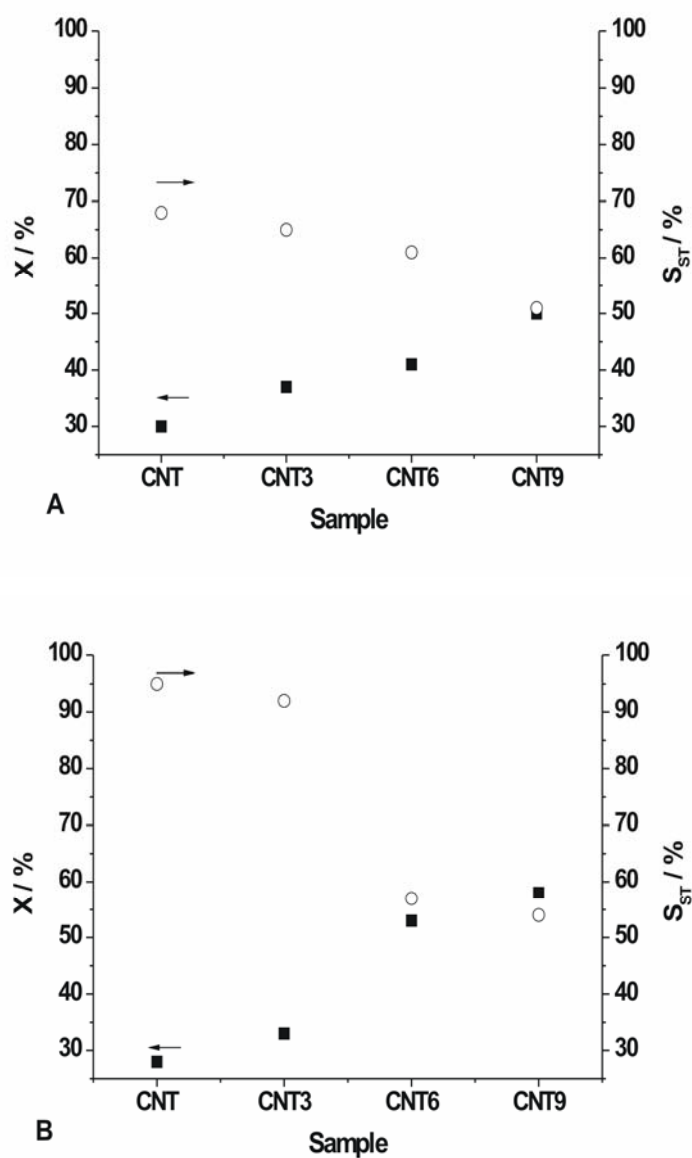


Figure 4.7. Effect of loading level of iron oxide in ODEB reaction on the ethylbenzene conversion (X) and styrene selectivity (S): in conventionally-heated (A) and microwave-assisted (B) reactors.

Effects of reaction temperature on the CNT3 performance

Influence of the reaction temperature on the CNT3 sample catalytic activity in ODEB was investigated using both microwave and conventional heating methods. Ethylbenzene conversion, styrene yield and selectivity as a function of reaction temperature in conventionally-heated reactor are shown in Fig. 4.8A. With an increase of the reaction temperature from 300 to 450 °C, ethylbenzene conversion increased monotonously, and styrene yield increased from 8 at initial temperature to 25% at final temperature, whereas styrene selectivity markedly decreased from 80% at 300 °C to 60% at 450 °C. Further rise of the reaction temperature resulted in increasing ethylbenzene conversion with larger decrease in the styrene selectivity. With an increase of the reaction temperature from 350 to 500 °C, the selectivity to CO₂ increased from 21 to 40% in conventionally-heated ODEB and from 20 to 38% in microwave-assisted reaction, indicating that the higher temperatures favour total oxidation of ethylbenzene.

Fig. 4.8B shows the effect of temperature on the catalytic activity and selectivity of CNT3 catalyst under microwave irradiation. The conversion of ethylbenzene increased monotonously in the temperature range from 300 to 450 °C and reached the efficiency of 35%, while the styrene selectivity slightly decreased from 92% at 350 °C to 86% at 450 °C. Apparently, the ethylbenzene conversion over CNT3 in the microwave-assisted reaction is similar to that under conventionally-heated condition. However, the styrene selectivity was more stable and considerably higher under microwave-assisted conditions at temperatures up to 450 °C, whereas it decreased monotonously during whole test in conventionally-heated reactor. Further temperature increase resulted in drastic decrease of CNT3 selectivity, and at 550 °C the main products were CO₂ and H₂O.

It should be noted that approximately similar ethylbenzene conversion rates were obtained at the same measured temperatures using both heating methods. This result which seems to be in contradiction with other ones published by other research groups [13-17] could be explained by the fact that, in our experimental conditions, contrary to what happens in the quoted references, there is no formation of microscopic hot spots. Zhang et al. [15-18] showed that the same conversion of methane can be achieved with microwave heating at temperatures which are about 200°C lower than those required when conventional heating was used. The effect was explained by the formation of microscopic hot-spots (so-called thermal runaways) [15], which then became the active centres for the catalytic reaction. The temperatures for these hot-spots were estimated to be 100-200°C higher than the average bulk

temperature measured in the catalyst bed. It was established, that the size of these microscopic hot-spots ranges from 150 till 1200 μm , when the average size of the prepared composites does not exceed 50 nm. It is worth to mention, in our heating experiments no difference was observed between the temperature values measured by a thermocouple or pyrometer even at the high microwave power input. Therefore, the temperature measured by the thermocouple could be related to the real temperature of every part of the catalyst material. Indeed, at temperatures higher than 450 $^{\circ}\text{C}$ the ethylbenzene conversion increased rapidly, indicating that at higher temperatures ethylbenzene was thermal oxidized. Thus, it could be concluded that the optimal temperature range for ODEB over MWCNTs modified by 3 wt.% Fe_2O_3 is 380-450 $^{\circ}\text{C}$.

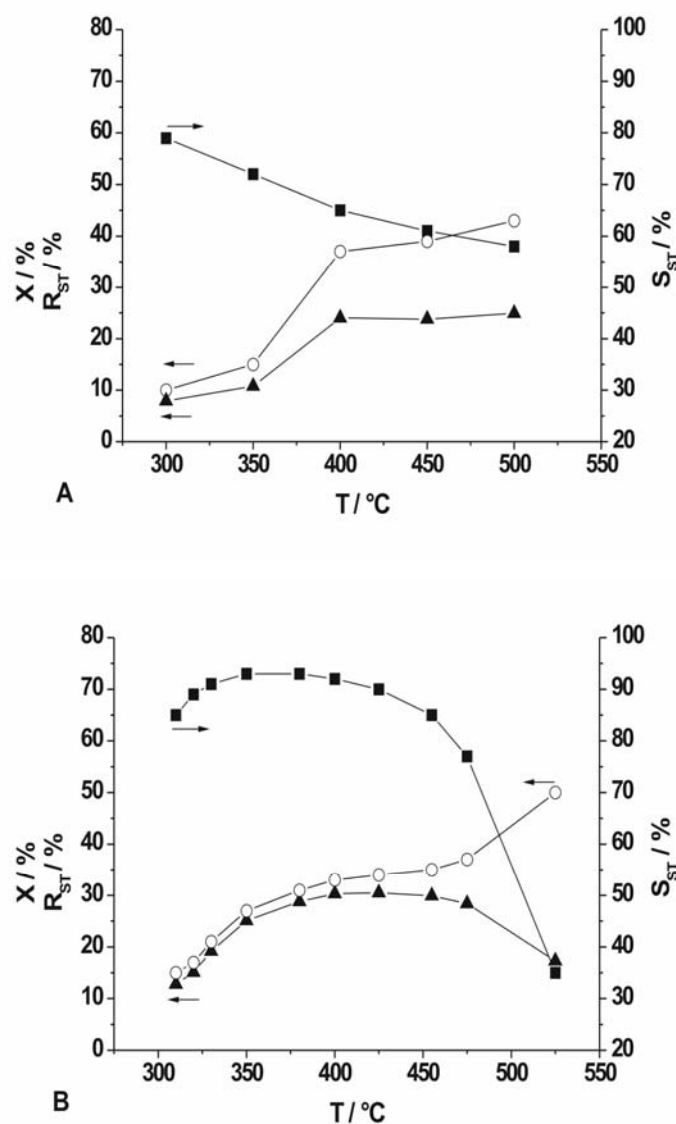


Figure 4.8. Effect of reaction temperature in ODEB over CNT3 catalyst on the ethylbenzene conversion (○), styrene yield (▲) and selectivity (■) in conventionally-heated (A) and microwave-assisted (B) reactors.

Long-term stability tests

Long-term stability tests with CNT3 sample were performed for conventional and microwave dielectric heating methods in order to investigate the influence of prolonged catalyst use on the activity and structure of catalyst. Ethylbenzene conversion and styrene selectivity rate on CNT3 catalyst at 400 °C are shown in Fig. 4.9 as a function of reaction time. As is clearly evident in Fig. 4.9, the synthesized composites displayed a high long-term stability under operating conditions in conventionally-heated reactor as well as in microwave field. Specifically, the conversion remained at 43 and 35% with a stable styrene selectivity of about 67 and 83% in conventionally-heated and microwave-assisted reactors respectively.

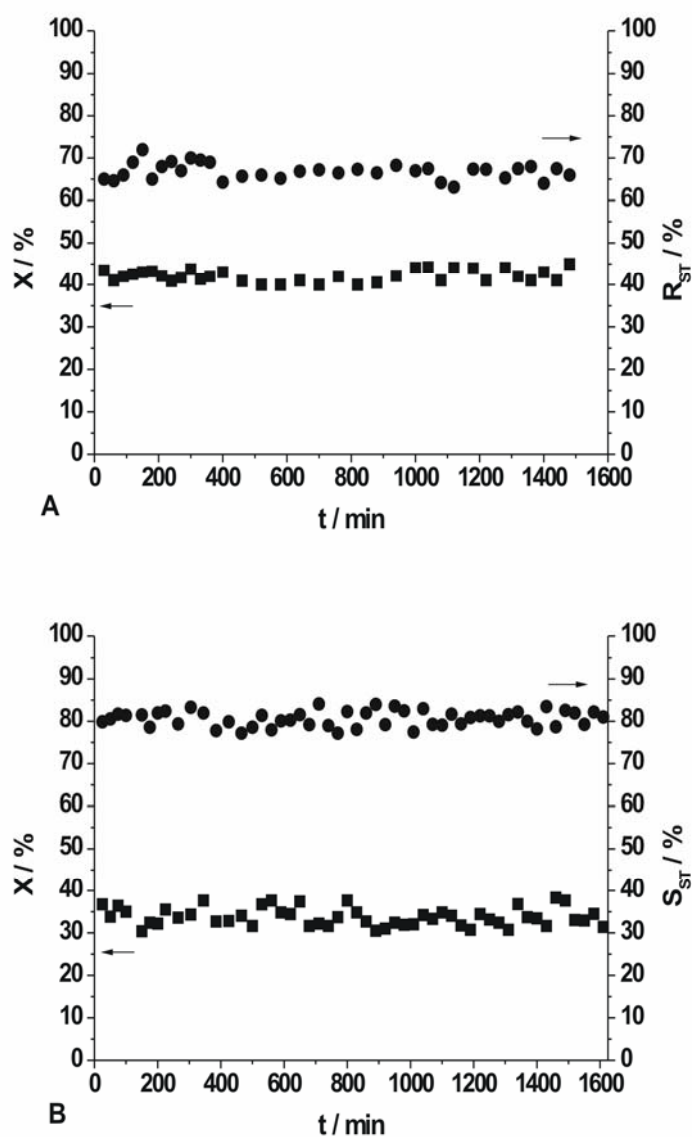


Figure 4.9. Effect of time on stream in ODEB reaction over CNT3 on the ethylbenzene conversion (X) and styrene selectivity (S) in conventionally-heated (A) and microwave-assisted (B) reactors.

4.2.3 Discussion

The results obtained during the long-term stability tests indicate that different catalytic ODEB mechanisms are at stake during conventional and microwave dielectric heating. In conventionally-heated ODEB, the higher ethylbenzene conversion and lower styrene selectivity on CNT3 catalyst could be correlated with the deposition of highly disordered carbon at the outer surface of the tubes during the reaction, as evidenced by TEM (Fig. 4.10), in comparison with TEM micrographs of fresh catalyst (Fig. 4.4), blocking C=O terminations on the basic surface of CNTs, which are proposed to be responsible for the dehydrogenating power of the catalyst [11-12, 19-21]. The surface of coke also contains C-O functionalities, generated during the reaction and plays the role of active sites for ODEB [22-26]. The stability of these active sites is considerably lower than that of basic, quinoidic carbonyl groups of sp^2 -carbon due to instability of coke in an oxidative atmosphere. Thus, the combustion of coke and building of new highly disordered carbon layers with further creation of C=O groups on the surface occur simultaneously. However, the combustion of coke occurs partially due to the low operating temperature and new layers of highly disordered carbon deposit on the surface, hindering the selectivity of catalyst.

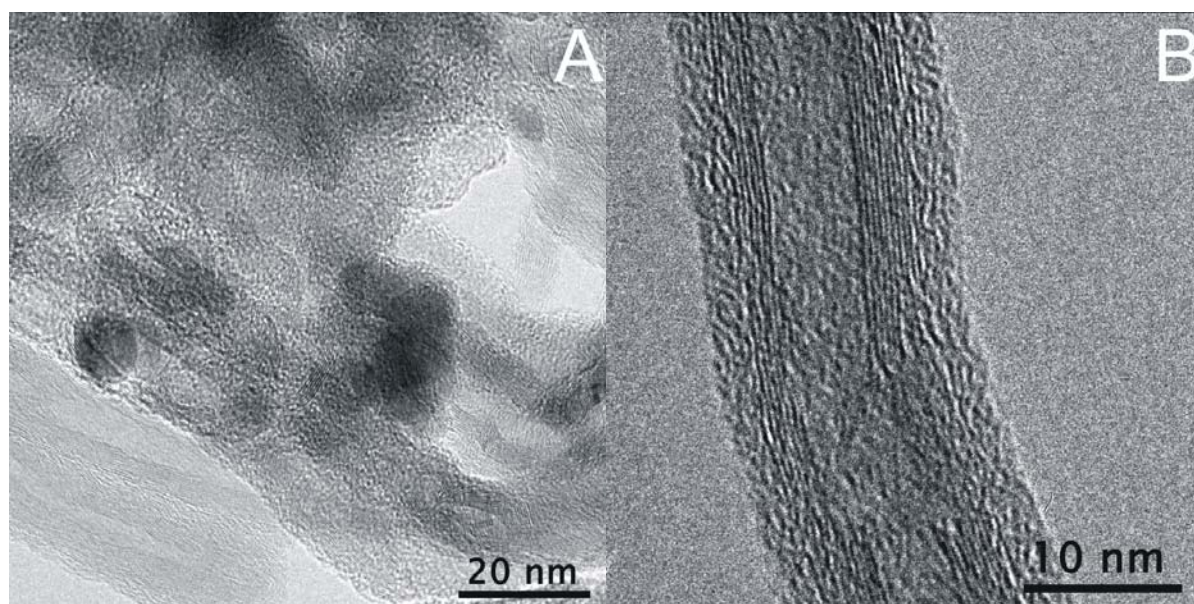


Figure 4.10. (A) TEM and (B) HRTEM images of CNT3 composite after conventionally-heated ODEB.

In contrast, during microwave dielectric heated ODEB no disordered carbon was observed on the surface of CNT3 catalyst (Fig. 4.11). Even at 400°C the coke was totally burned off, making the stable sp^2 -carbon oxygenated species accessible to the gas phase and as a consequence, increasing the selective properties of the catalyst.

As shown in Fig. 4.11, the CNT3 sample consists from unchanged MWCNTs without any deposited nanoparticles and graphite layers enclosing newborn particles instead of previously supported iron oxide. The average size of these particles ranges from 30 to 50 nm. Magnified images of newborn particles are shown in Fig. 4.12B and Fig. 4.12C. It could be observed that particles are encapsulated by carbon shell of high-ordered graphite layers, and the interlayer spacing is the same as that for the graphite (002) planes (SAED arrow in Fig. 4.11A). The EDX spectrum (Fig. 4.12) of one of this newborn particle includes only the signals of iron, carbon and copper, but no oxygen, indicating that the newborn particle is composed only of carbon and iron. Copper is detected from the used copper grid. The encapsulation occurs independently of the particle size and no iron oxide nanoparticles have been observed.

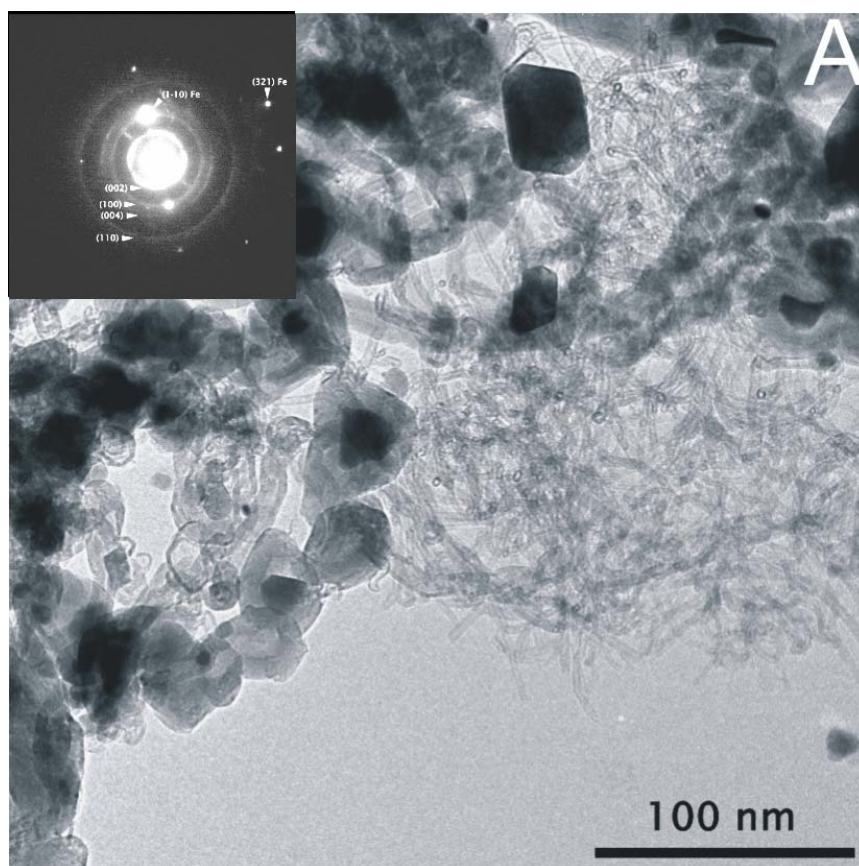


Figure 4.11. TEM image of CNT3 catalyst after microwave-assisted ODEB

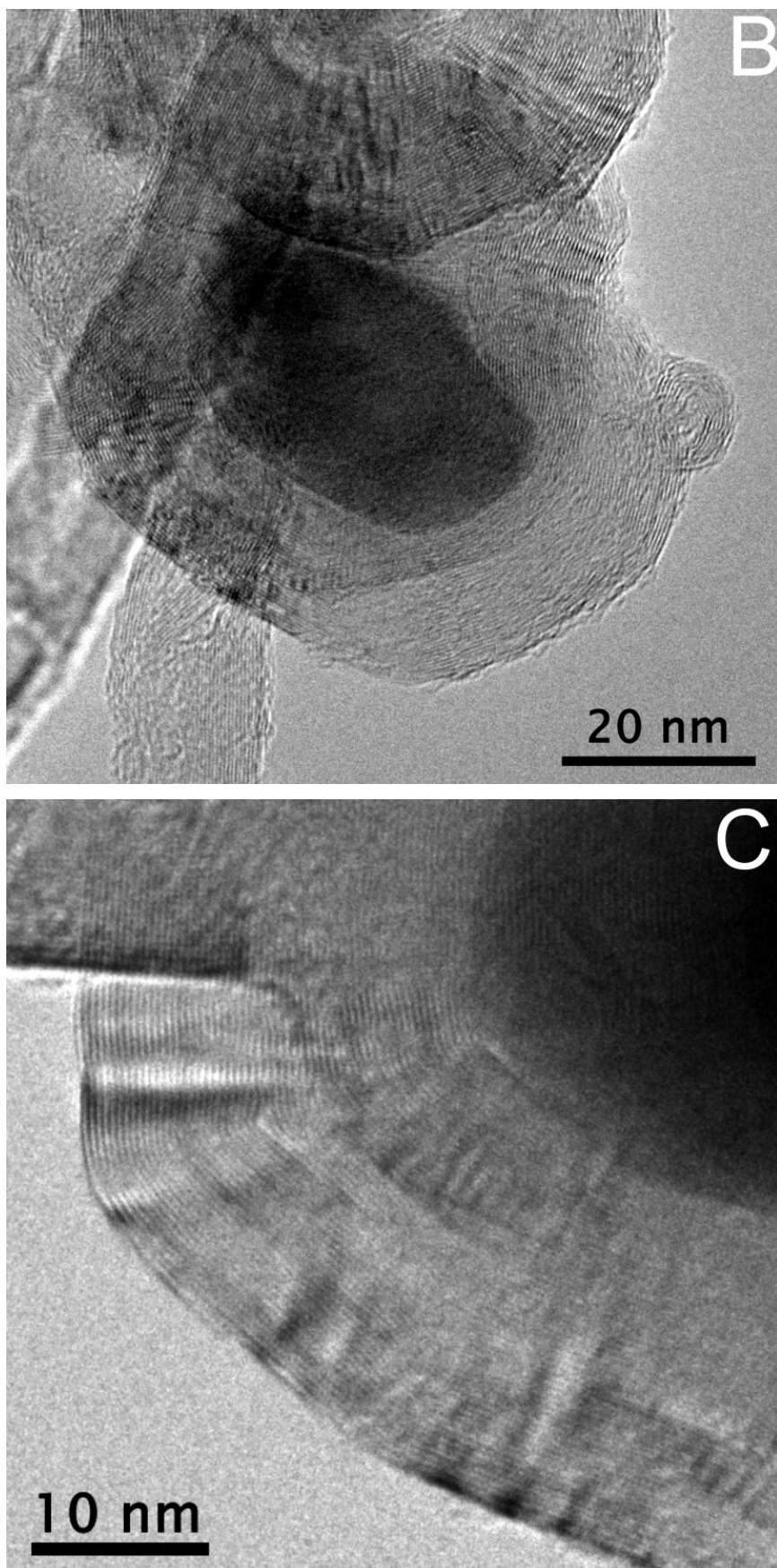


Figure 4.12. (B) TEM and (C) HRTEM micrographs of iron oxide particle encapsulated by carbon shell of high-ordered graphite layers.

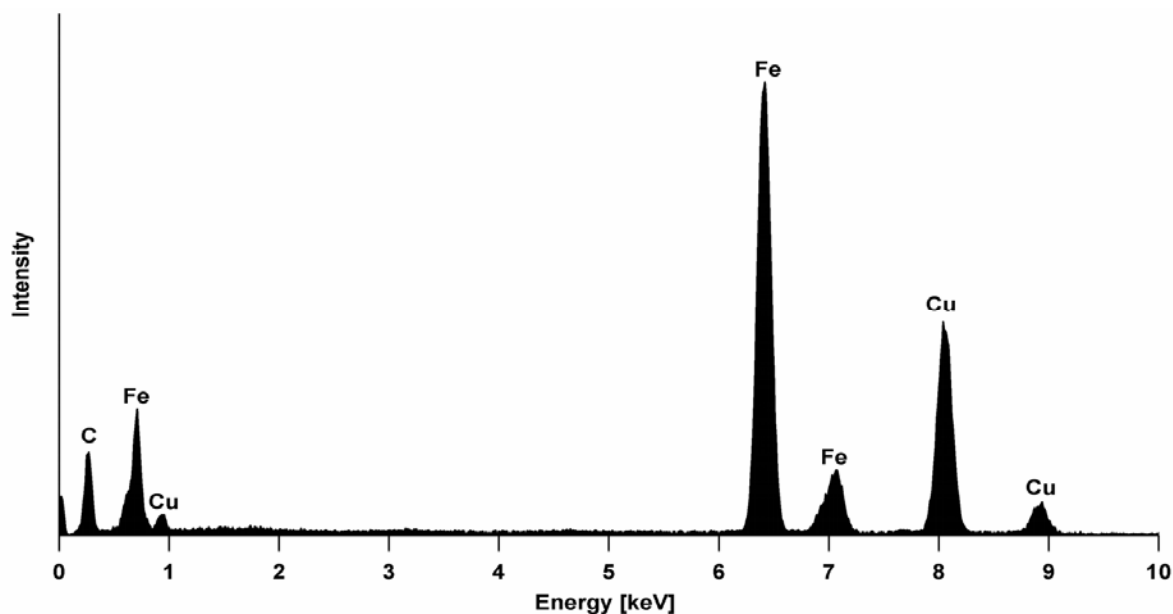


Figure 4.13. EDX spectrum of CNT3 catalyst after ODEB reaction under microwave-assisted conditions.

The XRD powder pattern of used CNT3 (Fig. 4.14c) detected the similar peaks as by X-ray diffraction pattern of fresh catalyst (Fig. 4.14a), indicating that the composition of catalyst remained unchanged after conventionally-heated ODEB. However, the chemical and structural results of TEM/EDX are in agreement with the XRD results of catalyst after ODEB reaction in microwave field (Fig. 4.14b). The new diffraction peaks assigned to single-phase metallic Fe at $2\theta = 44.84, 65.3, \text{ and } 82.72^\circ$ can be clearly seen right next to MWCNTs peaks, indicating that iron nanoparticles were reduced from iron oxide and have entered into narrow reciprocal combination with carbon [27]. Thus, different types of carbides such as Fe_3C , Fe_5C_2 , Fe_7C_3 superposed on $\alpha\text{-Fe}$ ($2\theta = 44.84^\circ$) could also play the role of foundation for further building of hexagonal graphite layers. The presence of iron oxide ($2\theta = 35.52, 53.54$) can probably be attributed to a certain concentration of oxygen as well as incomplete transformation of iron oxide inside of promoter nanoparticles [28].

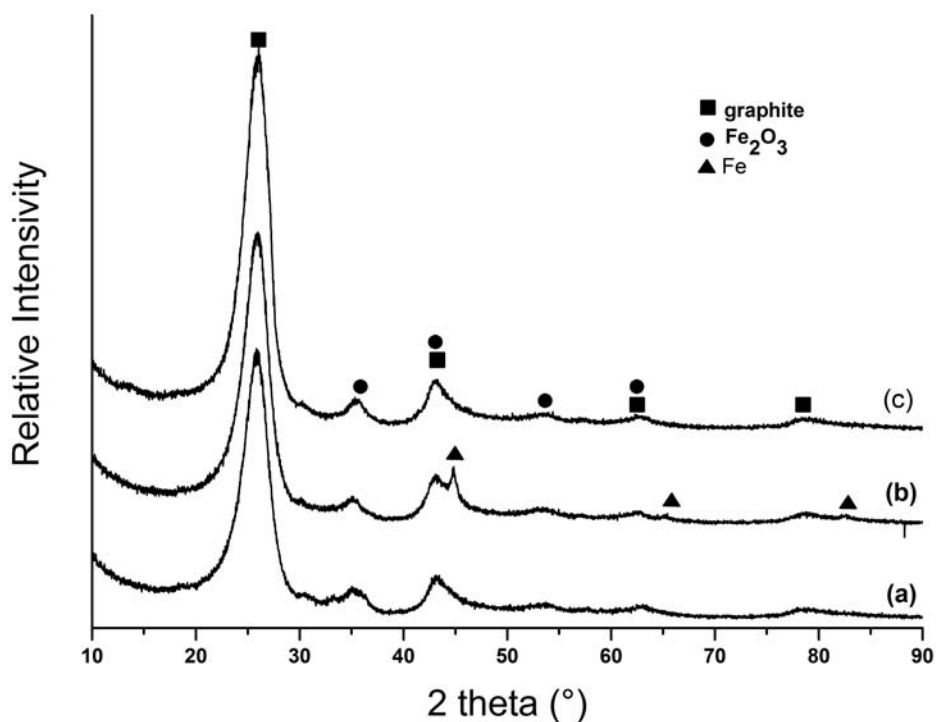


Figure 4.14. XRD patterns of CNT3 catalyst before (a) and after ODEB reaction in microwave-assisted (b) and conventionally-heated (c) reactors.

As it was reported by Rakov [29], the mechanism of carbon dissolution into iron, and its precipitation from the Fe-C and further deposition on the surface of iron was studied by many researchers, using Fe nanoparticles as catalyst for CNTs growing. The temperatures used for this process were 200-300 °C higher than that we carried out for our experiments in the microwave oven. Therefore, the application of microwave irradiation as a heating agent in preparation of MWCNTs via chemical vapour deposition method seems to be perspective, and the theoretical interpretation of microwave-assisted fluidized-bed reactor for the preparation of carbon nanotubes by catalytic pyrolysis is thoroughly described in the Chapter 5.

4.2.4 Upshot

In this chapter, comparison of the catalytic performance of Fe₂O₃/MWCNTs composites for ODEB in an integral fixed-bed and in microwave-assisted reactors is described. The highest ethylbenzene conversion and styrene selectivity were found for the 3wt.% Fe₂O₃ with a particle size less than 10 nm and almost isometric morphology supported on the outer surface of the MWCNTs in the temperature range 380 - 450 °C. The sample exhibited higher and more stable styrene selectivity under microwave conditions than that obtained using conventional heating at the same reaction conditions. In comparison to the large amounts of high disordered carbon displaced on the top layer of the catalyst during conventionally-heated ODEB no carbon deposition on the catalyst surface was observed for the microwave-assisted reaction. Apparently, the continuous burning of the disordered carbon leads to the higher styrene selectivity compared with that which was received with conventional heating. Under microwave reaction conditions the conversion of Fe₂O₃ nanoparticles supported on MWCNTs into carbon-encapsulated iron crystals occurred at temperatures by about 400 °C lower than that obtained in conventionally-heated reactors [27-30].

4.3. ODEB over Magnetite/Hematite nanopowders

In previous chapter, the influence of microwave irradiation on the structure and morphology of iron oxide loaded MWCNTs under reaction conditions was thoroughly investigated. Particularly, it was observed that during the ODEB iron oxide nanoparticles were reduced from iron oxide to iron and have entered into narrow reciprocal combination with carbon, resulting into the encapsulation of supported nanoparticles by carbon shell of high-ordered graphite layers. This leads one to assume, that the use of pure iron oxide particles under the same reaction conditions will be also followed by building of high-ordered graphite layers on their surface. The courageous theory of possible employment of the simple and cheap iron oxide without any doping agents as ODEB catalyst in conjunction with environmentally related and energy-saving method of heating – microwave irradiation – was advanced and experimentally proved.

Many oxidic iron compounds – iron oxides, oxide-hydroxides and hydroxides – not only play an important role in a variety of disciplines, but also serve as a model system of reduction and catalytic reactions [31]. The hematite $\alpha\text{-Fe}_2\text{O}_3$ being a major and thermodynamically most stable oxide among the 16 identified iron oxidic compounds is not a good microwave absorber; however the magnetite with cubic crystal system is related to materials with excellent magneto-dielectric properties. Therefore, the hematite was mixed with magnetite at various ratios and the catalytic properties of the obtained mixtures were investigated into microwave-assisted ODEB.

4.3.1 Characterization of fresh Magnetite/Hematite nanopowders

Iron oxides: Fe_2O_3 and Fe_3O_4 not only differ in their fundamental oxidation state, but are also usually regarded as non-stoichiometric compounds reflecting their natural tendency for oxidation $\text{Fe}^{2+} \rightarrow \text{Fe}^{3+}$. Their two appropriate formulas are given in Tab. 4.3. Structural information from an assembly of magnetite/hematite particles was obtained by X-Ray diffraction method (Fig. 4.15). The XRD spectrum from a prepared mixture showed that the position and relative intensity of all diffraction peaks match well with standard hematite and magnetite diffraction data. A set of (104), (110), (113) and (119) peaks belong to the hematite particles, however the magnetite signals are represented by (220), (311), (330) and (400) peaks. No impurity peaks are observed. The magnetite/hematite ratio 1:1 used by preparing of

the mixture was confirmed during the qualitative analyse of XRD data made by the Rietveld method.

Table 4.3

Non-stoichiometrical ferric oxides

Mineral	Stoichiometrical formula	Non-stoichiometrical formula
Hematite	$\alpha\text{-Fe}_2\text{O}_3$	$\text{Fe}_{2-x/3}(\text{OH})_x\text{O}_{3-x}$
Magnetite	Fe_3O_4	$\text{Fe}^{\text{II}}_{1-x}\text{Fe}^{\text{III}}_{2+x}\text{O}_{4+x/2}$ ($0 < x < 1$)

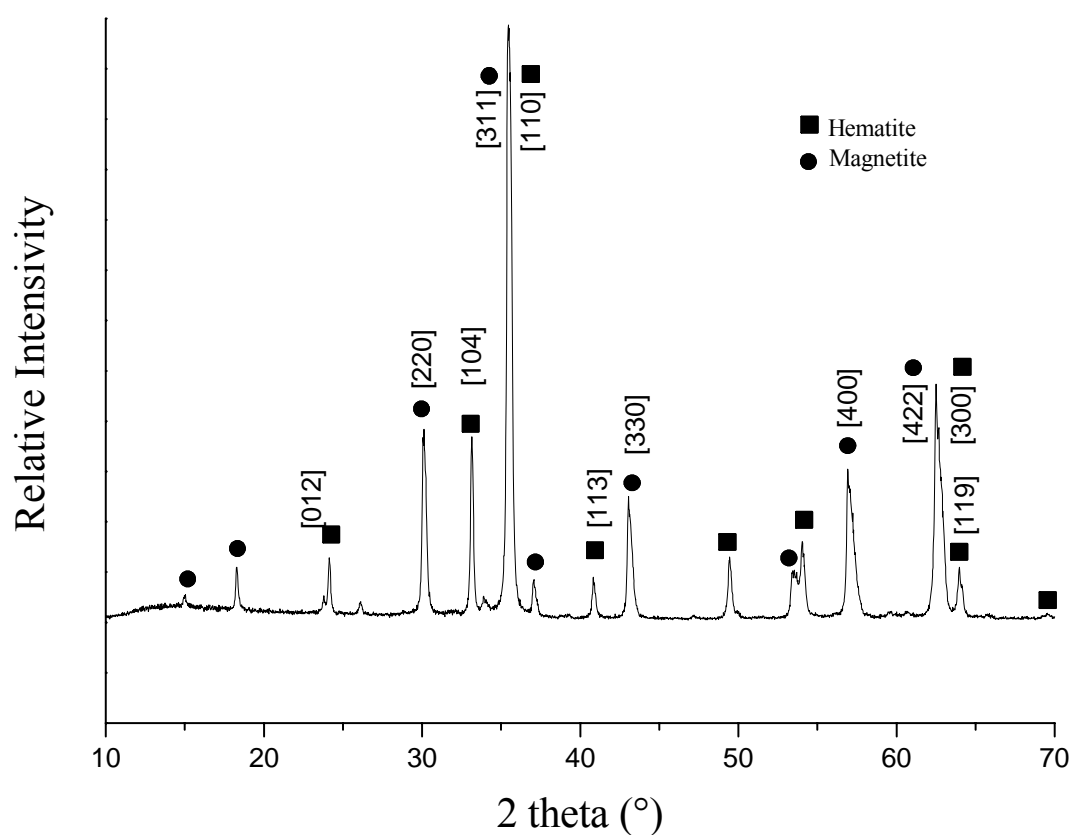


Figure 4.15. XRD spectrum of Magnetite/Hematite mixture.

The nanoparticles of investigated nanopowder were spherical with narrow size distribution, as shown in Fig. 4.16. The average particle diameter measured from TEM was 35 ± 5 nm, what is consistent with that estimated from Scherrer's formula during the XRD characterization. Fig. 4.17 depicts a selected area electron diffraction pattern from the magnetite (A) and hematite (B) nanoparticles. The calculated lattice spacing based on the multiple diffraction rings of magnetite (Fig. 4.17A) with their respective hkl indexes are given

in Tab. 4.4 [32]. The Fig. 4.17B showing the SAED of the circular α -Fe₂O₃ taken on α -Fe₂O₃ nanoparticle reveals the satisfactory crystallinity of the sample, which can be indexed to the pure rhombohedral phase of hematite.

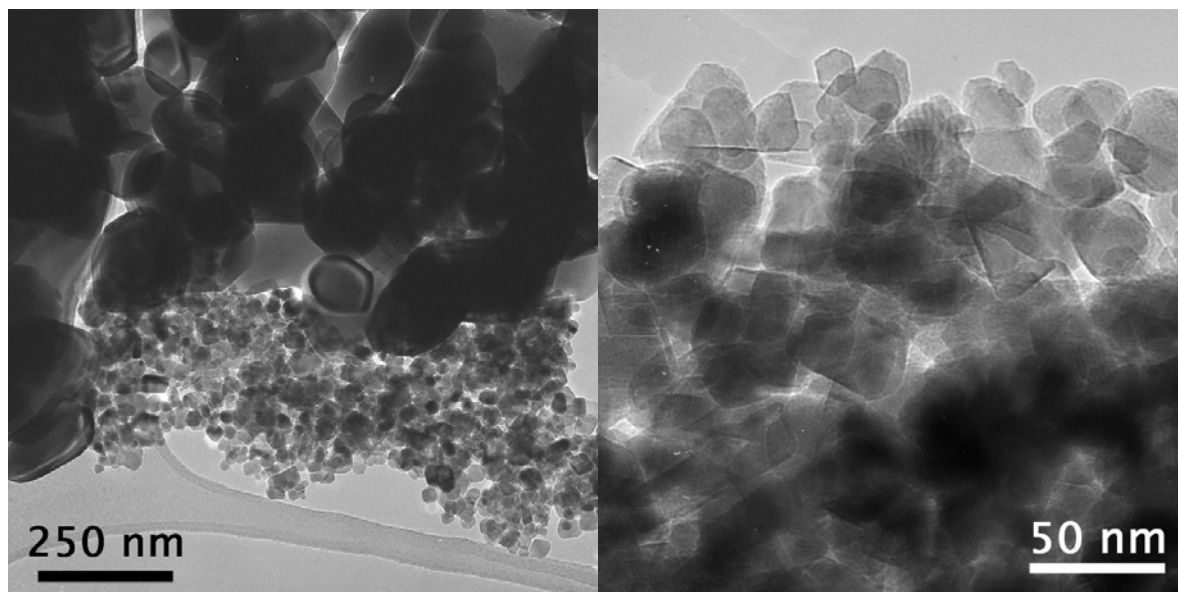


Figure 4.16. TEM images of fresh Magnetite/Hematite nanomixture.

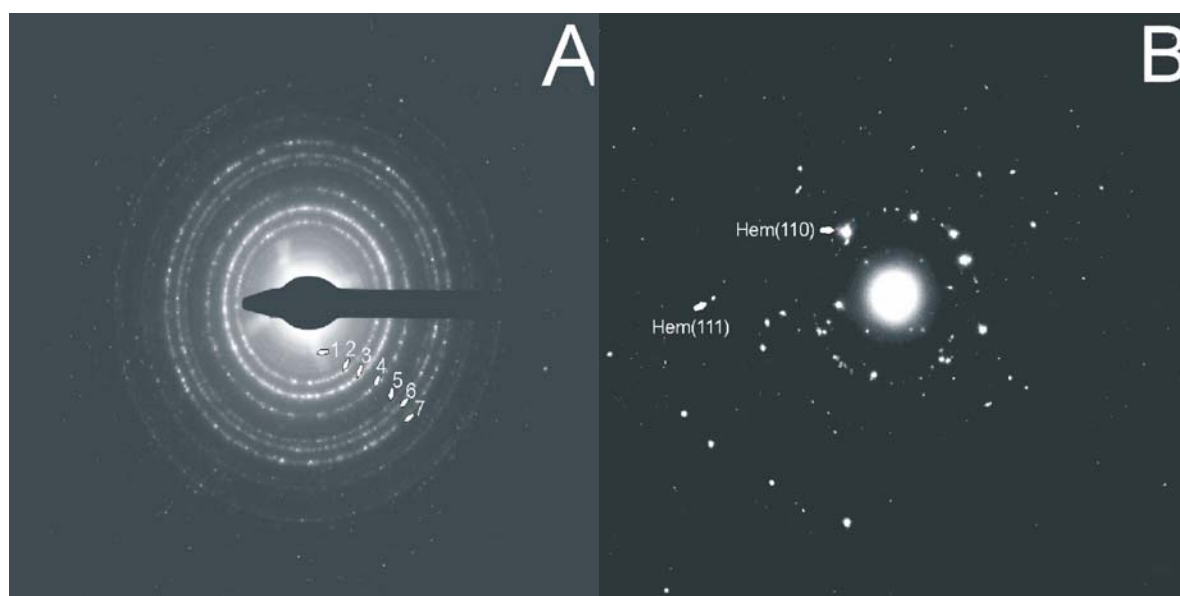


Figure 4.17. SAED images of fresh Magnetite (A) and Hematite (B) nanoparticles.

Table 4.4

Measured lattice spacing, $d(\text{\AA})$, of magnetite based on the rings in Fig. 4.15A and their respective hkl indexes.

	ring						
	1	2	3	4	5	6	7
d	4.89	2.98	2.54	2.12	1.73	1.63	1.5
hkl	111	220	311	400	422	511	440

4.3.2 Catalytic tests

The catalytic properties of pure micro- and nano-scaled magnetite as well as its mixtures with hematite nanopowder at various ratios were compared in order to determine which catalyst's composition exhibits the highest catalytic activity and stability in ODEB and to investigate the influence of the heating source on the catalytic properties of investigated systems. All tests were performed under identical experimental conditions that allowed the quantitative comparison.

Effect of particle size

Fig. 4.18 and 4.19 compare the influence of particle size as well as the influence of heating method on the catalytic behavior of micro- and nano-scaled magnetite. At the reaction temperature 250 °C, there was an insignificant difference in ethylbenzene conversion over micro- and nano-scaled magnetite (7.5 and 8% respectively) under microwave conditions. In conventionally-heated ODEB the nano-scaled magnetite exhibited the ethylbenzene conversion of 10%, while the ethylbenzene conversion over microparticles was only 5%. At low reaction temperature of 250 °C the selectivity to styrene seems to be identical for both heating methods. It was 35 and 40% for micro- and nano-scaled magnetite respectively. The increase of the temperature from 250 to 450 °C resulted in the remarkable decrease of styrene selectivity in conventionally-heated ODEB; the selectivity was 8 and 11% over micro- and nano-powders respectively. The same tendency could be observed over micro-scaled magnetite in microwave-assisted ODEB (styrene selectivity decreased from 35% at 250 °C to 15% at 450 °C), however, the nano-scaled magnetite exhibited relative constant selectivity during the temperature increase (35% at 450 °C in comparison to 40% at 250 °C). Under both conditions, the ethylbenzene conversion increased with temperature rise. The micro-scaled magnetite exhibited approximately the same ethylbenzene conversion of 25% at 450 °C under both heating methods, while the nanoparticles displayed different ethylbenzene conversion level. Indeed, it was 40 and 50% at 450 °C under conventional and microwave heating methods respectively. Thus, it could be concluded, that the highest conversion by relative stable and high styrene selectivity could be obtained over nano-scaled magnetite in microwave field.

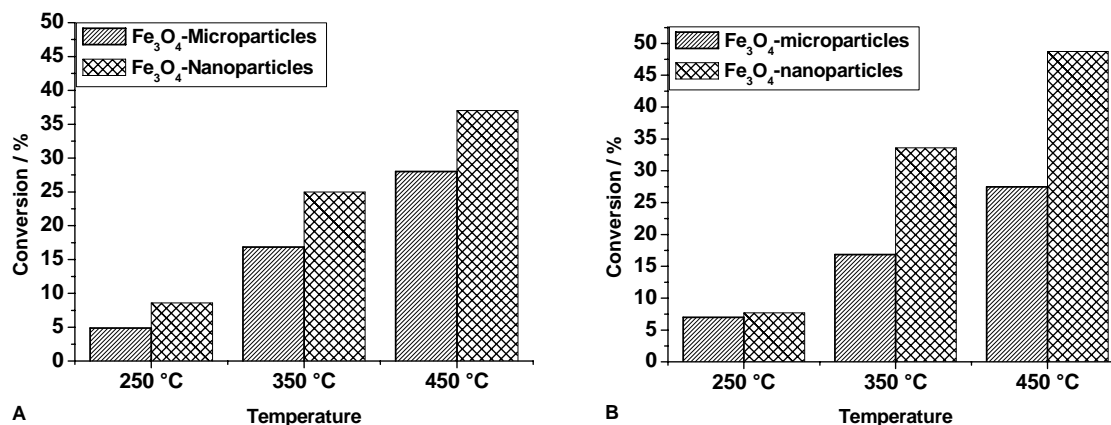


Figure 4.18. Conversion of ethylbenzene over micro- and nano-scaled magnetite as a function of temperature using both conventional (A) and microwave (B) heating

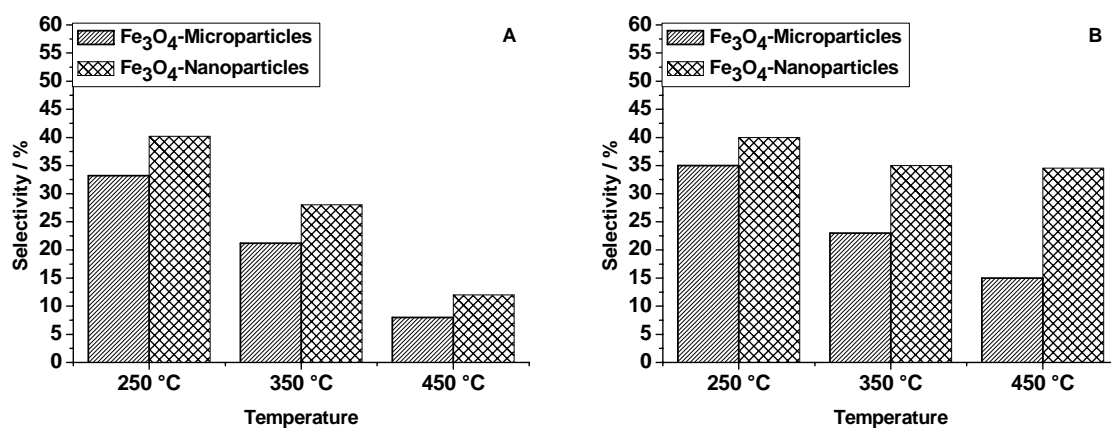


Figure 4.19. Styrene selectivity over micro- and nano-scaled magnetite as a function of temperature using both conventional (A) and microwave (B) heating

Effect of volume flow rate

Comparison of catalytic behavior at 8.5 and 1.1 l/h volume flow rates and the effect of microwave irradiation are given in Fig. 4.20. The catalyst used was a mixture of magnetite (75 wt.%) and hematite (25 wt.%) nanopowders. Around 36% increase in the ethylbenzene conversion and slight decrease in styrene selectivity by 6% at volume flow rate 8.5 l/h compared to 1.1 l/h was found in microwave-assisted ODEB at 350 °C. The same tendency in catalytic behavior with decreasing of volume flow rate was observed over the catalyst under conventional reaction conditions, and the increase in ethylbenzene conversion from 30 to 69% as well as decrease in styrene selectivity from 10 to 4% were ascertained by the

change of volume flow rate from 8.5 to 1.1 l/h. However, comparing results obtained under conventional reaction conditions with those obtained in microwave-assisted reactor at both volume flow rates, the styrene selectivity were considerably higher with microwave irradiation. Thus, the advantage of microwave heating at lower flow rates is obvious.

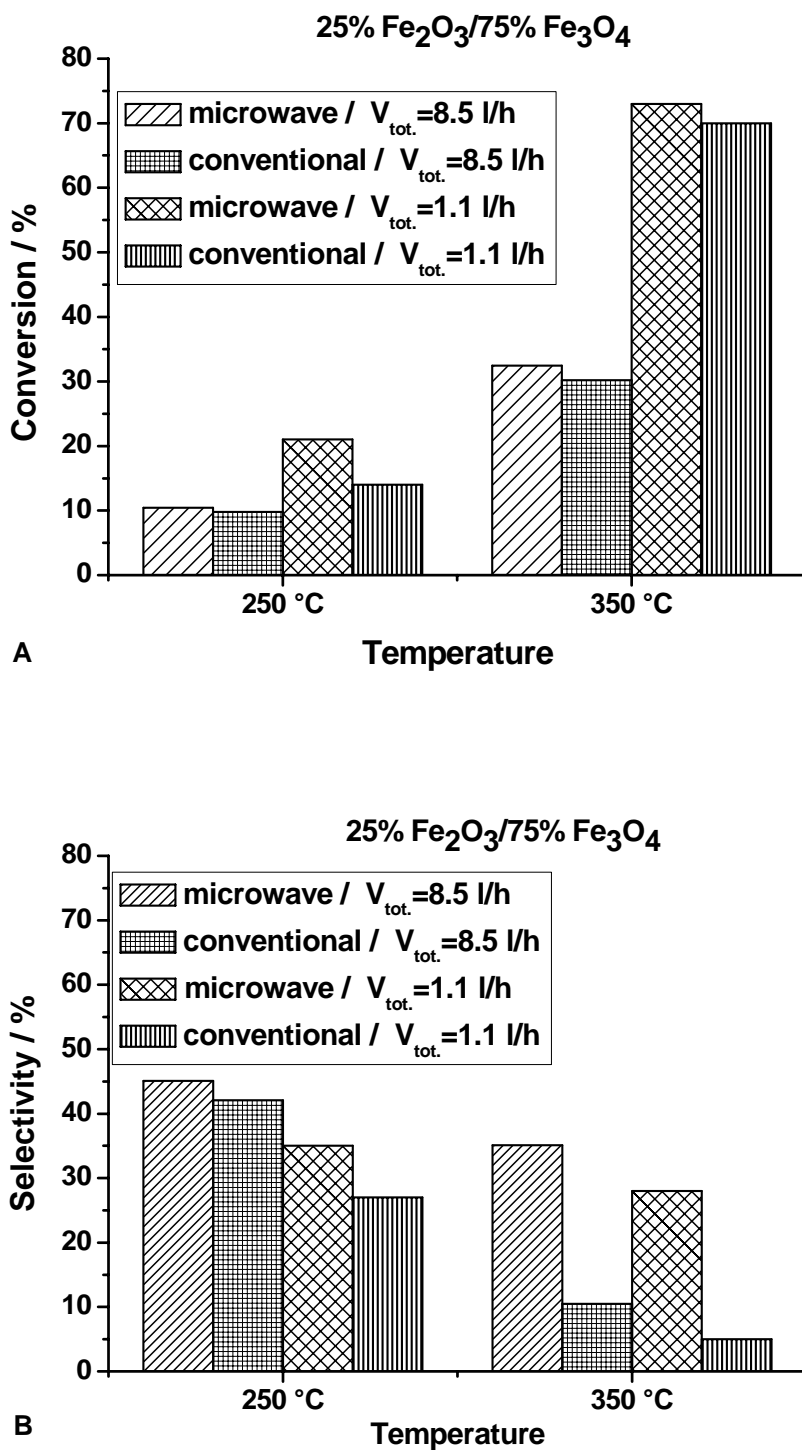


Figure 4.20. Ethylbenzene conversion (A) and styrene selectivity (B) over micro- and nano-scaled magnetite as a function of temperature using both conventional and microwave heating

The space velocity of 800-2000 h⁻¹ used in our investigations is considerably higher than that (5 h⁻¹) used in the industrial process of styrene production. Therefore, it could be assumed that further decrease of the volume flow rate could positively influence the catalytic activity.

Steady state results

Fig. 4.21 and 4.22 display the ethylbenzene conversion and styrene selectivity as a function of time on stream for conventionally-heated and microwave-assisted ODEB respectively over catalysts prepared via simple mixing of magnetite and hematite nanopowders. The following samples were used:

HEM25: 25 wt.% of hematite / 75 wt.% of magnetite

HEM50: 50 wt.% of hematite / 50 wt.% of magnetite

HEM70: 70 wt.% of hematite / 30 wt.% of magnetite

All the tested composites were active at 350 °C in conventionally-heated as well as in microwave-assisted ODEB. Indeed, HEM25 gave the highest ethylbenzene conversion amongst all the materials tested, and HEM70 with the smallest content of magnetite exhibited the lowest activity. The continuous increase of ethylbenzene conversion could be observed first 150 minutes of time on stream over all samples in both reactors. It could be related to the so called induction period of forming the carbon layers on the surface of catalysts as it was proposed by Schlögl et al. [20, 33]. After the induction period HEM25, HEM50 and HEM70 exhibited the steady state ethylbenzene conversion of 70, 55 and 38% respectively in microwave-assisted ODEB. In conventionally-heated ODEB the steady state conversions reached the values of 57, 50 and 40% over HEM25, HEM50 and HEM70 respectively. It seems to be that the magnetite has the positive influence on the catalytic activity.

The styrene selectivity increased during the initial time of reaction over all prepared samples in both reactors, and after 150 minutes of time on stream started to decrease continuously. This could be explained by deposition of high disordered coke, leading to the formation of typical by-products such as toluene, benzene and carbon oxides. However, HEM25 with highest content of magnetite exhibited the lowest styrene selectivity of 50 and 32% (150th minute of time on stream) in microwave-assisted and conventionally-heated ODEB respectively. On the other hand, the styrene selectivity was much higher on HEM70

with lowest content of magnetite, namely 85 and 47% (150th minute of time on stream) under microwave and conventional reaction conditions respectively.

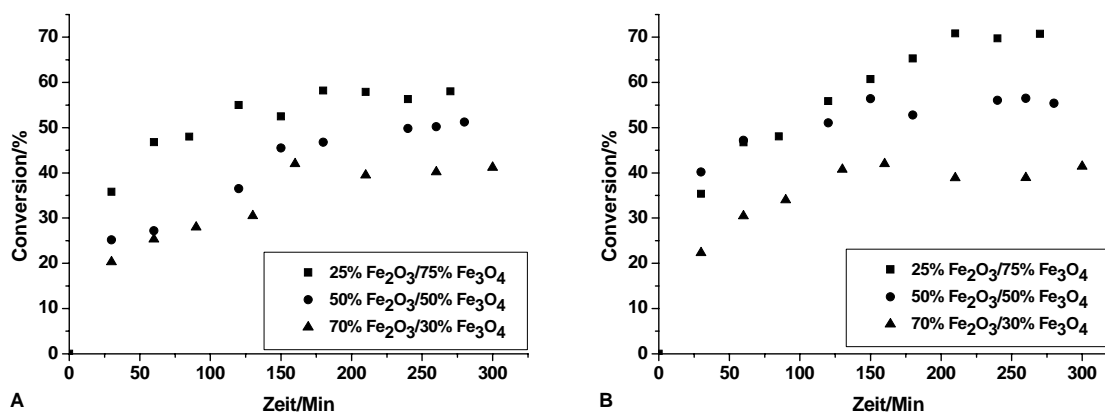


Figure 4.21. Effect of time on stream in ODEB reaction over CNT3 on the ethylbenzene conversion in conventionally-heated (A) and microwave-assisted (B) reactors

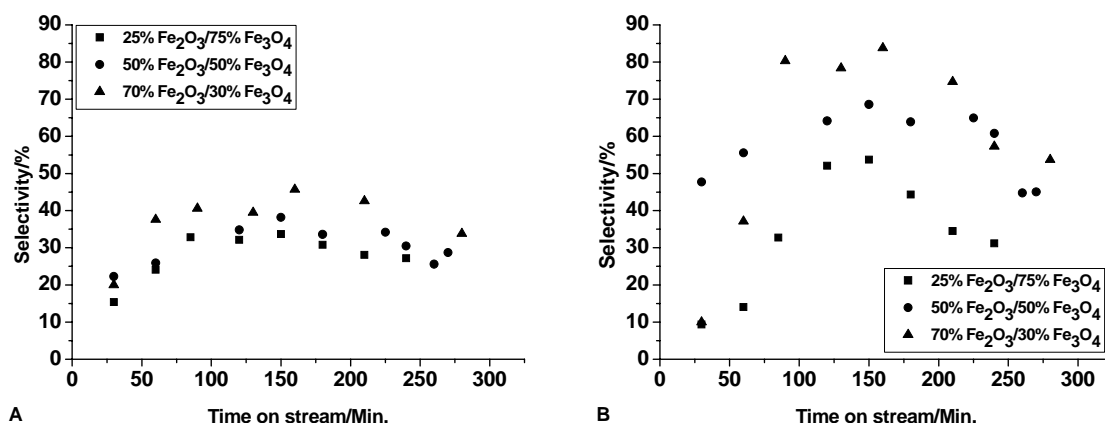


Figure 4.22. Effect of time on stream in ODEB reaction over CNT3 on the styrene selectivity in conventionally-heated (A) and microwave-assisted (B) reactors

Analyzing generally the catalytic results presented in Fig. 4.21 and Fig. 4.22, it should be noted, that the same development trends of ethylbenzene conversion and styrene selectivity were obtained during the steady state ODEB on the samples with various content of magnetite. Particularly, the samples with highest magnetite content (HEM25) exhibited the highest ethylbenzene conversion and the lowest styrene selectivity. In contrast to that, the lowest ethylbenzene conversion and highest styrene selectivity was achieved on HEM70 with lowest magnetite content. This tendency has been observed for both heating methods,

concluding that the magnetite gives higher ethylbenzene conversion, but lower styrene selectivity than the hematite.

4.3.3 Discussion

Fig. 4.23 presents the XRD patterns of HEM25 after the microwave-assisted ODEB in comparison with XRD data of three iron oxide phases: hematite, magnetite and maghemite in order to determine the transformations in the structure occurred during the reaction.

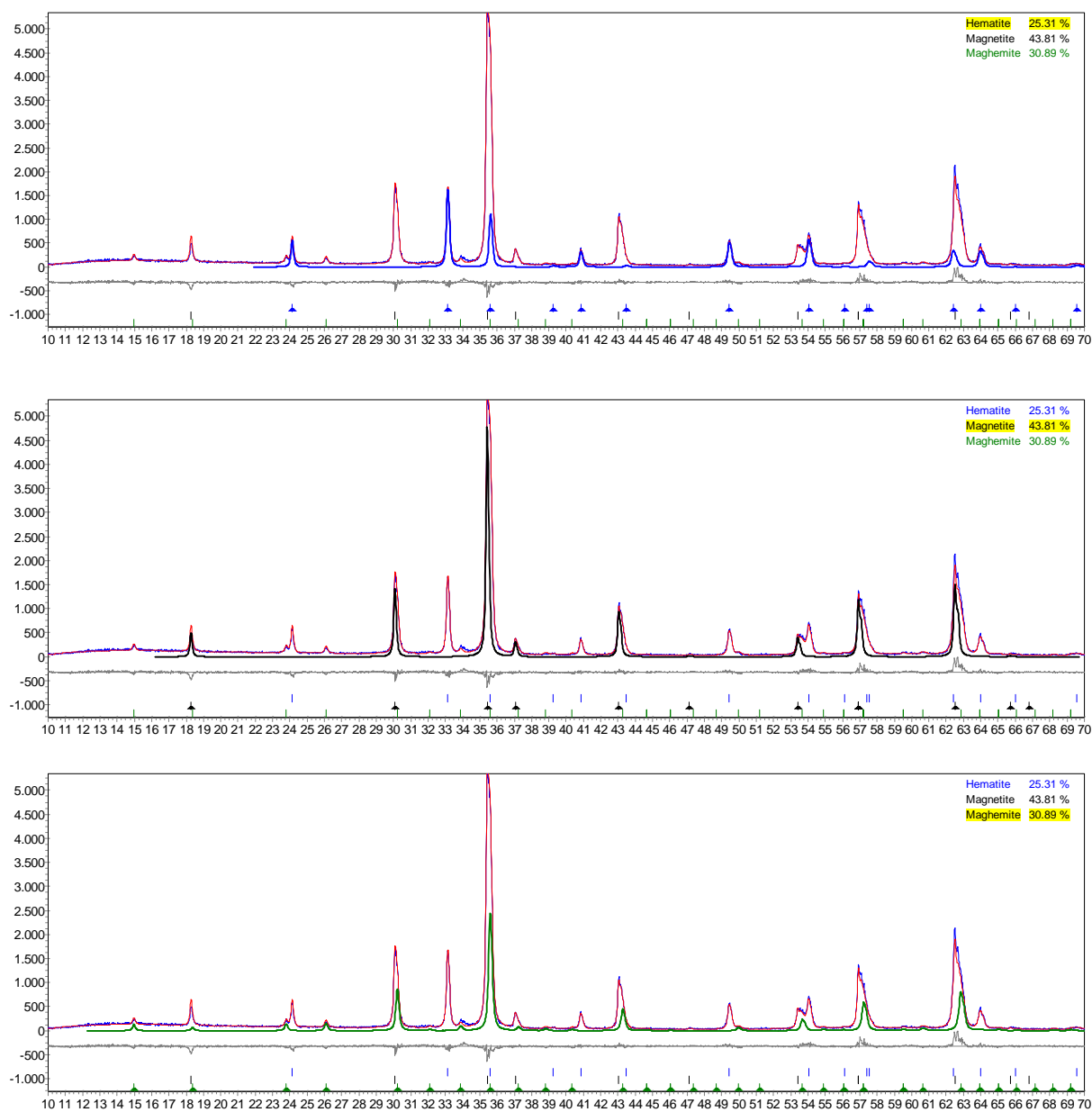


Figure 4.23. XRD spectrum of HEM25 after microwave assisted ODEB.

It seems to be that the process of iron oxide reduction to iron and its further encapsulation by carbon layers did not occur. No peaks of graphite or iron carbide could be observed. However, the presence of maghemite in the sample is evident, indicating that the oxidation of Fe_3O_4 under reaction conditions leads to $\gamma\text{-Fe}_2\text{O}_3$. The chemical compositions of hematite/magnetite mixtures after microwave-assisted and conventionally-heated ODEB are calculated on the base of XRD data and shown in Tab. 4.5.

Table 4.5

Hematite : Magnetite : Maghemite content ratios (%) for samples before and after ODEB in conventionally-heated (CH) and microwave irradiated (MW) reaction, derived from X-ray photoelectron spectra.

Sample	Hem:Magn (fresh)	State	Hem:Magn:Magh
Nano-scaled magnetite	0.1:100	CH-ODEB 450 °C	60:7:33
Nano-scaled magnetite	0.1:100	MW-ODEB 450 °C	62:8:30
HEM25	25:75	CH-ODEB 350 °C	25:28:47
HEM25	25:75	MW-ODEB 350 °C	25:33:42
HEM50	49:51	CH-ODEB 350 °C	49:30:31
HEM50	50:50	MW-ODEB 350 °C	50:26:24
HEM70	71:29	CH-ODEB 350 °C	71:8:21
HEM70	72:28	MW-ODEB 350 °C	72:12:16

It is to be recognized, that the transformation of magnetite to maghemite occurs under conventional as well as under microwave reaction conditions, whereas the partial oxidation of maghemite to hematite was observed only at the temperature of 450°C. These results are in accordance with results obtained by Sun [34]. He observed that the black assembly of magnetite nanoparticles was transformed to a red-brown one under O_2 at 250 °C, and the dark red-brown material of known $\alpha\text{-Fe}_2\text{O}_3$ was obtained after oxidation at 500°C.

Fig. 4.24 depicts the TEM image of HEM25 after microwave assisted ODEB. Sections 1-3 show magnified TEM images taken from different areas marked with numbers 1-3 in Fig. 4.24, respectively, in which sections 1 and 2 display the crystal lattice of iron oxide of different structure, and the section 3 displays the layers of high disordered carbon. In the section 1 the lattice spacing between two adjacent fringes is approximately 2.51 Å, corresponding to the spacing of (200) planes of $\alpha\text{-Fe}_2\text{O}_3$ with typical for hematite hexagonal lattice structure. The magnified image of the magnetite nanoparticles with a size of ~28 nm is shown in the section 2. The interplanar distances of $d_1=2.97$ Å and $d_2=2.94$ Å are very close to the plane d_{220} of magnetite phase in (111) zone axis. The section 3 displays the iron oxide

nanoparticle covered by highly disordered carbon layers occurred during the deactivation process of coke deposition what is characteristic of ODEB.

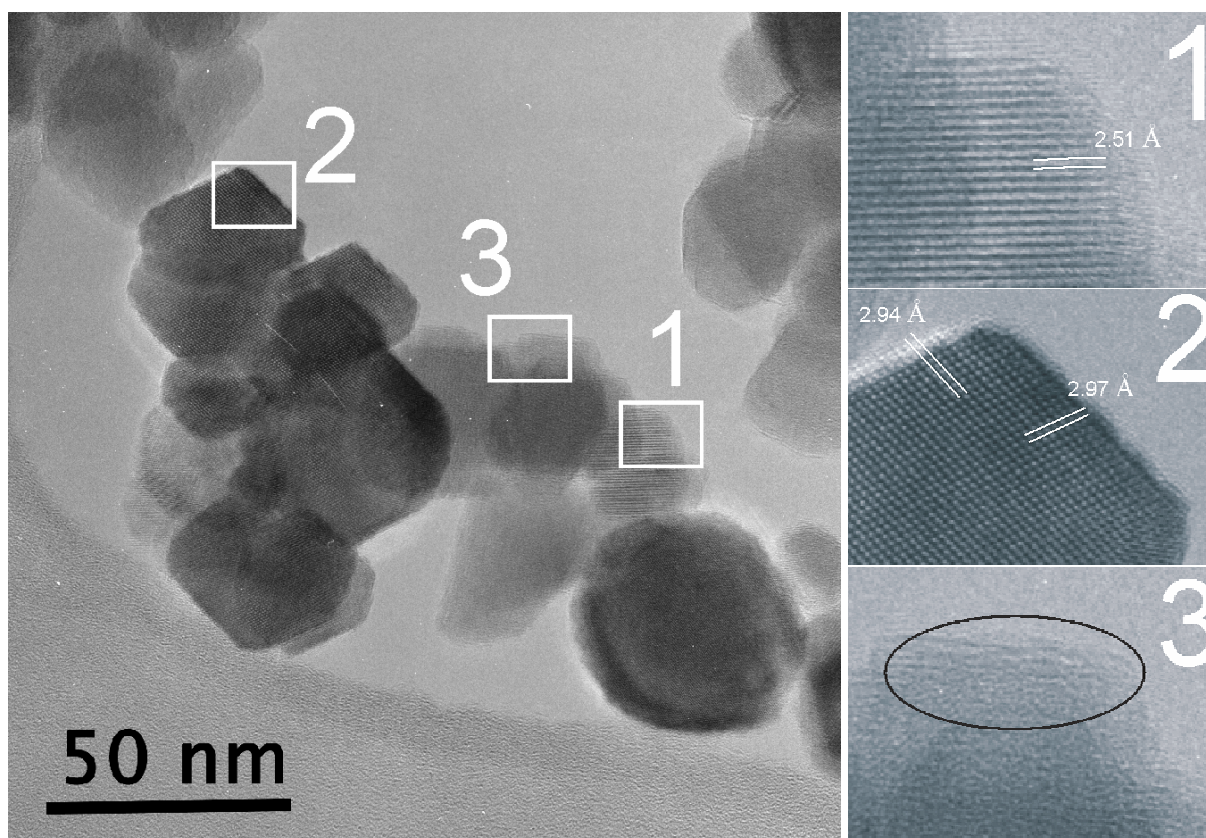


Figure 4.24. TEM images of HEM25 after microwave-assisted ODEB.

4.3.4 Upshot

By summarizing the results a trend towards a higher ethylbenzene conversion and styrene selectivity was observed using microwave radiation. The nanoparticles of magnetite exhibited higher catalytic activity than micro-scaled particles. The change of volume flow rate from 8.5 to 1.1 l/h influenced the ethylbenzene conversion in conventionally- heated and microwave-assisted ODEB over HEM25 positively, while the styrene selectivity decreased under both reaction conditions. The stable ethylbenzene conversion of 70% was found for the HEM25 during the steady state experiments in microwave oven (Panasonic) on the 4th hour of time on stream. All samples exhibited non-stable styrene selectivity which decreased continuously after 3h of time on stream for both heating methods. Moreover, the oxidation of Fe_3O_4 to $\gamma\text{-Fe}_2\text{O}_3$ as well as the formation of highly disordered carbon instead of the expected iron oxide reduction to iron and its further encapsulation by graphite layers was determined during the post reaction characterization. It could be assumed that in the previous tests the sp^2

structure of MWCNTs in conjunction with microwave-assisted reaction conditions resulted in the deposition of sp^2 carbon layers on the whole surface of catalyst including the iron oxide nanoparticles. During the encapsulation of $\gamma\text{-Fe}_2\text{O}_3$ particles the reduction of iron oxide to iron occurred slowly in direction from the outside to inside of the particle. Thus, the formation of iron carbide is proposed to be only the consequence of coke deposition in the form of sp^2 carbon but not conversely. The non-thermal effect of microwave irradiation should be also taken into consideration because the above described processes were observed on the surface of the promoted MWCNTs only after microwave-assisted ODEB, whereas the conventionally-heated reaction conditions resulted in appearance of high disordered amorphous carbon, what is typical for many dehydrogenation reactions. To prove the given explanation the following tests with unpromoted MWCNTs will be performed. However, the advantage of microwave energy as heating agent investigated in gas-phase catalytic reactions is obvious and the tests in this area will be also continued.

4.4. ODEB over functionalized carbon nanotubes

The aim of this chapter is to investigate the effect of gas- and liquid-phase oxidation on the surface and catalytic properties of MWCNTs, as well as to prove if the formation of new graphite layers on the surface of carbon nanotubes occurs during the ODEB. Oxidative treatment typically produces a wide range of functionalities including carboxylic acids, alcohols, aldehydes, ethers, lactones, epoxides, etc. These oxygen-containing surface groups are formed not only by reaction with oxidizing gases (e.g. O₂, O₃, CO₂), but also by treatment with aqueous solutions of HNO₃, H₂SO₄, H₂O₂ or KMnO₄ [35-37]. Literature screening shows that the treatment with solutions of nitric acid produces mainly carboxylic as well as carbonyl groups, which proposed to be the active sites for ODEB on carbon materials [38]. The nitric acid was used to oxidize carbon nanotubes, because the NO₂⁺ ion, is able to attack aromatic compounds, which is probably the first step in the introduction of oxygen-containing surface groups. Therefore the severity of the oxidation treatment depends on the treatment time and the concentration of NO₂⁺ [39]. However, the conditions of treatment differ largely from one author to another, e.g., the acid concentration varies in the range of 15-70 wt.%, the initial concentration of carbon nanotubes varies from 0.1 to 10 mg/ml, and the treatment duration from 1 to 48 h. In this investigation MWCNTs were pretreated with 6 molar nitric acid for 24 h in order to obtain the maximum number of oxygen-containing surface groups. The oxidative treatment with oxygen was performed as reported by Pereira et al. [25].

4.4.1 Characterization of functionalized MWCNTs before ODEB

Fig. 4.25A displays TEM image of untreated MWCNTs. The images of MWCNTs pretreated with oxygen (OMWCNTs) and nitric acid (NMWCNTs) are shown in Fig. 4.25B and 4.25C respectively. The oxidation with oxygen brings more significant changes in the starting material. OMWCNTs are clearly shorter and, differently to what was observed in Fig. 4.25A nanotubes, most of the carbon nanotubes are open. It seems to be that gasification by oxygen starts at the ends of MWCNTs and then proceeds further on to reduce their lengths [40]. Thus, the significant decrease of the sample volume and weight observed can be explained by simple combustion of nanotubes. However, the oxidation with HNO₃ leads to no significant change, since the MWCNTs maintain their size; and the walls do not seem to be affected [41].

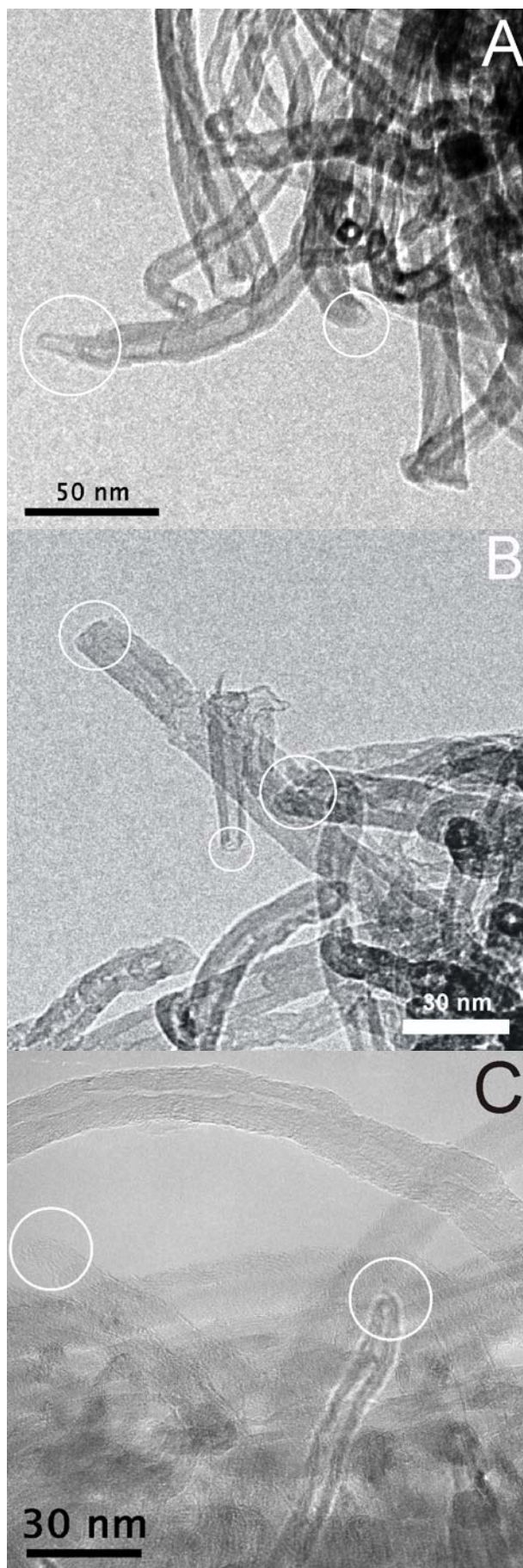


Figure 4.25. HRTEM images of untreated (A) and pre-treated with oxygen (B) and nitric acid (C) MWCNTs.

Tab. 4.6 presents the numerical values corresponding to weight loss and volume decrease of MWCNTs after the treatment with oxygen using both heating methods. After the reaction in conventionally-heated reactor the weight loss of 23% was observed, while the catalyst volume remained unchanged. However, the microwave-assisted treatment of MWCNTs with O₂ resulted in huge weight loss (66%) as well as volume decrease (50%). Even by the treatment with two fold lower concentration of oxygen in what the weight loss of 45% as well as the volume decrease of 35% was obtained. Thus, it could be concluded that the gas-phase oxidizing of MWCNTs under microwave reaction conditions influences their structural stability negatively.

Table 4.6

Effect of treatment procedure on the weight and volume of MWCNTs

Source of heating	O ₂ concentration, %	Weight loss, %	Volume decrease, %
Conventional Heating	5	33	2
Microwave irradiation	5	66	50
Microwave irradiation	2.5	48	35

4.4.2 Catalytic tests

The kinetic results for conventionally-heated and microwave-assisted ODEB are summarized in Tab. 4.7 and Tab. 4.8, respectively. It seems to be that OMWCNTs exhibited mostly higher ethylbenzene conversion and styrene selectivity than that obtained over MWCNTs and CNT3 in previous experiments. The selectivity achieved in microwave-assisted reactor was higher than that observed under conventional reaction conditions. The increase of the reaction temperature from 350 to 450 °C resulted in increasing ethylbenzene conversion with slight decrease in the styrene selectivity. The weight and the volume of OMWCNTs remained unchanged after dehydrogenation in microwave field as well as in conventionally-heated reactor, indicating that no catalyst was combusted. However, NMWCNTs showed the highest ethylbenzene conversion for both heating methods in the temperature range from 350 to 450 °C, whilst the selectivity seems to be a little bit lower than that obtained with OMWCNTs. It could be related to the more rapid desorption process of products occurred on fined down during the oxidative treatment OMWCNTs.

Table 4.7

The experimental results for conventionally-heated ODEB over untreated, iron oxide loaded and functionalized MWCNTs.

Sample	350 °C		400 °C		450 °C	
	X _{EB}	S _{ST}	X _{EB}	S _{ST}	X _{EB}	S _{ST}
MWCNTs	15	77	30	68	31	67
CNT3	15	75	38	66	37	63
OMWCNTs	9	81	27	79	43	73
NMWCNTs	38	79	45	75	51	68

Table 4.8

The experimental results for microwave-assisted ODEB over untreated, iron oxide loaded and functionalized MWCNTs.

Sample	350 °C		400 °C		450 °C	
	X _{EB}	S _{ST}	X _{EB}	S _{ST}	X _{EB}	S _{ST}
MWCNTs	26	97	28	89	31	80
CNT3	27	92	32	82	35	75
OMWCNTs	33	91	27	89	43	83
NMWCNTs	58	87	70	84	75	75

Fig. 4.26 presents ethylbenzene conversion and styrene selectivity rate on NMWCNTs as a function of reaction time. In order to investigate the influence of oxidation treatment on the catalytic activity of NMWCNTs long-term stability tests were performed for conventionally-heated and microwave-assisted ODEB. The results were compared with those obtained on CNT3 in previous investigations. As it is clearly evident in Fig. 4.26, the synthesized composites displayed a high long-term stability under operating conditions in both reactors. MWCNTs exhibited the stable styrene yield of 34% in conventionally-heated reactor, what is actually 3% higher than that obtained on CNT3, thus the insignificant but definitely positive influence of the treatment with nitric acid on the catalytic activity is ascertained. However, the application of functionalized NMWCNTs in conjunction with microwave field as heating agent resulted in a great catalytic performance. Specifically, the styrene yield of 59% remained unchanged during the long-term stability test on NMWCNTs after 80 h on stream. The styrene selectivity seems to be similar on CNT3, OMWCNTs and NMWCNTs, however, the ethylbenzene conversion is 35 and 30% higher than that achieved on CNT3 and OMWCNTs respectively.

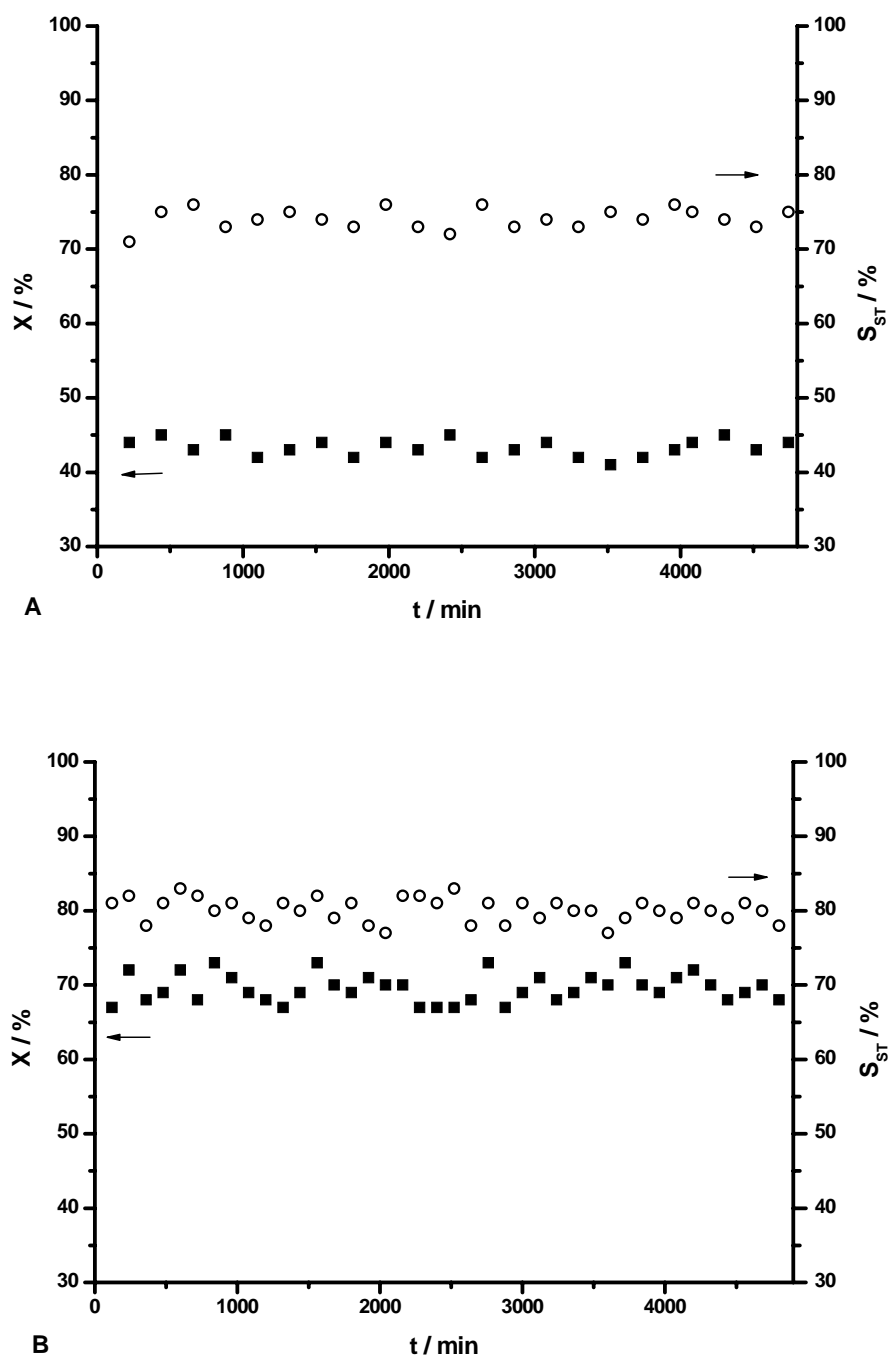


Figure 4.26. Effect of time on stream in ODEB reaction over NMWCNTs on the conversion (X) and styrene selectivity (S) in conventionally-heated (A) and microwave-assisted (B) reactors

In order to give the comprehensive comparison of efficiency of conventional and microwave heating methods in ODEB, the energy consumption of each reactor was measured (s. Appendix A). The power consumption has been determined with an electricity meter at the microwave oven and the resistance wire. It was found, that the energy efficiency of

microwave heating method is more than four times higher than the conventional procedure considering the production of 1 gram of styrene over 5 cm³ of catalyst under the same reaction conditions.

4.4.3 Discussion

Fig. 4.27A displays TEM image of NMWCNTs after conventionally-heated ODEB. At first sight, the catalyst seems to be unaltered, but HRTEM examination (Fig. 4.27B) clearly detects the coke deposition on the surface of NMWCNTs, what is in corresponding with results obtained in the Chapter 4.2 [42]. In contrast, insignificant amount of high disordered carbon could be observed on the surface of NMWCNTs tested in microwave-assisted reactor (Fig. 4.28). However, the CNTs themselves appear to be considerably thicker than those before the reaction (Fig. 4.25C). It can be seen, that the surface of used NMWCNTs was covered by graphitized over-layers after 80 h of time on stream in microwave oven (MLS), which can correspond to deposited carbon during the reaction due to the polymerization of reactants or products.

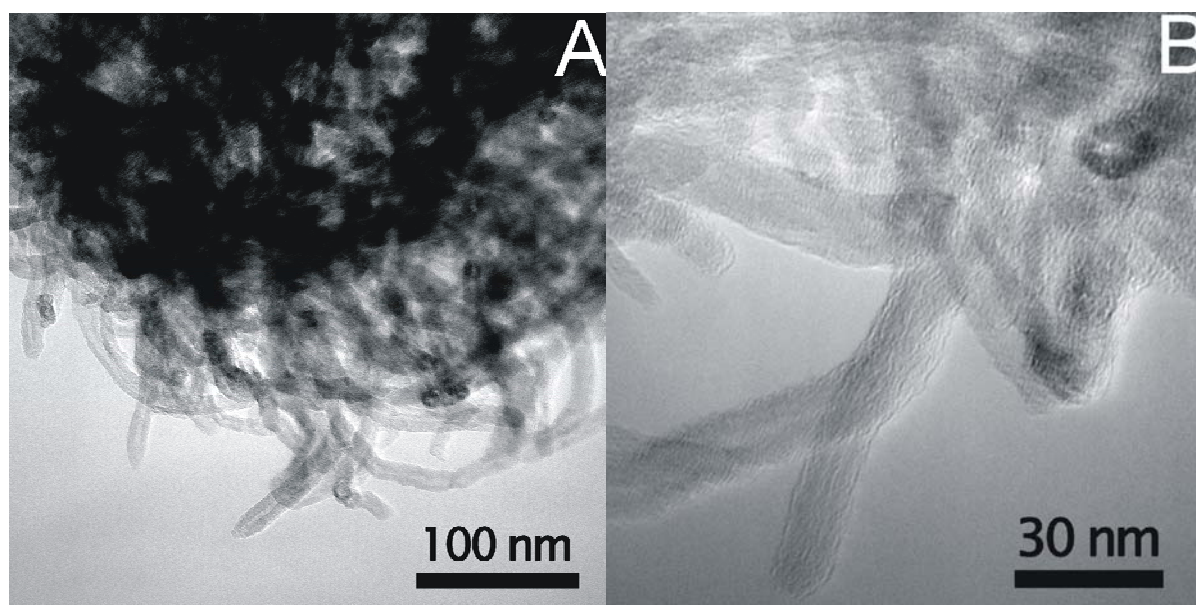


Figure 4.27. (A) TEM and (B) HRTEM images of NMWCNTs after conventionally-heated ODEB.

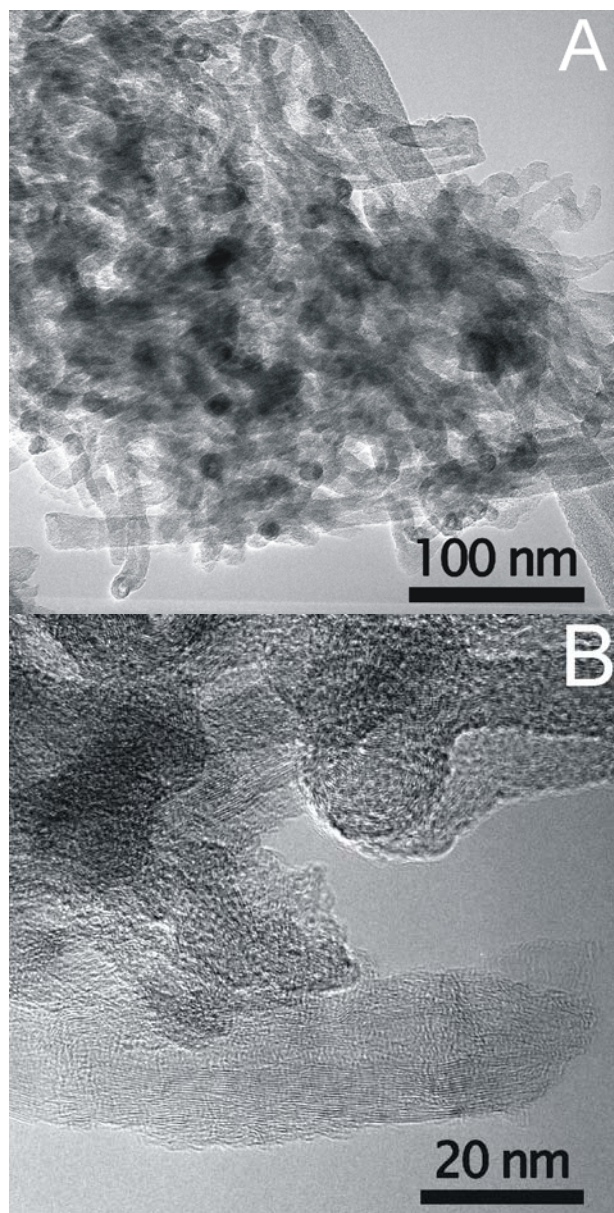


Figure 4.28. (A) TEM and (B) HRTEM images of NMWCNTs after microwave-assisted ODEB.

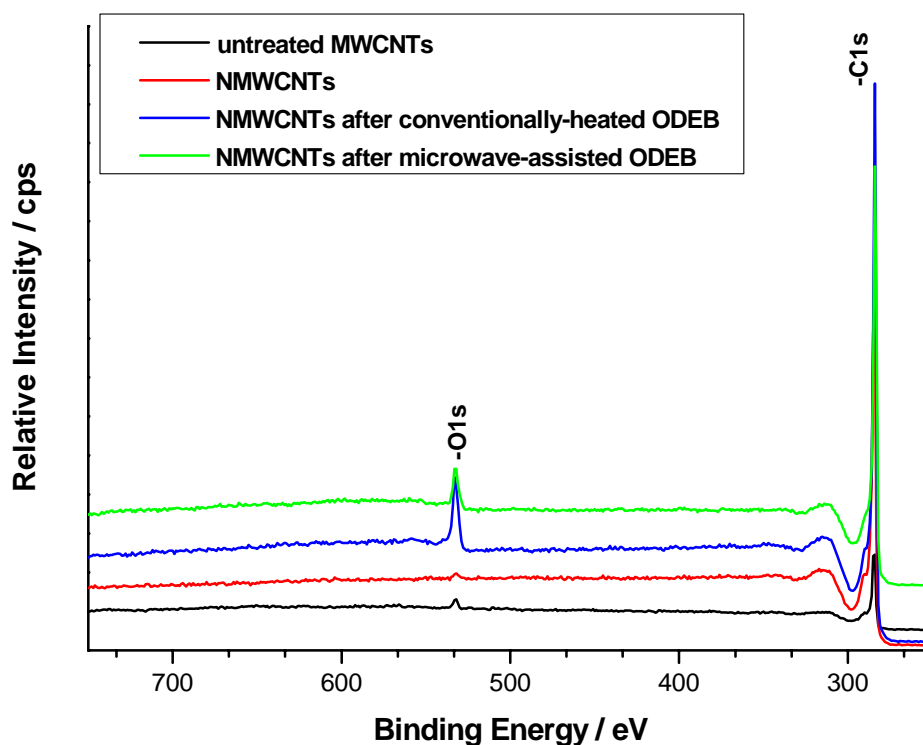


Figure 4.29. XPS Spectra of MWCNTs, NMWCNTs before and after conventionally-heated and microwave-assisted ODEB.

The examination of the bonding state on the surface of MWCNTs and NMWCNTs before and after conventionally-heated and microwave-assisted ODEB has been provided by XPS analysis. All samples exhibited only C1s and O1s XPS spectra around 288 and 533 eV respectively (Fig. 4.29). During the deconvolution of each spectrum it was found that the C1s peak is composed of four peaks, which could be assigned to graphitic carbon (284 eV), hydroxyl carbon (286 eV), carbonyl carbon (287 eV) and carboxyl carbon (288.9 eV), whereas the O1s peak revealed three different chemical environments for oxygen, assigned to C=O (531 eV), -OH (532 eV) and adsorbed water (534eV) (s. Appendix B). The results of peak areas analysis are summarized in Tab. 4.9.

Table 4.9

Component peaks and their attributions of XPS spectra as well as their calculated areas related to each sample.

Binding energy / eV	Chemical group	Peak area / % around 285 eV			
		untreated MWCNTs	NMWCNTs	NMWCNTs after conventionally-heated ODEB	NMWCNTs after microwave-assisted ODEB
284	C	71.26	62.07	68.92	70.09

286	C-O	16.56	27.12	19.83	19.07
287	C=O	6.91	6.60	6.79	6.43
288.9	-COOH-	5.26	4.22	4.46	4.40
	Oxygen	Peak area / % around 531 eV			
531	C=O	1.97	2.17	0.00	13.06
532	-OH	49.58	56.66	40.62	26.07
534	H ₂ O ^{adsorbed}	48.56	41.17	59.38	60.86

It is to be recognized, that the oxidative treatment of MWCNTs resulted in rising amount of oxidized carbon, associated with occurrence of new hydroxyl carbon (286 and 532 eV). However, the relation between peak areas of graphitic carbon and oxidized carbon in the samples after conventionally-heated and microwave-assisted ODEB seems to be similar to that observed before the oxidative treatment, probably due to the coke deposition (carbon – 284 eV). The analysis of the peak areas around 531 eV shows that approximately 13% of strongly basic C=O bonds, which are responsible for the dehydrogenating power of the catalyst [43], were generated during ODEB in microwave field. In contrast, only peaks, assigned to hydroxyl carbon and adsorbed water were observed in the O1s Spectra of MWCNTs after conventionally-heated ODEB. Massive appearance of C=O bonds could be explained by the influence of non-thermal microwave effect on the last elementary steps of reaction, whereas the activated oxygen reacts with the hydroxyl groups to re-form the basic, chinoidic oxygen functionalities accompanied by water desorption [12], as it was suggested by Maksimova (s. Appendix C). Presumably, the microwaves accelerate the water desorption process, generating the carbonyl active sites on the surface of carbon catalyst, and thus, more molecules of ethylbenzene could react with the oxygenated species at the prismatic planes leading to the more selective dehydrogenation to styrene.

4.4.4 Upshot

To summarize, the results of the practical investigations on the functionalization of MWCNTs in gas- and liquid-phases were reviewed. The MWCNTs treatment with oxygen in microwave field results in significant weight loss and volume decrease, however, the conventionally-heated oxidation leads only to an insignificant weight loss. Thus, the gas-phase oxidizing should be performed only in conventionally-heated reactor due to the destroying influence of microwave field on the cells of sp²-structural carbon material in

aggressive oxidizing environment. The OMWCNTs exhibited the highest styrene yield in microwave-assisted ODEB. Altogether, the catalytic activity of OMWCNTs was higher than that of untreated as well as iron loaded MWCNTs.

The graphite-like structure of MWCNTs remained intact after the oxidation with nitric acid. The stable styrene yield of 34% was obtained in conventionally-heated reactor with NMWCNTs, what is actually 3% higher than styrene yield obtained on CNT3 and OMWCNTs. Thus, the insignificant but definitely positive influence of the treatment with nitric acid on the catalytic activity is ascertained. Otherwise, the great enhancement in activity of catalyst pre-treated with nitric acid was observed in microwave field. NMWCNTs show a stable styrene yield of 58% during 80 h under reaction conditions. The XPS analysis of samples indicates the appearance of non-thermal microwave effect in the mechanism of ODEB, most likely by the water desorption, which enables new interaction of ethylbenzene with the catalyst.

References

- [1] A. Miyakoshi, A. Ueno, M. Ichikawa. *Appl. Catal. A* 216 (2001) 137-146.
- [2] I. Serafin, A. Kotarba, M. Grzywa, et al. *J. Catal.* 239 (2006) 137-144.
- [3] N. Dulamita, A. Maicananu, D. Sayle, et al. *Appl. Catal. A* 287 (2005) 9-18.
- [4] D. Hong, V. Vislovskiy, S. Park, et al. *Bull. Korean. Chem. Soc.* 26 (2005) 1713-1748.
- [5] X. Li, W. Li, K. Xie. *Catal. Lett.* 105 (2005) 223-227.
- [6] Y. Sakurai, T. Suzaki, N. Ikenaga, et al. *Appl. Catal. A* 192, (2000) 281-288.
- [7] Y. Sakurai, T. Suzaki, K. Nakagawa, et al. *J. Catal.* 209 (2002) 16-24.
- [8] V. Vislovskiy, J. Chang, M. Park, et al. *Catal. Comm.* 3 (2002) 227-231.
- [9] M. Park, V. Vislovskiy, J. Chang, et al. *Catal. Today* 87 (2003) 205-212.
- [10] Z. Fang, X. Cao, C. Li, et al. *Carbon* 44 (2006) 3368-3370.

- [11] D. Su, N. Maksimova, J. Delgado, et al. *Catal. Today* 102-103 (2005) 110-114.
- [12] N. Maksimova. PhD Dissertation, Berlin, Germany, 2002.
- [13] C. Chen, P. Hong, S. Dai, et al. *React. Kinet. Catal. Lett.* 61 (1997) 181-185.
- [14] X. Bi, P. Hong, X. Xie, et al. *React. Kinet. Catal. Lett.* 66 (1999) 381-386.
- [15] X. Zhang, D. Hayward, C. Lee, et al. *Appl. Catal. B* 33 (2001) 137-148.
- [16] X. Zhang, C. Lee, D. Mingos, et al. *Appl. Catal. A* 249 (2003) 151-164.
- [17] X. Zhang, D. Hayward. *Inorg. Chim. Acta* 359 (2006) 3421-3433.
- [18] X. Zhang, D. Hayward, D. Mingos. *Ind. Eng. Chem. Res.* 40 (2001) 2810-2817.
- [19] P. Li, T. Li, J. Zhou, et al. *Micro. Mes. Mater.* 95 (2006) 1-7.
- [20] Max-Planck-Gesellschaft. Press information: PRI C 23 / T 15 / 2002 (99).
- [21] N. Maksimova, G. Mestl, R. Schlögl. *Stud. Surf. Sci. Catal.* 133 (2001) 383-389.
- [22] M. Pereira, J. Orfão, J. Figueiredo. *Appl. Catal. A* 184 (1999) 153-160.
- [23] M. Pereira, J. Orfão, J. Figueiredo. *Appl. Catal. A* 196 (2000) 43-54.
- [24] M. Pereira, J. Orfão, J. Figueiredo. *Appl. Catal. A* 218 (2001) 307-318.
- [25] M. Pereira, J. Orfão, J. Figueiredo. *Coll. Surf. A: Physicochem. Eng. Aspects* 241 (2004) 165-171.
- [26] D. Su, N. Maksimova, G. Mestl, et al. *Carbon* 45 (2007) 2145-2151.
- [27] B. David, N. Pizúrová, O. Schneeweiss, et al. *J. Alloys Comp.* 378 (2004) 112-116.
- [28] F. Yu, J. Wang, Z. Sheng, et al. *Carbon* 43 (2005) 3018-3021.
- [29] E. Rakov. *Russ. Chem. Rev.* 76 (2007) 1-22.
- [30] J. Cheng, X. Zhang, G. Yi, et al. *J. Alloys Comp.* 455 (2008) 5-9.
- [31] R. Cornell, U. Schwertmann. *The Iron oxides*. VCH Publishers, New York (1996) 175.
- [32] T. Yang, R. Brown, L. Kempel, et al. *J. Magn. Magn. Mater.* X (2008) XX-XX.
- [33] O. Shekhah, W. Ranke, A. Schüle, et al. *Angew. Chem. Int. Ed.* 42 (2003) 5760-5763.
- [34] S. Sun, H. Zeng, D. Robinson, et al. *J. Am. Chem. Soc.* 126 (2004) 273-279.
- [35] A. Rasheed, J. Howe, M. Dadmun, et al. *Carbon* 45 (2007) 1072-1080.
- [36] Z. Yu, L. Brus. *J. Phys. Chem. A* 141 (2004) 113-122.
- [37] F. Mercury, A. Sgamellotti. *Inorg. Chim. Acta* 360 (2007) 785-793.
- [38] I. Rosca, F. Watari, M. Uo, etc. *Carbon* 43 (2005) 3124-3131.
- [39] T. Ros, A. van Dillen, J. Geus, etc. *Chem. Eur. J.* 8 (2002) 1151-1162.
- [40] B. Clare, D. Kepert. *Inorg. Chim. Acta* 343 (2003) 1-17.
- [41] R. Giordano, P. Serp, P. Kalck, et al. *Eur. J. Inorg. Chem.* 4 (2003) 610-617.
- [42] B. Nigrovski, U. Zavyalova, P. Scholz, et al. *Carbon* 46 (2008) 1678-1686.

[43] N. Keller, N. Maksimova, V.Roddatis, et al. *Angew. Chem. Int. Ed.* 41 (2002) 1885-1888.

Chapter 5. Microwave-assisted synthesis of magnetite nanoparticles used as a catalyst for the irradiated pyrolysis of carbon nanotubes in fluidized-bed reactor

In the previous chapters the application of catalytic systems based on MWCNTs for conventionally-heated as well as microwave-assisted ODEB was investigated, and the highest catalytic activity on MWCNTs oxidized with nitric acid was observed. The MWCNTs were received commercially; however there are all necessary conditions in our institute to produce the MWCNTs of better properties and by use of alternative energy sources. Moreover, what a deductive idea to perform industrially important reactions in microwave-assisted reactor on

the carbon nanomaterials which could be synthesized via irradiated pyrolysis on the magnetite nanoparticles prepared by the hydrothermal process using also microwave as energy source?

"I think it would be a good idea."

Mahatma Gandhi

In this chapter the preparation of magnetite nanoparticles through irradiated hydrothermal process as well as their further application as the catalyst for the synthesis of carbon nanotubes in microwave-assisted fluidized-bed reactor is observed in order to complete this science research related to the application of microwave heating in gas-phase heterogeneous catalysis as well as in the synthesis of nanomaterials.

5.1 Selection of the MWCNTs preparation method

There are three general methods to synthesize CNT: arc-discharge, laser-ablation and catalysis. The arc-discharge method is the simplest and most common method. However, during the preparation many side products are formed, such as fullerenes, amorphous carbon and graphite sheets; and the separation procedures of high costs are required to recover the CNT from the crude product containing soot, catalytic metals and various side products [1-4]. The advantages of the laser-ablation method are as follows: relatively high purity single wall CNT are synthesized, room temperature is feasible with a continuous laser beam and the conditions are easily optimized by modifying the nature of the gas and its pressure [5-6]. However, this technique is suitable only for the lab-scale synthesis of single-wall CNT. MWCNT growth is impossible and the scale up is not feasible since a laser is required and capital costs will become too high. Chemical vapour deposition (CVD) is considered to be the most promising process for low-cost and large-scale synthesis of high quality CNT, either in the thermal mode or the plasma enhanced CVD mode [7-10]. The other methods such as the electrolysis, the chemical reduction of certain organic derivatives with alkali and alkaline-earth metals, the chlorination of metal carbides or the thermal exfoliation play far less important roles [11].

The CVD technique involves the decomposition of hydrocarbons on heating in the presence of catalyst, which can proceed through many routes to ultimately yield elemental carbon. The hydrocarbon enters the reactor with an inert gas under different conditions, namely, the temperature of the process may vary nearly ambient to above 1000 °C, while the

pressure may be both below and above the atmospheric pressure. The most common catalysts used for CVD are iron, nickel or cobalt, because the carbon has a low solubility in these materials at high temperatures and thus the carbon will precipitate to form nanotubes. The simplest and most frequently applied method is the CVD with powder catalysts. The two main reactor types used for CNT synthesis by CVD are fixed and fluidized beds. The latter are most popular because of several reasons. Firstly, the fluidized bed technique provides a large effective surface area and a large amount of space for CNT growth. Secondly, the excellent temperature uniformity could be achieved in fluidized bed reactor due to a good mixing. Recent studies [12-17] reported the fluidized bed synthesis of MWCNTs using bulk catalysts. In most cases iron nanoparticles were found as a perfect catalyst for fluidized bed CVD and high carbon yields greater than 75% were obtained [12-13,15]. However, all these investigations were performed in conventionally-heated reactors mercilessly disregarding the alternative energy sources such as microwave heating. In order to fill a gap in this field the first practical investigations on topic “MWCNTs synthesis on magnetite nanoparticles in microwave-assisted fluidized-bed reactor by catalytic pyrolysis” are given below.

5.2 Synthesis of magnetite nanoparticles

The choice of the efficient catalyst seems to be the one of the most important tasks. It should exhibit not only the highest yield, but also have the great dielectric properties. Several catalysts such as Ni, Cu, Mo and Fe dispersed upon different substrates such as Al_2O_3 , SiO_2 and MgO have been used in CVD. The nanoparticles of elemental iron as well as its compositions with molybdenum on various supports were found to be the most suitable for CVD at the atmospheric pressure [11]. A simple model for the gas-phase synthesis of carbon nanotubes on iron oxide nanoparticles in the presence of carbon monoxide has been developed by Celnik et al. [18].

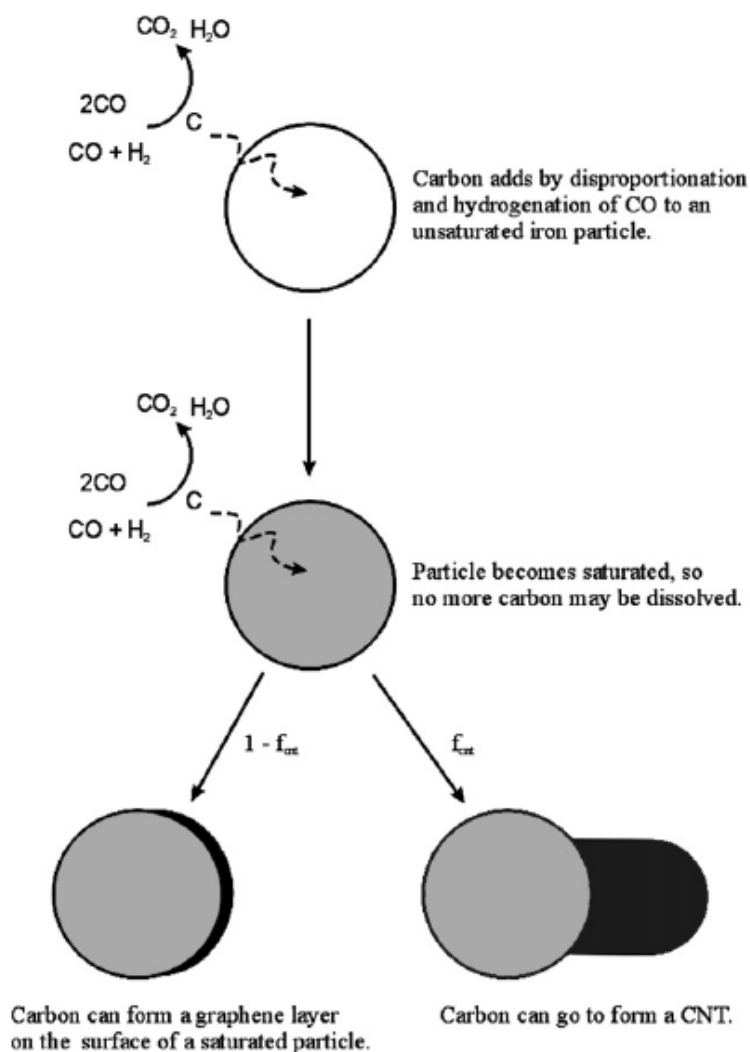


Figure 5.1. Scheme of carbon paths on a catalyst particle. Adapted from Celnik [18].

Fig. 5.1 shows the formation scheme of carbon nanotubes on iron catalyst nanoparticles. It can be seen, that the deposits appear to be formed by a thermal catalytic mechanism in which CO decomposes to carbon at the surface of iron particles. The carbon diffuses through these particles and precipitates as more or less graphitic filaments which as they grow often carry the particle at their head. The same conversion of hydrocarbons to carbon on iron was observed during the decomposition of various gas phase precursors, such as methane [19], carbon dioxide [20] and ethene [21]. At last, it was found that the magnetite, which exceptional dielectric properties are well known, could also lead to the carbon deposition from a large vary in precursors such as CO₂, CO, CH₄, C₂H₆ and C₂H₂ at temperatures of 300-1000 °C [22-25]. The deposition of carbon occurred on the metallic iron (Fe²⁺/Fe³⁺ sites) formed in the magnetite under reaction conditions. Therefore, the nanoparticles of magnetite are proposed to be the great catalyst for the production of

MWCNTs in microwave field. However, the quantity and quality of MWCNTs depends not only on the synthesis conditions and catalyst structure, but also on the diameter of the catalyst particles [11]. Thus, to grow MWCNTs with diameter not larger than 10 nm the magnetite particles of 15-27 nm should be prepared.

Synthesis

The highly crystalline magnetite nanoparticles were prepared by the microwave-assisted hydrothermal process [26-27]. The materials used were ferrous chloride ($\text{FeCl}_2 \cdot 4\text{H}_2\text{O}$), sodium hydroxide (NaOH), hydrazine hydrate ($\text{H}_4\text{N}_2 \cdot \text{H}_2\text{O}$) and distilled water. The synthesis was performed as followed:

- I. $\text{FeCl}_2 \cdot 4\text{H}_2\text{O}$ (0.5150 g) was dissolved in 13 ml of distilled water, which was earlier degassed with continuous nitrogen flow approximately for half an hour. The solution A of the yellowish colour was obtained.
- II. NaOH (0.2609 g) was dissolved in 2.174 ml of $\text{N}_2\text{H}_4 \cdot \text{H}_2\text{O}$. Colourless solution B was obtained.
- III. The solution B was dropped into Teflon[®] vessel with the solution A in nitrogen atmosphere. Green precipitate immediately appeared in aqueous solution of Fe (II) ions.
- IV. The vessel was closed with a lid to keep the nitrogen atmosphere in the system and put into a Milestone ETHOS TC microwave digestion system. The sample was kept at the temperature of 100°C for 2 h and then naturally cooled to room temperature.
- V. Colourless transparent solution with black colloids in the bottom was obtained. To separate the particles triple stage centrifugation was applied. The sample was washed with distilled water twice and once with ethanol.
- VI. Finally, the sample was dried in the vacuum oven at room temperature for 2 days.

Characterization

Prepared sample was characterized by XRD using an X-Ray diffractometer (Model X'Pert PRO Philips, Eindhoven, Netherlands) and TEM (Philips XL-30). The XRD pattern

shows that the sample is a pure magnetite without impurity phases (Fig.5.2a). The average particles size calculated using the Debye - Scherrer formula from the reflection peak (2 2 2) is approximately 28 nm. The procedure of microwave-assisted hydrothermal synthesis of magnetite was repeated in four vessels in order to obtain more material for the further investigations as well as characterization procedures. The XRD of the black powder prepared to prove out the method (Fig. 5.2b) seems to be absolute identical to the XRD pattern of the initially obtained sample.

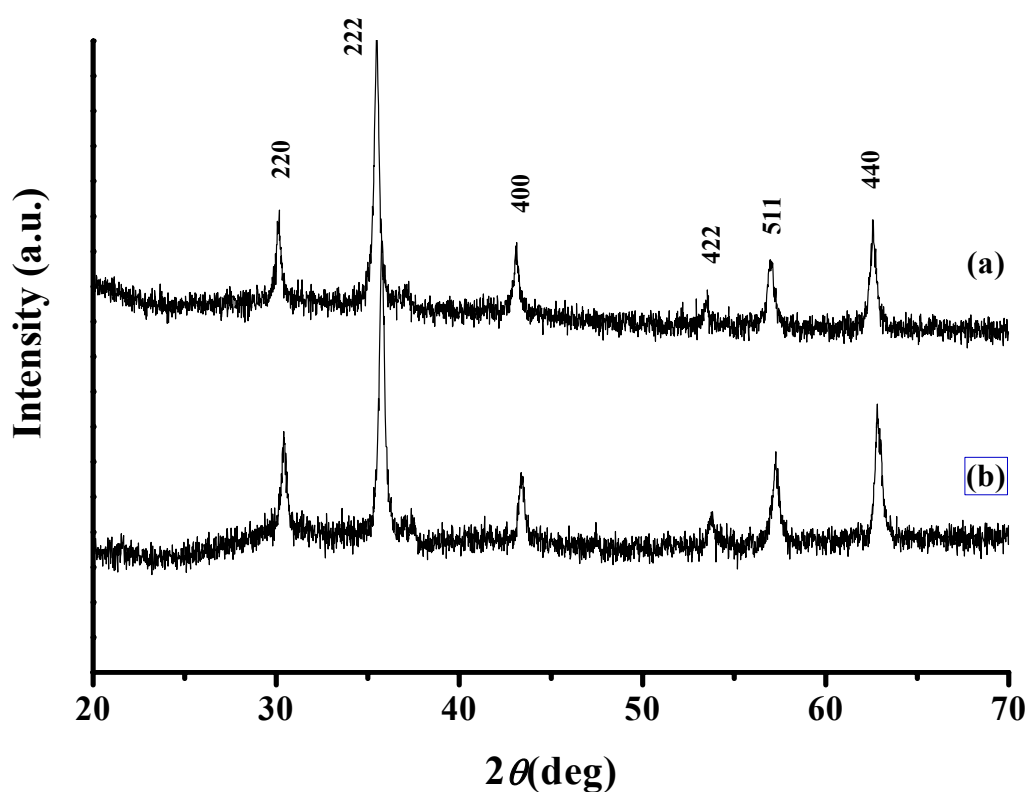


Figure 5.2. XRD patterns of samples obtained during the initial (a) and repeated (b) synthesis.

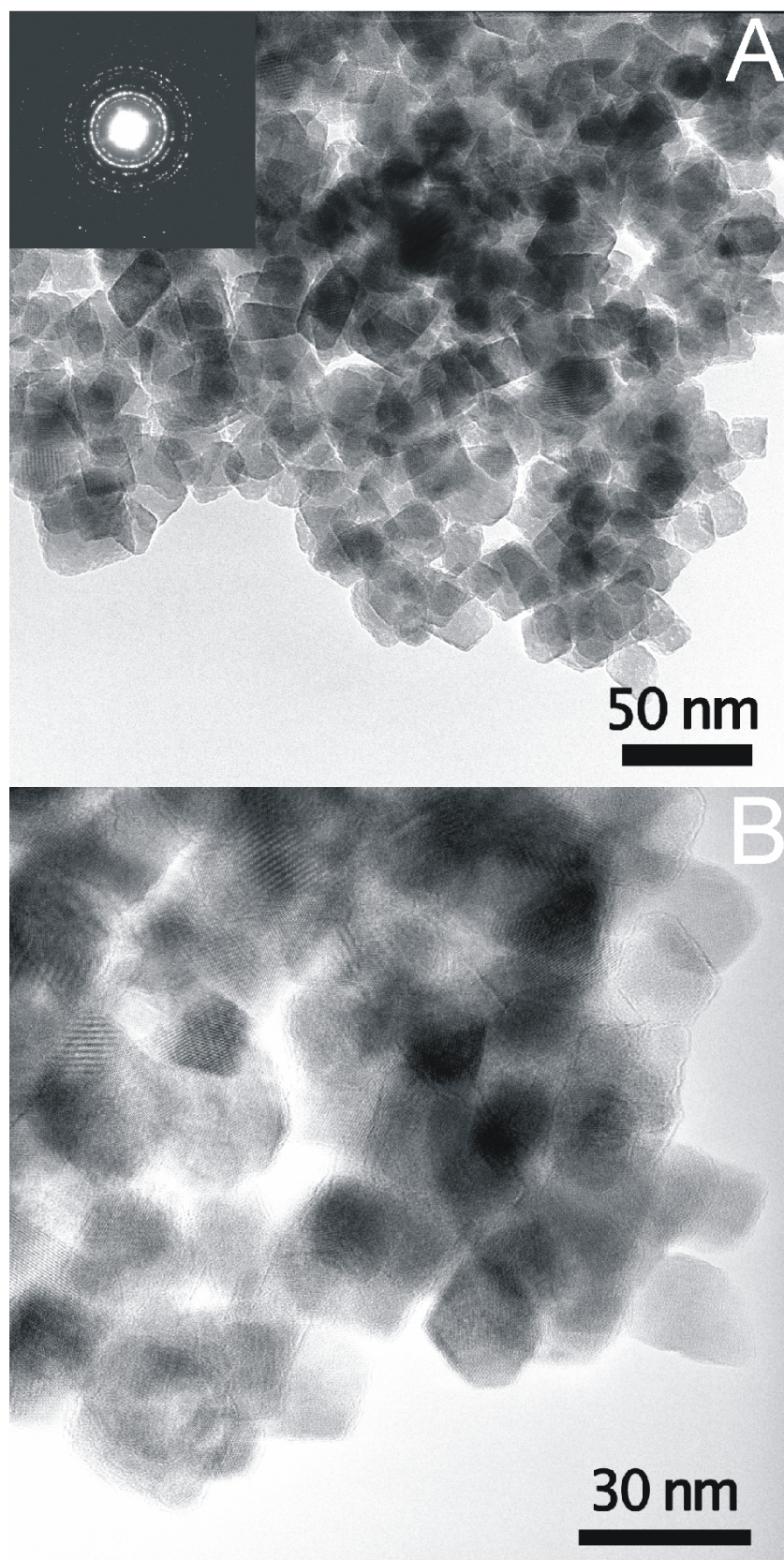


Figure 5.3. (A) TEM image of magnetite produced by microwave assisted hydrothermal synthesis. (B) HRTEM image of the sample. The inset of (A) shows the SAED pattern of magnetite nanoparticles.

The size and morphology of synthesized magnetite were examined by TEM. Fig. 5.3 shows the typical TEM photograph of Fe_3O_4 nanocrystallines. It seems to be, that all nanoparticles are spherical and the average size of those is approximately 15-20 nm in contrast to 28 nm obtained by analysis of XRD pattern. The inset showing the SAED pattern of the magnetite nanoparticles taken on a mass of Fe_3O_4 reveals the crystallinity of the sample, which can be indexed to the pure octahedral phase of magnetite.

5.3 Microwave-assisted fluidized-bed reactor

A schematic drawing of the microwave-assisted fluidized-bed reactor is depicted in Fig. 5.4. The reactor is made of quartz, with an inner diameter of 20 mm and height of 500 mm. The catalyst is located between two flaps in order to avoid the loss of nanomaterials. Additionally, the bag filter is installed above the reactor to collect the nanoparticles of catalyst or carbon penetrated through the top flap. The flow rates of working gases are regulated by electronic flow controllers. Pressure sensors allow monitoring the differential pressure drop between the bottom and top parts of the reactor. The operating procedure is quite simple: initially a controlled amount of particles is loaded into the reactor and then a bed fluidized with a constant flow rate of pure nitrogen and heated by microwave (MLS-ETHOS 1600; 1000 W). As soon as the thermal regime reached, the flow rate of nitrogen is lowered to a pre-calculated value of deposition and simultaneously the hydrocarbon is introduced into the bed. In case of the application of liquid carbon sources such as ethanol the saturator is also installed.

The process of hydrocarbon decomposition will be performed under different conditions. Particularly, the pyrolysis is recommended to be carried out at a reduced total pressure in the system and a low partial pressure of the main reagent in order to minimize the non-catalytic decomposition of gaseous monoatomic and hereatomic hydrocarbons. However, for industrial applications it would be desirable to work at atmospheric pressure, and therefore, the synthesis is reasonable to perform at the pressure close to atmospheric

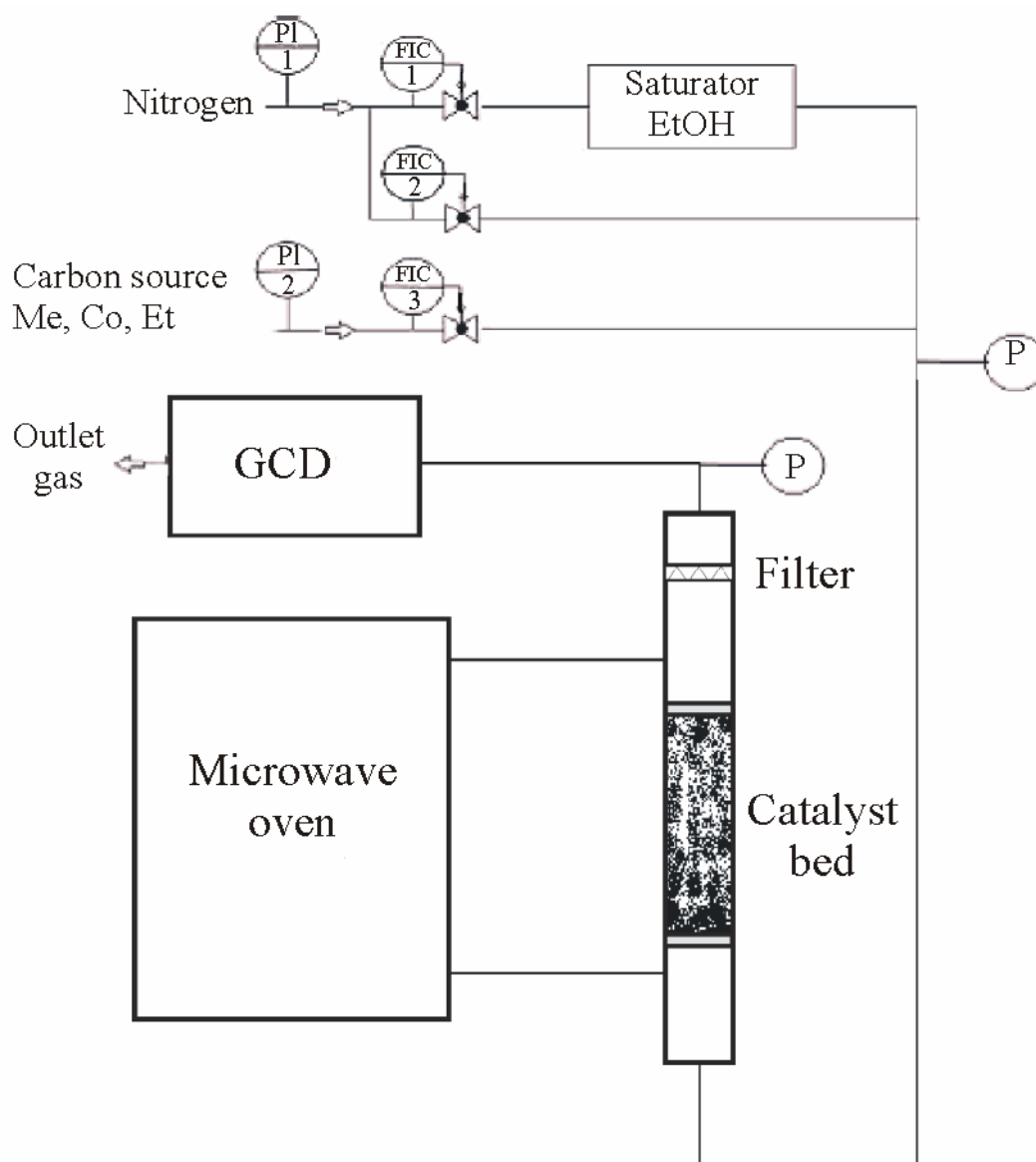


Figure 5.4. Schematic draw of the microwave assisted catalytic CVD system.

5.3 Fluidization characteristics of the magnetite nanopowder in fluidized-bed reactor

The fluidization characteristics of the magnetite nanopowder (Sigma-Aldrich) in a microwave-assisted fluidized-bed laboratory reactor were performed in order to investigate the suitable conditions of the fluid catalyst bed at which the deposition of hydrocarbons into MWCNTs will be carried out. The minimal fluidization velocity for the bulk is given by [26]:

$$u_w = \frac{\varepsilon_w^4 \cdot (1 - \varepsilon_w) \cdot g \cdot (\rho_T - \rho_f) \cdot d^2}{12 \cdot \Psi \cdot \nu \cdot \rho_f}$$

where g is the gravitational acceleration, ρ_T – density of the catalyst material, ρ_f – density of fluid, Ψ – form factor, d – particle diameter, ν – kinematic viscosity of fluid and ε_w – pores volume. Considering the nano scale of the material, ε_w could be approximated on pore volume of the material in dormant state:

$$\varepsilon = \frac{\rho_T - \rho_S}{\rho_T}$$

where ρ_S is the bulk density.

For the calculation of pressure drop across the bed two equilibriums from different sources [28-29] were used:

$$\Delta p_1 = \frac{h_0 \rho_f w^2 c_w}{2d}$$

$$\Delta p_2 = \frac{3}{2} \cdot \frac{1 - \varepsilon}{\varepsilon^3 \Psi} \left(\frac{133}{\text{Re}} + 2,34 \right) \frac{h_0}{d} \cdot \frac{\rho_f w^2}{2}$$

where Re is Reynolds number, w – average stream velocity, h_0 – the height of fill and c_w – the resistance coefficient of bulk. Since the resistance coefficient is a function of Reynolds number, the c_w could be given by:

$$c_w = \Psi \cdot \frac{24}{\text{Re} \cdot \varepsilon^4}$$

The main properties of fluid and bulk are given in Table 5.1. The magnetite nanoparticles mean diameter is about 25 nm, and their minimum fluidization velocity (for $\text{Re} < 2$) at room temperature is $8.54 \cdot 10^{-9}$ m/s. However, such a low velocity seems to be problematic to achieve on the operating set-up. Thus, the experiments were carried out in a fluidized-bed reactor at a gas flow from 0.1 to 45 l/h. Table 5.2 presents the bed characteristics of magnetite under operating conditions. The results show that the pressure drop increases as the gas flow increases. A similar trend was obtained for Reynolds number.

Table 5.1

The main properties of fluid and bulk.

ρ_T kg/m ³	ρ_S kg/m ³	ρ_f kg/m ³	ε	Ψ	ν 10 ⁻⁶ m ² /s	d 10 ⁻⁹ m	u_w 10 ⁻¹² m/s
5,12	0,777	1,251	0,848	~1	16,33	25	8,54

Table 5.2

Bed characteristics of magnetite.

h_0 m	V l/h	w 10 ⁻⁵ m/s	Re 10 ⁻⁶	Δp_1 10 ⁶ kg/m·s ²	Δp_2 10 ⁶ kg/m·s ²
~0,02*		0,1	8,85	0,14	1,34
~0,02*		0,2	17,69	0,27	2,68
~0,02*		0,3	26,54	0,41	4,02
~0,02*		0,4	35,39	0,54	5,36
~0,02*		0,5	44,23	0,68	6,70
~0,02*		0,6	53,08	0,81	8,04
~0,02*		0,7	61,92	0,95	9,38
~0,02*		0,8	70,77	1,08	10,72
~0,02*		0,9	79,62	1,22	12,06
~0,02*		1	88,46	1,35	13,40
~0,02*		1,1	97,31	1,49	15,48
0,021		1,3	115,00	1,76	19,16
0,022		2	176,93	2,71	29,48
0,023		5	442,32	6,77	77,05
0,024		8	707,71	10,83	128,65
0,025		10	884,64	13,54	167,51
0,026		20	1769,29	27,09	348,42
0,029		25	2211,61	33,86	485,77
0,035		30	2653,93	40,63	703,53
0,05		35	3096,25	47,40	1172,55
0,06		45	3980,89	60,94	1809,08

* The measurement of the increase of bulk height is complicated

The difference in values of pressure drop calculated by equations from different sources is insignificant and could be related to the integral error. At the gas flow higher than 4 l/h the powder fountains of different height were observed, concluding that the extensive mixing of the material occurred. The dependence of the pressure drop on the volumetric flow rate is presented in Fig. 5.3. Continuous increase in the pressure drop as well as the assembly of magnetite powder observed on the filter after the experiments indicates that the fluidization process is located in the stage of bulk discharge.

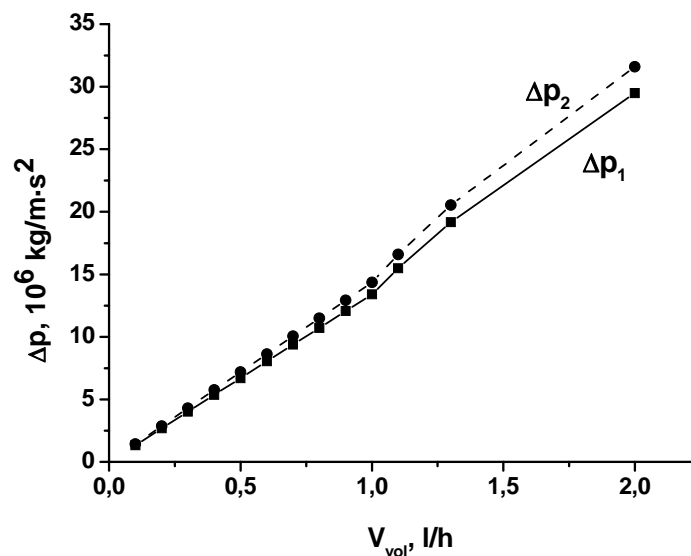


Figure 5.5. The dependence of the pressure drop on the volumetric flow rate.

5.5 Upshot

Microwave-assisted fluidized-bed reactor for the preparation of carbon nanotubes by CVD is presented. Fe_3O_4 was chosen as the perfect candidate for the catalyst due to its exceptional microwave dielectric properties. The magnetite particles with average size of 15-20 nm were successfully prepared by the microwave-assisted hydrothermal process, and the preparation time was three times shorter than that using the conventional heating [26-27]. The fluidization characteristics of nano-scaled Fe_3O_4 in the microwave-assisted fluidized-bed reactor were found and at higher velocities the insignificant discharge of the bulk was observed. Finally, the first tests with magnetite nanoparticles were successfully performed in new microwave-assisted fluidized bed reactor and are revealed a perfect fundamental for the further investigations.

References

- [1] S. Iijima. *Nature* 354 (1991) 56-58.
- [2] V. Popov. *Mater. Sci. Eng. Reports* 43 (2004) 61-102.
- [3] T. Ebbesen, P. Ajayan. 358 (1992) 220-222.
- [4] S. Iijima, T. Ichihashi. *Nature* 363 (1993) 603-605.
- [5] A. Thess, R. Lee, P. Nikolaev, et al. *Science* 273 (1996) 483-485.
- [6] T. Guo. *Chem. Phys. Lett.* 243 (1995) 49-54.
- [7] M. Perez-Cabero, D. Kuvshinov, A. Ruiz, et al. *Mater. Res. Bulletin* 43 (2008) 1737-1742.
- [8] K. Kouravelou, S. Sotirchos, X. Verykios. *Surface Coat. Technol.* 201 (2007) 9226-9231.
- [9] S. Inoue, Y. Kikuchi, Y. Matsumura. *Diamond Related Mater.* (2008) in Press.
- [10] K. Hata, D. Futaba, K. Mizuno, et al. *Science* 306 (2004) 1362-1369.
- [11] E. Rakov. *Russian Chem. Rev.* 76 (2007) 1-7.
- [12] Y. Wang, F. Wie, G. Luo, et al. *Chem. Phys. Lett.* 364 (2002) 568-572.
- [13] A. Weidenkaff, S. Ebbinghaus, P. Mauron, et al. *Mater. Science Eng. C* 19 (2002) 119-123.
- [14] B. Liu, Q. Liang, T. Shui Hua, et al. *Chinese J. Chem.* 19 (2001) 983-986.
- [15] M. Corrias, B. Caussat, A. Ayrat, et al. *Chem. Eng. Science* 58 (2003) 4475-5582.
- [16] Q. Weizhong, L. Tang, W. Zhanwen, et al. *Appl. Catal. A* 260 (2004) 223-228.
- [17] G. Ning, F. Wei, G. Luo, et al. *Appl. Catal. A* 78 (2004) 955-959.
- [18] M. Celnik, R. West, N. Morgan, et al. *Carbon* 46 (2008) 422-433.
- [19] U. Narkiewicz, W. Arabczuk, W. Konicki, et al. *Rev. Adv. Mater. Sci.* 8 (2004) 53-58.
- [20] I. Morjan, I. Soare, R. Alexandrescu, et al. *Inf. Phys. Tech.* 51 (2008) 186-197.
- [21] S. Hoffmann, M. Cantoro, B. Kleinsorge, et al. *J. Appl. Phys.* 98 (2005) 34308-34315.
- [22] G. Allen, K. Hallam. *J. Nucl. Mater.* 252 (1998) 135-144.
- [23] J. Geng, D. Jefferson, B. Johnson. *Chem. Comm.* (2004) 2442-2443.
- [24] C. Zhanga, S. Lib, L. Wang, et al. *Mater. Chem. Phys.* 62 (2000) 44-51.
- [25] E. Yamasue, H. Yamaguchi, H. Okumura, et al. *J. Alloys Comp.* 434-435 (2007) 803-805.
- [26] T.J. Daou, G. Pourroy, et al. *Chemical Materials.* 18 (2006) 4399-4404.
- [27] J. Wang, J. Sun, Q. Sun, et al. *Materials Research Bulletin* 38 (2003) 1113-1118.
- [29] А. Касаткин. Основные процессы и аппараты химической технологии. Издательство Химия, Москва (1973) 107-112.

Chapter 6. Conclusions

In the present work, the application of microwave irradiation as an alternative heating source in gas-phase heterogeneous catalysis was investigated. The catalytic activity of various composites such as untreated, iron loaded and functionalized multi-wall carbon nanotubes as well as mixtures of magnetite and hematite nanopowders was tested in conventionally-heated and microwave-assisted ODEB to styrene. The comparative characterizations of catalysts before and after reaction with TEM, XPS, XRD and BET surface area techniques allowed to develop a structure-activity relationship as well as to determine the influence of microwave field on the morphology and catalytic properties of prepared systems.

Iron oxide with a particle size less than 10 nm and almost isometric morphology was successfully supported on the outer surface of the MWCNTs by the simple impregnation method. The highest ethylbenzene conversion and styrene selectivity were found for the catalyst with 3 wt.% Fe_2O_3 in the temperature range 380 - 450 °C. All prepared samples exhibited higher and more stable styrene selectivity under microwave conditions than that obtained using conventional heating at the same reaction conditions. In comparison to the large amounts of high disordered carbon displaced on the top layer of the catalyst during conventionally-heated ODEB no carbon deposition on the catalyst surface was observed for the microwave-assisted reaction. Apparently, the continuous burning of the disordered carbon leads to the higher styrene selectivity compared with that which was received with conventional heating. It was found that under microwave reaction conditions the conversion of Fe_2O_3 nanoparticles supported on MWCNTs into carbon-encapsulated iron crystals occurred at temperatures by about 400 °C lower than that obtained in conventionally-heated reactors. Alluding to these results, it was assumed that microwave-assisted ODEB with unpromoted Fe_2O_3 nanoparticles could lead to the conversion of iron oxide into carbon-encapsulated iron crystals, which play the role of active catalyst for this reaction.

The mixtures of hematite and magnetite nanopowders were prepared by the common mixing. All samples exhibited higher ethylbenzene conversion and styrene selectivity using microwave radiation than those obtained in conventionally-heated reactor. The nanoparticles of magnetite exhibited higher catalytic activity than micro-scaled particles. The change of volume flow rate from 8.5 to 1.1 l/h influenced positively on the ethylbenzene conversion in conventionally-heated and microwave assisted ODEB over HEM25, while the styrene selectivity decreased rapidly under both reaction conditions. The highest ethylbenzene conversion was found for HEM25 during the steady state tests at 350 °C. All samples

exhibited unstable styrene selectivity decreased continuously after 3h of time on stream for both heating methods. Moreover, the oxidation of Fe_3O_4 to $\gamma\text{-Fe}_2\text{O}_3$ as well as the formation of highly disordered carbon was observed during the post reaction characterization. Altogether, the catalytic results of prepared iron oxide mixtures in ODEB seems to be not really encouraged, as soon as the expected iron oxide reduction to iron and its further encapsulation with graphite layers did not occur.

Different methods of oxidizing treatment were used to improve the catalytic properties of MWCNTs in ODEB. It was found that treatment of MWCNTs with oxygen should be performed only in conventionally-heated reactor because the use of microwave irradiation results in significant weight loss and volume decrease. OMWCNTs exhibited the highest styrene yield in microwave-assisted ODEB. Altogether, the catalytic activity of OMWCNTs was higher than that of untreated as well as iron loaded MWCNTs.

The graphite-like structure of MWCNTs remained intact after the oxidation with nitric acid. The stable styrene yield of 34% was obtained in conventionally-heated reactor with NMWCNTs, what is actually 3% higher than styrene yield obtained on CNT3. Thus, the insignificant but definitely positive influence of the treatment with nitric acid on the catalytic activity is ascertained. Otherwise, the great enhancement in activity of catalyst pre-treated with nitric acid was observed in microwave field. NMWCNTs show a stable styrene yield of 58% during 80 hours under reaction conditions. The bonding state on the surface of MWCNTs and NMWCNTs before and after conventionally-heated and microwave-assisted ODEB was examined. The XPS analysis indicates the appearance of non-thermal microwave effect in the mechanism of ODEB, most likely by the water desorption, which enables new interaction of ethylbenzene with the catalyst.

The power consumption of each reactor was measured and it was found, that the energy efficiency of microwave heating method is more than four times higher than the conventional procedure considering the production of 1 gram of styrene over 5 cm^3 of catalyst under the same reaction conditions.

The magnetite particles with average size of 15-20 nm were successfully prepared by the microwave-assisted hydrothermal process, and the preparation time was three times shorter than that using the conventional heating. The fluidization characteristics of nano-scaled Fe_3O_4 in the microwave-assisted fluidized-bed reactor were found and at higher velocities the insignificant discharge of the bulk was observed. Finally, the first tests with magnetite nanoparticles were successfully performed in new microwave-assisted fluidized-bed reactor and are revealed a perfect fundamental for the further investigations.

Appendix A. Energy consumption during 80-hour test for both heating methods

Type of reactor	Energy needed to heat the whole volume of the reactor during 80h test		
	$V_{\text{reactor.}} / \text{cm}^3$	$E_{80\text{h}} / \text{kWh}$	$E_{80\text{h}} / \text{MJ}$
conventionally-heated	90	0,247	0,8892
microwave-assisted	39270	48	172,8

Energy needed to heat 5 cm ³ of catalyst during 80h test	
$V_{\text{cat.}} /$	$E_{80\text{h}} / \text{MJ}$
5	0,053
5	0,022

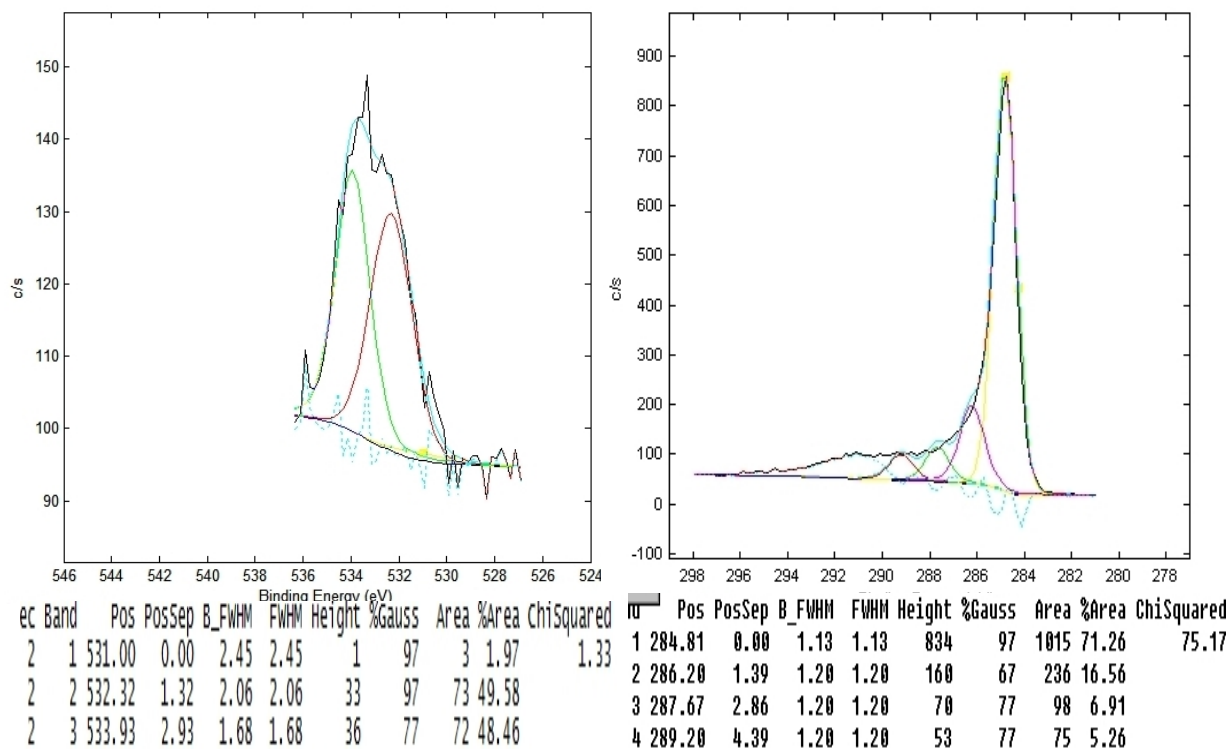
Reactor	Productivity of the catalyst during the 80h test			
	$V_{\text{EB}} / \text{l/h}$	$M_{\text{EB}} / \text{g/h}$	Yield / %	$M_{\text{ST}} / \text{g/h}$
conventionally-heated	0,0264	0,122	33,75	0,041
microwave-assisted	0,0264	0,122	60,5	0,073

Energy needed to produce 1 g of styrene over 5 cm ³ of catalyst in one hour	
E^* / MJ	
	0,016
	0,0038

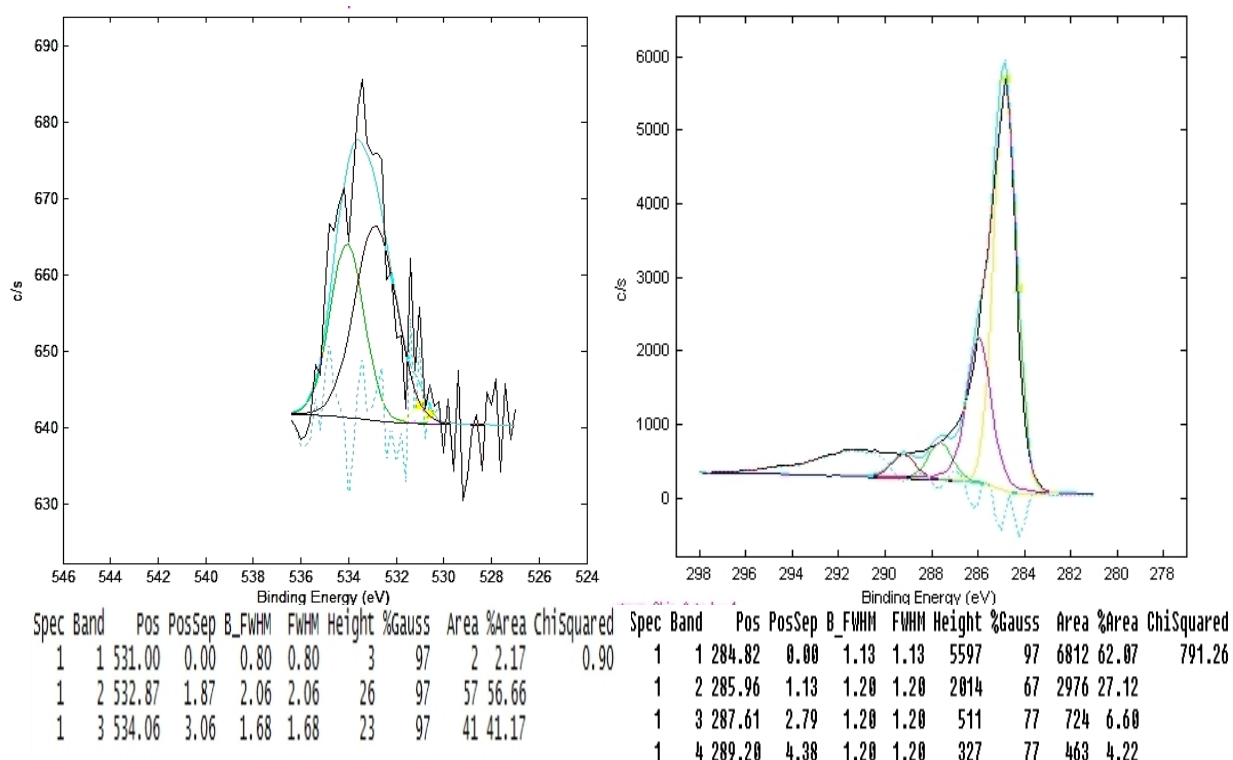
The power consumption of microwave heating method is 4.2 fold higher than that under conventional reaction conditions considering the production of 1 gram of styrene over 5 cm³ of catalyst under the same reaction conditions.

Appendix B. Deconvolution of C1s and O1s XPS spectra around 288 and 533 eV respectively

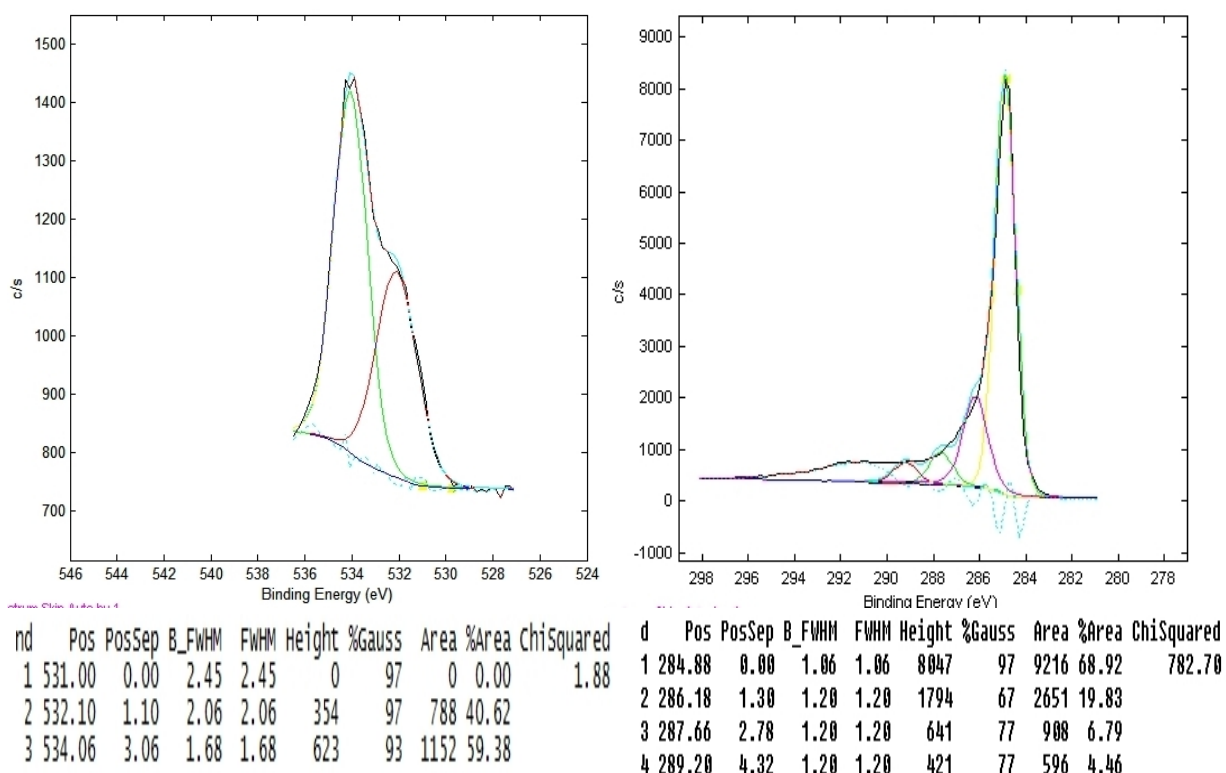
1. Untreated MWCNTs



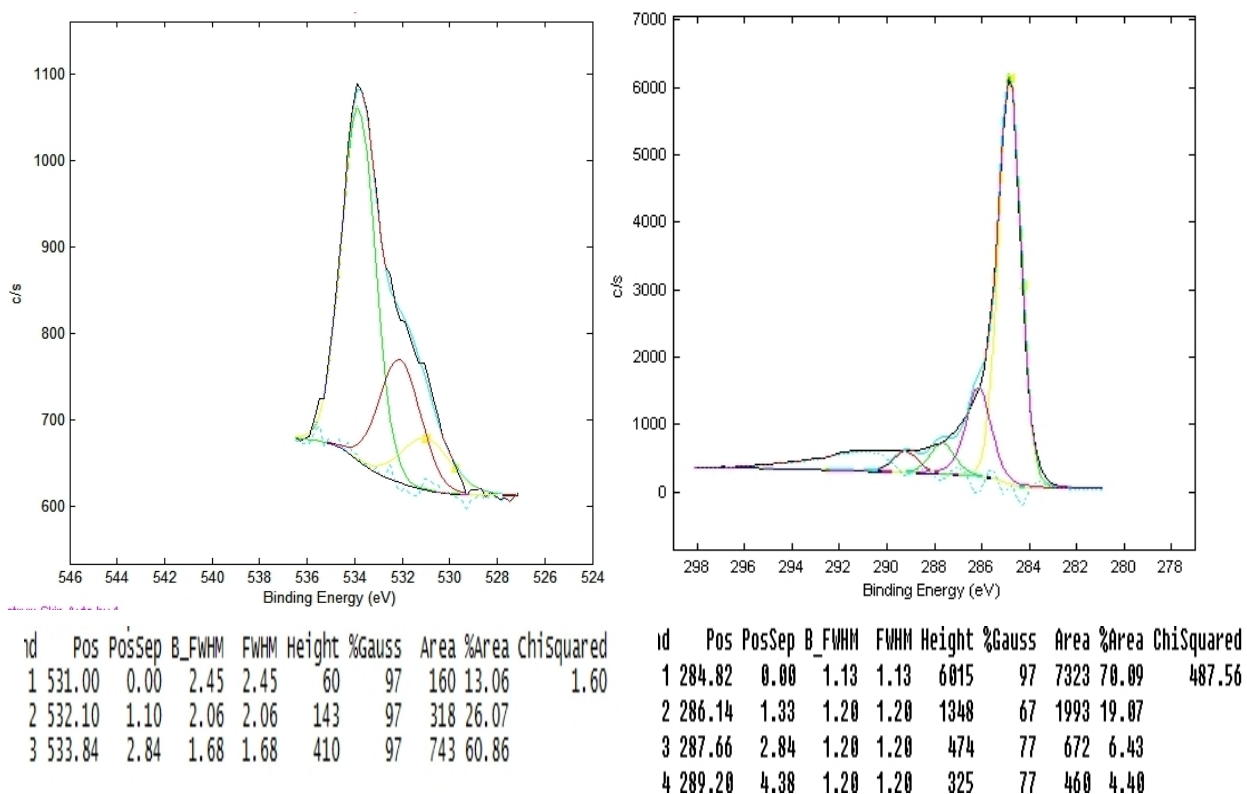
2. NMWCNTs before ODEB



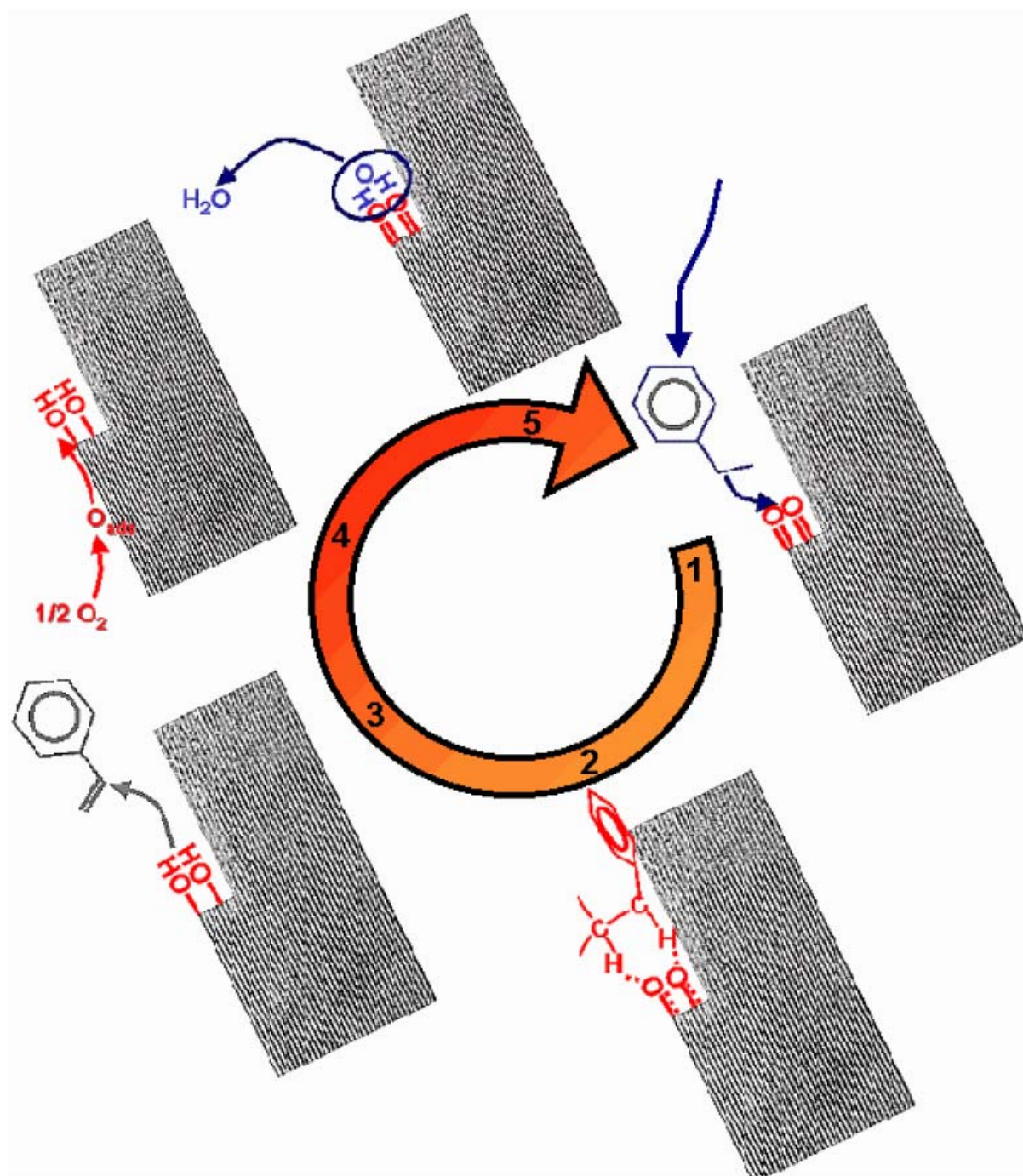
3. NMWCNTs after conventionally-heated ODEB



4. NMWCNTs after microwave-assisted ODEB



Appendix C. Schematic drawing of the catalytic ODEB over carbon nanofilaments by Maximova et al. [12]



- 1 - Adsorption of ethylbenzene
- 2 - Dehydrogenation at basic centers
- 3 - Desorption of styrene
- 4 - Adsorption of oxygen and reaction with OH groups
- 5 - Desorption of water.

Appendix D. Abbreviations

ODEB – Oxidative Dehydrogenation of Ethylbenzene

DEB – Dehydrogenation of Ethylbenzene

CNT – Carbon Nanotubes

MWCNTs – Multi-Wall Carbon Nanotubes

CAT1 – mixture consisted of 75 wt.% of Fe_2O_3 / 3 wt.% of Cr_2O_3 / 10 wt.% of K_2CO_3 / 6 wt.% of TiO_2 / 6 wt.% of CeO_2

CAT2 – mixture consisted of 55 wt.% of Fe_2O_3 / 20 wt.% of MnO_2 / 5 wt.% of K_2CO_3 / 20 wt.% of ZrO_2

CAT3 – mixture consisted of 75 wt.% of Fe_2O_3 / 5 wt.% of K_2CO_3 / 20 wt.% of ZrO_2

CAT4 – mixture consisted of 25 wt.% of MnO_2 / 50 wt.% of V_2O_5 / 25 wt.% of ZrO_2

CAT5 – mixture consisted of 50 wt.% of MnO_2 / 50 wt.% of ZrO_2

CNT3 – MWCNTs with theoretical Fe_2O_3 nanoparticles content of 3 wt.%

CNT6 – MWCNTs with theoretical Fe_2O_3 nanoparticles content of 6 wt.%

CNT9 – MWCNTs with theoretical Fe_2O_3 nanoparticles content of 9 wt.%

HEM25 – mixture consisted of 25 wt.% of hematite / 75 wt.% of magnetite

HEM50 – mixture consisted of 50 wt.% of hematite / 50 wt.% of magnetite

HEM70 – mixture consisted of 70 wt.% of hematite / 30 wt.% of magnetite

OMWCNTs – MWCNTs pretreated with oxygen

NMWCNTs – MWCNTs pretreated with nitric acid

XRD – X-Ray Diffraction Characterization

BET – Specific Surface Area determination

TEM – Transmission Electron Microscopy

HRTEM – High Resolution Transmission Electron Microscopy

XPS – X-Ray-induced Photoelectron Spectroscopy

EDX – Energy Dispersive X-ray Detector

GC – Gas Chromatography

Appendix E. Table of Figures

Figure 2.1. Schematic life cycle of a prototype styrene catalyst without any promoter additives.....	6
Figure 2.2. Reactor configuration in the process for hydrocarbons dehydrogenation (Shell).....	9
Figure 2.3. The electromagnetic spectrum.....	16
Figure 2.4. Relationship between the dielectric loss factor and ability to absorb microwave power for some common materials.....	20
Figure 2.5. Inverse temperature profile by microwave heating (a) and conventional heating (b).....	22
Figure 2.6. Schematic diagram of the inductively coupled plasma infrared imaging system.....	24
Figure 2.7. The evolution of microwave oven from gigantic "Radarange" (A) to the retro oven from 60s (B) and modern Panasonic microwave (C).....	25
Figure 2.8. Sectional view of a typical magnetron.....	26
Figure 2.9. Reaction network for the oxidative coupling of methane.....	31
Figure 3.1. Scheme of the experimental set-up.....	45
Figure 4.1. Effect of reaction temperature in ODEB over CAT1, CAT2 and CAT3 catalysts.....	49
Figure 4.2. Effect of reaction temperature in ODEB in the presence of carbon dioxide over CAT4 and CAT5..	49
Figure 4.3. (A) TEM and (B) HRTEM images of unpromoted MWCNTs before the reaction.....	53
Figure 4.4. TEM micrographs of fresh Fe ₂ O ₃ decorated MWCNTs. a) The nanoparticle adhere to the outer surface of the nanotubes and are randomly distributed. b) High-resolution images. The nanocrystals (indicated by an arrow) are crystalline and have a grain size of less than 10 nm.....	54
Figure 4.5 XRD pattern of (a) pure MWCNTs and (b) Fe ₂ O ₃ /MWCNTs nanocomposite before dehydrogenation.....	55
Figure 4.6. The effect of microwave power input on the temperature of catalyst bulk.....	56
Figure 4.7. Effect of loading level of iron oxide in ODEB reaction on the ethylbenzene conversion (X) and styrene selectivity (S): in conventionally-heated (A) and microwave-assisted (B) reactor.....	57
Figure 4.8. Effect of reaction temperature in ODEB over CNT3 catalyst on the ethylbenzene conversion (○), styrene yield (▲) and selectivity (■) in conventionally-heated (A) and microwave-assisted (B) reactors.....	59
Figure 4.9. Effect of time on stream in ODEB reaction over CNT3 on the ethylbenzene conversion (X) and styrene selectivity (S) in conventionally-heated (A) and microwave-assisted (B) reactors.....	60
Figure 4.10. (A) TEM and (B) HRTEM images of CNT3 composite after conventionally-heated ODEB.....	61
Figure 4.11. TEM image of CNT3 catalyst after microwave-assisted ODEB.....	62
Figure 4.12. (A) TEM and (B) HRTEM micrographs of iron oxide particle encapsulated by carbon shell of high-ordered graphite layers.....	63
Figure 4.13. EDX spectrum of CNT3 catalyst after ODEB reaction under microwave-assisted conditions.....	64
Figure 4.14. XRD patterns of CNT3 catalyst before (a) and after ODEB reaction in microwave-assisted (b) and conventionally-heated (c) reactors.....	65
Figure 4.15. XRD spectrum of Magnetite/Hematite mixture.....	68
Figure 4.16. TEM images of fresh Magnetite/Hematite nanocomposites.....	69
Figure 4.17. SAED images of fresh Magnetite/Hematite nanocomposites.....	69

Figure 4.18. Conversion of ethylbenzene over micro- and nano-scaled magnetite as a function of temperature using both conventional (A) and microwave (B) heating.....	71
Figure 4.19. Styrene Selectivity over micro- and nano-scaled magnetite as a function of temperature using both conventional (A) and microwave (B) heating.....	71
Figure 4.20. Ethylbenzene conversion (A) and styrene selectivity (B) over micro- and nano-scaled magnetite as a function of temperature using both conventional and microwave heating.....	72
Figure 4.21. Effect of time on stream in ODEB reaction over CNT3 on the ethylbenzene conversion in conventionally-heated (A) and microwave-assisted (B) reactors.....	74
Figure 4.22. Effect of time on stream in ODEB reaction over CNT3 on the styrene selectivity in conventionally-heated (A) and microwave-assisted (B) reactors.....	74
Figure 4.23. XRD spectrum of HEM25 after microwave assisted ODEB.....	75
Figure 4.24. TEM images of HEM25 after microwave assisted ODEB.....	77
Figure 4.25. HRTEM images of untreated (A) and pre-treated with oxygen (B) and nitric acid (C) MWCNTs.	80
Figure 4.26. Effect of time on stream in ODEB reaction over NMWCNTs on the conversion (X) and styrene selectivity (S) in conventionally-heated (A) and microwave-assisted (B) reactors.....	83
Figure 4.27. (A) TEM and (B) HRTEM images of NMWCNTs after conventionally-heated ODEB.....	84
Figure 4.28. (A) TEM and (B) HRTEM images of NMWCNTs after microwave-assisted ODEB.....	85
Figure 4.29. XPS Spectra of MWCNTs, NMWCNTs before and after conventionally-heated and microwave-assisted ODEB.....	85
Figure 5.1. Schematic of carbon paths on a catalyst particle. Adapted from Celnik.....	92
Figure 5.2. XRD patterns of samples obtained during the initial (a) and repeated (b) synthesis.....	94
Figure 5.3. (A) TEM image of magnetite produced by microwave assisted hydrothermal synthesis. (B) HRTEM image of the sample. The inset of (A) shows the SAED pattern of magnetite nanoparticles.....	95
Figure 5.4. Schematic of the microwave assisted catalytic CVD system.....	97
Figure 5.5. The dependence of the pressure drop on the volumetric flow rate.....	100

Appendix F. List of Tables

Table 3.1 The properties of MWCNT.....	41
Table 3.2 Compositions and abbreviations of powder catalysts prepared by the simple mixings.....	42
Table 4.1 Effect of microwave irradiation on the temperature of powder catalysts.....	51
Table 4.2 Effect of the iron oxide loading on the pore volumen and surface area of the prepared composites....	52
Table 4.3 Non-stoichiometrical ferric oxides.....	68
Table 4.4 Measured lattice spacing, $d(\text{Å})$, of magnetite based on the rings in Fig. 4.15 and their respective hkl indexes.....	69
Table 4.5 Hematite:Magnetite:Maghemite content ratios (%) for samples before and after ODEB in conventionally heated (CH) and microwave irritated (MW) reaction.....	76
Table 4.6 Effect of treatment procedure on the weight and volume of MWCNTs.....	81
Table 4.7 The experimental results for conventionally-heated ODEB over untreated, iron oxide loaded, and functionalized MWCNTs.....	82
Table 4.8 The experimental results for microwave-assisted ODEB over untreated, iron oxide loaded, and functionalized MWCNTs.....	82
Table 4.9 Component peaks and their attributions of XPS spectra as well as their calculated areas related to each sample.....	86
Table 5.1 The main properties of fluid and bulk.....	99
Table 5.2 Bed characteristics of magnetite.....	99

Kurzzusammenfassung

Ziel der vorliegenden Arbeit ist ein Beitrag zum besseren Verständnis der mikrowellenassistierten heterogenen Gasphasen-Katalyse am Beispiel der oxidativen Dehydrierung von Ethylbenzol zu Styrol.

Diese Reaktion wurde wegen ihrer industriellen Bedeutung ausgewählt. Styrol ist einer der ältesten und wichtigsten Ausgangsstoffe für die Herstellung von Kunststoffen, speziell von synthetischem Kautschuk und Polystyrol, aus dem viele alltägliche Gebrauchsartikel für den Haushalt wie Kleiderbügel oder Wäscheklammern, ebenso wie Gehäuse für elektronische Geräte oder für Lebensmittel geeignete Verpackungen gefertigt werden. Derzeit wird Styrol fast ausschließlich durch Dehydrierung von Ethylbenzol bei Temperaturen zwischen 600 bis 700°C im Beisein vom Wasserdampf über Kalium-promovierten Eisenoxidkatalysatoren erzeugt. Der Wasserdampf liefert die Wärme und unterdrückt außerdem die ablaufenden Deaktivierungsprozesse, wie zum Beispiel die Koksablagerung. Dieses Verfahren ist besonders energieaufwendig und dies zu einem Zeitpunkt an dem der Energiehunger der Welt, egal ob aus Öl, Kohle, Gas oder Atomkraft, immer größer wird.

Einen Beitrag zur Entschärfung dieser Probleme kann die oxidative Dehydrierung von Ethylbenzol zu Styrol unter mikrowellen-assistierten Bedingungen sein.

Seit den 80er Jahren des vergangenen Jahrhunderts gewinnen nicht-klassische Verfahren, insbesondere die Mikrowellentechnik, zur thermischen Unterstützung von heterogen katalysierten Reaktionen in der Forschung verstärkt an Bedeutung. Mikrowellen können sehr gezielt und innerhalb kürzester Zeit polare Moleküle aufheizen, wie zum Beispiel Wasser. Die Erzeugung von Wärme beruht dabei auf der Dissipation hochfrequenter elektromagnetischer Strahlung auf Grund dielektrischer Verluste von mikrowellenaktiven Stoffen. Die Selektivität der Erwärmung polarer Moleküle kann gerade bei mehrphasigen Systemen die Grundlage für neue Anwendungen sein, die sowohl im Produktionsschritt als auch bei der Wechselwirkung der Strahlung mit den Endprodukten liegen können. Es muß dabei beachtet werden, daß auf diesem Gebiet ein großer Forschungsbedarf besteht, da die heterogene Katalyse im Mikrowellenfeld derzeit nahezu vollständig auf Katalysatormassen von wenigen Gramm und damit auch geringe Gasdurchsätze beschränkt ist. Die experimentellen Forschungsergebnisse im Labor konnten bisher auf Grund einiger Probleme, z.B. der apparativen Gestaltung der Anlage, die elektrotechnische Ausführung der Mikrowellen-Generatoren sowie die Entwicklung von geeigneten Katalysatormaterialien nicht

in technische Maßstäbe umgesetzt werden. Aber die Forschungen werden weiter geführt und die Entwicklungen der letzten Zeit im Bereich der Mikroreaktortechnik machen die Anwendung der elektromagnetischen Strahlung als Energiequelle in der Industrie realistischer.

Aufgrund obengenannter Tatsachen stellt die oxidative Dehydrierung von Ethylbenzol zu Styrol im Mikrowellenfeld eine interessante Alternative zur technisch durchgeführten Dehydrierung von Ethylbenzol dar. Dafür müssen jedoch Katalysatoren entwickelt werden, die eine hohe Ausbeute und eine hohe Selektivität zum Wertprodukt Styrol zeigen.

Die Untersuchung der katalytischen Eigenschaften von Multi-Wall Carbon Nanotubes für die oxidative Dehydrierung von Ethylbenzol im Mikrowellenfeld sowie die Optimierung von katalytischen Eigenschaften der Nanoröhrchen durch Funktionalisierung ihrer Oberfläche mit Eisenoxid-Nanopartikeln sowie fallweise mittels Bearbeitung mit Sauerstoff oder Salpetersäure stellt die Grundlage zur sukzessiven Erreichung des Zieles dieser Arbeit dar. Die Arbeit gliedert sich in drei Teile:

1. In erstem Teil wird die oxidative Dehydrierung von Ethylbenzol zum Styrol über die Multi-Wall Carbon Nanotubes im Mikrowellenfeld wie im konventionell geheizten Reaktor durchgeführt. Diese Nanoröhren gehören zu den sp^2 -hybridisierten, nanostrukturierten Kohlenstoffen, die durch hohe Oxidationsstabilität sehr gut für die extremen Reaktionsbedingungen der katalytischen oxidativen Dehydrierung geeignet sind. Sie wurden zusätzlich mit Eisenoxid Nanopartikeln versetzt und mittels beider Heizmethoden unter gleichen Reaktionsbedingungen untersucht, um die Ergebnisse vergleichen zu können.
2. Die Forschung des zweiten Teils der Arbeit beruht auf den Erkenntnissen vorangegangener Untersuchungen. Es wurde erkannt, daß die Eisenoxidpartikel, welche an die Multi-Wall Carbon Nanotubes promoviert sind, während der Dehydrierung von Ethylbenzol von mehreren Sechseck-Struktur-Schichten hochgeordneten Graphits eingekapselt wurden. Aus diesem Grund wurde das Gemisch aus reinem Nanopulver von Magnetit und Maghemit unter gleichen Reaktionsbedingungen untersucht, um diese Wirkung ohne Multi-Wall Carbon Nanotubes als Träger zu untersuchen.

3. Zuletzt wurden die Multi-Wall Carbon Nanotubes mit verschiedenen Methoden funktionalisiert und für die oxidative Dehydrierung von Ethylbenzol verwendet. Der Einfluß der Funktionalisierung sowie der Art der Heizung auf katalytische Eigenschaften und Struktur von präparierten Systemen wurden mit Hilfe mehrerer Charakterisierungsmethoden (TEM, XRD, BET, XPS) ermittelt.

Abschließend werden die wichtigsten Schlußfolgerungen der Arbeit, die Erklärungen der verwendeten Abkürzungen und die Liste aller Abbildungen und Tabellen vorgestellt.

Lebenslauf



Angaben zur Person

Nachname / Vorname	Boriss Nigrovski
Adresse	Stauffenbergstraße 2, D-07747 Jena
Telefon	(+49) 176 2395 6032
E-mail	boriss.nigrovski@mail.org
Staatsangehörigkeit	Estnisch / EU
Geburtsdatum	29.03.1983 in Nahodka, Rußland
Geschlecht	Männlich
Familienstand	ledig

Schul- und Berufsbildung

Datum	10.2005 – 12.2008
Studienabschluss	Doktor der Naturwissenschaften
Thema der Promotionsarbeit	„Oxidative Dehydrierung von Ethylbenzol zu Styrol im Mikrowellenfeld“
Name und Art der Bildungs- oder Ausbildungseinrichtung	Institut für Technische und Umweltchemie Friedrich-Schiller Universität Jena
Datum	09.2000 – 06.2005
Studienabschluss	Diplom – Ingenieur / Gesamtnote: gut
Name und Art der Ausbildungseinrichtung	Institut für Umweltchemie Technische Universität Tallinn
Datum	09.1989 – 06.2000
Schulabschluss	Abitur / Gesamtnote: sehr gut
Name, Ort und Art der Schule	Linnamäe Gymnasium in Tallinn, Estland

Jena, 17.10.2008

Publikationsliste

1. B. Nigrovski, P. Scholz, B. Ondruschka, et al. Katalysatoren zur Totaloxidation von flüchtigen organischen Komponenten. Chem. Ing. Tech. 79 (2007) 2083 – 2088.
2. U. Zavyalova, B. Nigrovski, K. Pollok, et al. Gel-combustion synthesis of nanocrystalline spinel catalysts for VOCs elimination. Appl. Catal. B: Environ. 83 (2008) 221-228.
3. B. Nigrovski, U. Zavyalova, P. Scholz, et al. Microwave-assisted catalytic oxidative dehydrogenation of ethylbenzene on iron oxide loaded carbon nanotubes. Carbon 46 (2008) 1678-1686.
4. B. Nigrovski, P. Scholz, B. Ondruschka. Catalytic performance of carbon nanotubes iron oxide composites (Fe₂O₃/CNT) in microwave-assisted oxidative dehydrogenation of ethylbenzene (ODEB) to styrene. 41. Jahrestreffen Deutscher Katalytiker, Weimar. Poster (February, 2008).
5. Boriss Nigrovski, Peter Scholz, Bernd Ondruschka. Katalysatoren zur Totaloxidation von flüchtigen organischen Komponenten. Universität Jena 1558-2008, Goethe Galerie. Poster (April, 2008).

Selbsterklärung

Ich erkläre, daß ich die vorliegende Arbeit selbstständig und unter Verwendung der angegebenen Hilfsmittel, persönlichen Mitteilungen und Quellen angefertigt habe.

Jena, 17.10.2008